

# Error Control Coding Schemes for Ultra-wideband Impulse Radio Systems

PROEFSCHRIFT

ter verkrijging van de graad van doctor  
aan de Technische Universiteit Delft,  
op gezag van de Rector Magnificus Prof. ir. K.C.A.M. Luyben,  
voorzitter van het College voor Promoties,  
in het openbaar te verdedigen op vrijdag 12 februari 2010 om 10.00 uur

door

Michał Mirosław PIETRZYK

magister inżynier elektrotechniki,  
Kielce University of Technology  
geboren te Kielce, Polen.

Dit proefschrift is goedgekeurd door de promotor:

Prof. dr. ir. I.G.M.M. Niemegeers

Copromotor: Dr. ir. J.H. Weber

Samenstelling promotiecommissie:

Rector Magnificus	voorzitter
Prof. dr. ir. I.G.M.M. Niemegeers	Technische Universiteit Delft, promotor
Dr. ir. J.H. Weber	Technische Universiteit Delft, copromotor
Prof. dr. ir. P.G.M. Baltus	Technische Universiteit Eindhoven
Prof. dr. ir. J. Biemond	Technische Universiteit Delft
Prof. dr. ir. L.P. Ligthart	Technische Universiteit Delft
Prof. dr. ir. W.C. van Etten	Universiteit Twente
Prof. dr. ir. T. Wysocki	University of Nebraska

ISBN 978-90-9024663-5

Copyright © 2010 by Michał M. Pietrzyk

All rights reserved. No part of the material protected by this copyright notice may be reproduced or utilized in any form or by any means, electronic or mechanical, including photocopying, recording or by any information storage and retrieval system, without the prior permission of the author.

Printed in the Netherlands by Wöhrmann Print Service

Cover design by Aneta Pietrzyk

Author email: [m.m.pietrzyk@ieee.org](mailto:m.m.pietrzyk@ieee.org)

*To Aneta and Klaudia*



# Summary

It is envisioned that wireless systems beyond the third generation (3G) will enable connectivity for everybody and everything at any place and any time. This highly pervasive nature of future communication will require an integration of existing and future wireless standards, ranging from metropolitan area networks (MANs), wireless local area networks (WLANs), wireless personal area networks (WPANs) to wireless body area networks (WBANs). Today's WLAN and WPAN technologies cannot meet the needs of tomorrow's connectivity that requires high data rate, is able to sense the environment, and is based on ambient intelligence and pervasive computing paradigms.

Ultra-wideband (UWB) is a promising technology that offers a potential solution for the data rate, cost, power consumption and physical size requirements of the next generation wireless devices. UWB may also play an important role in the realization of future heterogeneous networking. This technology has recently gained significant interest from both academia and industry leading to the specification of the IEEE 802.15.3 and IEEE 802.15.4 standards. The strength of the UWB lies in the very large instantaneous bandwidth that is used and the potential for simple transceiver architectures.

This thesis deals with several important aspects of the UWB technology, including modeling of feasible ultra-wideband impulse radio (UWB-IR) systems, their performance characterizations, and suitable methods for protection against errors. The main goal of this thesis is to propose and evaluate novel error control techniques particularly suitable for UWB-IR systems operating in severe multipath interference prone environments. The proposed methods exploit the temporal diversity brought by the UWB channels through multipaths and as a result allow for the alleviation of destructive effects of inter-symbol (ISI), inter-frame (IFI), and inter-pulse (IPI) interference. We found that rearranging the order of UWB chips or UWB frames results in a bit error rate (BER) performance improvement. This improvement is particularly apparent in case of UWB-IR systems with frame repetition (FR) as the method of protection against errors. For the case of UWB-IR systems with superorthogonal (SOC) coding, the introduced gain is smaller.

This thesis starts with an introduction to the UWB technology and a literature survey on relevant topics. Next, the UWB-IR system model considered throughout the thesis is presented. It provides details on the proposed techniques, channel model, pulse shape, antenna characteristics and receiver architecture. Moreover, hardware implementation challenges are

being addressed. The considered channel coding schemes suitable for UWB systems include frame repetition, bit repetition and SOC coding. We present the criteria for their selection. Furthermore, selected aspects of the hardware implementation of a decoding algorithm available in the literature are reviewed. The performance of UWB-IR systems is characterized through theoretical- and Monte-Carlo-simulation-based analyzes. The BER performance of single-user UWB-IR systems operating on additive white Gaussian noise (AWGN) and multipath fading channels is studied in detail. The novelty of the presented analysis is that it considers ISI, IFI, and IPI effects, RF front-end issues and real antenna characteristics that are often neglected by the researchers. Moreover, they are presented, for the first time, for the given type of the simple incoherent receiver architecture (differential autocorrelation receiver), channel coding scheme (SOC coding), and channel model (IEEE 802.15.3a multipath fading channel).

Our results indicate that for UWB-IR systems with SOC coding, and for a given set of system parameters explained in detail in Chapter 4, it is possible to achieve BER levels of the order of  $10^{-4}$  at  $E_b/N_0$  (bit energy to noise spectral density ratio) values lower than 12.5 dB. UWB-IR systems with frame repetition perform much poorer, and for the same BER levels the required  $E_b/N_0$  is more than 16 dB. Our findings also show that rearranging the order of chips in a one-to-one random manner brings better performance improvement comparing to rearrangement of frames or bits. Moreover, altering the system parameters settings (within the considered values) while maintaining the data rate does not affect the BER performance of UWB-IR systems with FR. This is not the case for UWB-IR systems with SOC coding, where a tendency favoring low code-rate codes is visible. The obtained simulation results are in good agreement with the derived lower and upper bounds on the BER.

A novel design of a deterministic chip interleaver based on time-hopping hyperbolic congruence sequences is also proposed. This scheme together with SOC coding or frame repetition constitutes an effective method of protection against errors in scarcely populated UWB-IR systems operating in severe multipath interference prone environments. The BER performance of UWB-IR systems operating on multipath fading channels with and without the proposed scheme is evaluated by referring to bounds based on the Poisson distribution and intensive Monte Carlo simulations. Our contribution includes the design of the chip interleaver based on time-hopping hyperbolic congruence sequences and its main parameters determination.

Our findings indicate that the Interleaved Coding-Modulation (ICM) method introduces performance improvements also for scarcely populated multi-user scenarios. The proposed deterministic chip interleaver may be favored over the random interleaver due to its simpler implementation. Our results show that the presented Poisson-based analysis may be helpful in a rough approximation of the BER performance of UWB-IR systems without the ICM method.

The last part of this thesis presents the study of application of UWB-IR technology in

body area networks (BANs). It starts with an introduction to the BAN concept. Next, a description of several considered scenarios, system, and channel models is given. Performance of BANs based on UWB-IR technology is evaluated by Monte-Carlo simulations.

Our results indicate that for low data rate BANs, the frame repetition and SOC coding enable better BER performance than that for the case of high-data-rate systems. Moreover, the ICM method offers BER performance improvements which are significant for FR scheme with the data rate of 31.25 Mbps. For the case of data rates lower than 31.25 Mbps, this method introduces performance improvements but only when the  $E_b/N_0$  is larger than a certain value.





# Contents

<b>Contents</b>	<b>v</b>
<b>1 Introduction</b>	<b>1</b>
1.1 Introduction to UWB technology . . . . .	1
1.1.1 History of UWB . . . . .	2
1.1.2 Basics of UWB-IR . . . . .	3
1.1.3 Distinctive properties of UWB . . . . .	3
1.1.4 UWB cognitive radio . . . . .	5
1.1.5 Potential applications . . . . .	7
1.1.6 Regulatory issues . . . . .	8
1.2 Channel coding . . . . .	10
1.2.1 Block codes . . . . .	10
1.2.2 Convolutional codes . . . . .	11
1.2.3 Iteratively decodable codes . . . . .	11
1.3 Prior research . . . . .	13
1.3.1 Channel coding schemes for UWB systems . . . . .	13
1.3.2 UWB receiver architectures . . . . .	15
1.4 Aim and outline of the thesis . . . . .	16
1.4.1 Aim of the thesis . . . . .	16
1.4.2 Thesis outline . . . . .	17
1.4.3 Framework . . . . .	18
<b>2 UWB-IR system model</b>	<b>21</b>
2.1 System model . . . . .	21

2.1.1	Principle of ICM+PR – UWB-IR transmitter . . . . .	21
2.1.2	Channel models . . . . .	24
2.1.3	Pulse shape . . . . .	29
2.1.4	Antenna characteristics . . . . .	31
2.1.5	Principle of ICM+PR – UWB-IR receiver . . . . .	33
2.2	Hardware implementation issues . . . . .	35
2.2.1	General issues . . . . .	35
2.2.2	A view on hardware realization of the ICM technique . . . . .	36
2.3	Summary . . . . .	37
<b>3</b>	<b>Channel coding</b>	<b>39</b>
3.1	Channel coding selection criteria . . . . .	39
3.2	Investigated channel coding schemes . . . . .	40
3.2.1	Frame repetition . . . . .	40
3.2.2	Bit repetition . . . . .	41
3.2.3	Superorthogonal convolutional coding . . . . .	41
3.3	Hardware implementation of a Viterbi decoder . . . . .	45
3.4	Summary . . . . .	46
<b>4</b>	<b>Performance analysis</b>	<b>47</b>
4.1	Bounds on the bit error probabilities . . . . .	47
4.1.1	Bounds on the bit error probabilities on AWGN channels . . . . .	48
4.1.2	Bounds on the bit error probabilities on multipath fading channels . .	50
4.1.3	Bit error probabilities of a RAKE receiver on multipath fading channels	52
4.2	Simulation results . . . . .	53
4.2.1	Results - no interleaving nor PR case . . . . .	53
4.2.2	Results - interleaving and/or PR case . . . . .	54
4.2.3	Results - influence of the system parameters . . . . .	58
4.2.4	Results - influence of the channel parameters . . . . .	60
4.2.5	Results - comparison with other systems . . . . .	62
4.3	Summary . . . . .	66

<b>5</b>	<b>Multi-user UWB-IR systems</b>	<b>67</b>
5.1	System model . . . . .	67
5.1.1	UWB-IR Transmitter . . . . .	69
5.1.2	UWB-IR Receiver . . . . .	69
5.2	Chip interleaver design based on TH sequences . . . . .	72
5.2.1	Hyperbolic congruence sequence design . . . . .	72
5.2.2	Interleaver properties . . . . .	72
5.3	Bounds on the bit error probabilities . . . . .	77
5.3.1	Frame Repetition . . . . .	78
5.3.2	SOC Coding . . . . .	78
5.4	Simulation results - interleaving in scarcely populated UWB-IR systems . . .	79
5.5	Summary . . . . .	82
<b>6</b>	<b>UWB-IR based Body Area Networks</b>	<b>83</b>
6.1	Introduction . . . . .	83
6.1.1	Definitions . . . . .	84
6.1.2	Main features . . . . .	85
6.1.3	Applications . . . . .	86
6.1.4	Topologies . . . . .	86
6.1.5	Technological challenges . . . . .	87
6.1.6	Social issues . . . . .	88
6.2	System model . . . . .	89
6.2.1	UWB-IR transmitter and receiver . . . . .	89
6.2.2	Body area radio propagation channel model . . . . .	89
6.3	Performance evaluation . . . . .	95
6.4	Summary . . . . .	98
<b>7</b>	<b>Conclusions</b>	<b>99</b>
7.1	Contributions of this thesis . . . . .	99
7.1.1	Single-user high-data-rate UWB-IR systems . . . . .	99
7.1.2	Multi-user high-data rate UWB-IR systems . . . . .	100

7.1.3	Single-user low-data rate UWB-IR systems for BAN applications . . .	101
7.2	Future research directions . . . . .	102
	<b>Bibliography</b>	<b>103</b>
	<b>A Publications by the Author</b>	<b>117</b>
	<b>Acknowledgements</b>	<b>127</b>

# Preface

It was the year 1981 and I was a 4-years-old boy, when my adventure with telecommunications started. At that time, I was given for the first time a short-wave amateur radio and was enjoying chatting with my father. Several years later, I started my first experiments with electronics and circuits which changed my entire life thereafter. I have built my first long-wave radio at the age of 10. Then, in 1992, just before starting the education at a technical electronics college, I have designed my first short wave transceiver operating in the 27 MHz band. As a final project at my technical college, I designed a wireless timer that could measure the lap time for short distance running (up to 100 m). Two simultaneous timers could be started and lap times recorded at the finish when two students crossed infra-red links. The start unit was communicating wirelessly with the main unit placed at the finish. The timer was based on the 89C51-family microcontroller. I proposed, designed, built, and tested all the electrical circuits and wrote the assembler code all by myself. These required among others vast knowledge of radio communications and test equipment, and problem solving skills. My assignment won the Best Prize in the Student Contest for the Most Useful Final Project Put in Practice at my college. Since 1999, when I had been awarded the Harmonized Amateur Radio Certificate, I have been a licensed ham radio operator, and can build prototypes of transceivers and make radio calls with people all over the world.

Nowadays, telecommunication devices look much different than the ham radio transceivers. They are much smaller, lighter, of increased functionality, and at the same time offering numerous services. However, the principles of the radio wireless communication technology that they are based on, remain the same.

The main topic of this thesis is proposal, design, and performance evaluation of novel error control coding techniques for ultra-wideband communication systems.



# Chapter 1

## Introduction

Extremely popular these days ubiquitous wireless connectivity has been changing our lifestyles by providing conveniences for mobile computing. It is not far from now that consumers will demand the same conveniences in their digital homes connecting their camcorders to high definition TV (HDTV), connecting gaming consoles, digital cameras, personal digital assistants (PDAs), and mobile phones to each other in wireless personal and body area networks. However, today's WLAN and WPAN technologies cannot meet the needs of tomorrow's connectivity especially when the available bandwidth is scarce and extremely expensive. The ultra-wideband technology has recently become a potential solution to many of today's problems related to the spectrum management and radio systems engineering. The unconventional approach underlying the use of UWB is based on sharing the existing radio spectrum resources rather than looking for available frequency bands.

### 1.1 Introduction to UWB technology

The UWB technology has been approved by the Federal Communication Commission (FCC) in the USA in 2002 and by the Electronic Communication Committee (ECC) of the European Conference of Postal and Telecommunications Administration (CEPT) in the Europe in 2007. The FCC defines ultra-wideband device as any wireless radio device emitting signals with a fractional bandwidth being at least 20% or an absolute bandwidth being at least 500 MHz [25]. The fractional bandwidth is defined as  $2(f_H - f_L)/(f_H + f_L)$ , where  $f_H$  and  $f_L$  are the upper and lower frequencies at the -10 dB emission point, respectively. The UWB systems are allowed to transmit signals with very limited power across wide range of frequencies between 3.1 GHz to 10.6 GHz (in the USA) and therefore such signals may be perceived by wireless communication systems, e.g., IEEE 802.11a WLANs operating around

the frequency of 5.20 MHz, as noise. High bandwidth that is occupied by the UWB systems yields high temporal resolution that allows for lower fading margins than in narrowband systems. It also enables very fine (centimeter) accuracy ranging and positioning capabilities that may be combined with data transmission.

### 1.1.1 History of UWB

It is generally agreed that the ultra-wideband technology has its origins in early 1960s with the pioneering work of Gerald Ross at Sperry Research Center in 1963 [89] and Henning Harmuth in 1969 at the Catholic University of America [43]. The work concerned a description of a certain class of microwave networks through their impulse responses. However, one decade earlier, in 1952, Louis de Rosa was granted a U.S. patent No. 2671896 for a random impulse system to provide a method and means to generate a series of random pulses which when used for modulation of a carrier would greatly minimize the possibility of jamming. Moreover, in 1961, Conrad H. Hoepfner was granted a patent for a pulse communications system that could reduce interference and jamming. In fact, one may argue that the UWB technology actually had its origins in the spark-gap transmission designs by Marconi and Hertz in the late 1890s and in Marconi's celebrated cross-Atlantic transmission using spark techniques on 12 December 1901. In a general sense, this first wireless communication system was based on the UWB technology. Due to the technical limitations, narrowband communication was preferred to UWB. Similarly to CDMA systems, which originated in military applications during World War II as means for defeating enemy torpedoes and which reached commercial applications, only some 40 years later, the UWB technology followed somewhat similar path, with early systems designed for military and with commercial interest being recognized much later. For up until 1962, when Hewlett-Packard introduced the time-domain sampling oscilloscope, there were no convenient ways to observe nor measure waveforms of sub-nanosecond durations. However, the first receiver that could detect short pulses known as a threshold receiver, was built based on the avalanche transistor and tunnel diode detectors in early 1970s. The tunnel diode invented by Esaki in 1957 who later, in 1973, received the Nobel Prize for this accomplishment, was the first element permitting sub-nanosecond pulse detection as well as generation. Through the late 1980s, the UWB technology was alternately referred to as baseband, carrier-free or impulse. The term "ultra-wideband" originated with the Department of Defense of the USA around 1989 to describe a way of communication via transmission and reception of impulses. By that time, UWB theory, techniques and hardware approaches had experienced nearly 30 years of extensive development. By 1989, Sperry Research Center had been awarded over 50 patents in the field of UWB technology including applications in communications, radar, automobile collision avoidance, positioning systems, sensing and altimetry. After 1994, when some of the research activities were declassified [92] and when the FCC issued a Notice of Inquiry in 1998 the research activities in UWB 'sparked' worldwide. The next milestone, the Report and Order issued by the FCC in 2002



[67] allowing for a commercial development of UWB technology, generated interest among the public and within academia and governments of many countries.

### 1.1.2 Basics of UWB-IR

The most traditional way of emitting a UWB signal is based on radiating ultra-short pulses. This transmission method is used in ultra-wideband impulse radio (UWB-IR). The way in which information data bits are represented by pulses may differ depending on the modulation scheme applied and might include pulse position modulation (PPM), pulse amplitude modulation (PAM), pulse shape modulation (PSM) or differential autocorrelation modulation (DAM). In addition to modulation schemes, pseudorandom codes may be used to spread the impulses in time in order to avoid co-channel interference in multi-user scenarios which refers to time hopping ultra-wideband (TH-UWB) approach. Alternatively, pseudorandom sequences might be used for spread spectrum purposes as in CDMA systems, and as such leading to direct sequence ultra-wideband (DS-UWB) radio.

Another approach is based on the orthogonal frequency division multiplexing (OFDM) technique. OFDM is a highly spectral efficient version of a multicarrier transmission that permits orthogonal subcarriers to overlap in the frequency domain without causing mutual interference. Multiple users can be supported by allocating each user a group of subcarriers depending on the particular quality-of-service (QoS) requirements. The key advantage of such an approach lies in the fact that some subcarriers, although being of low quality to one user, may be of higher quality to the other users. UWB-OFDM has been proposed as a physical layer for high data rate, short range communications in the IEEE 802.15.3a standard. Unlike narrowband OFDM, the OFDM-UWB spectrum has gaps between subcarriers. The whole spectrum is divided into 14 sub-bands, each having a bandwidth of 528 MHz. Information is being transmitted using OFDM symbols that correspond to three different bands interleaved in time. The modulation proposed is the quadrature phase-shift keying (QPSK). The OFDM technique has some drawbacks, e.g., it requires the use of digital logic circuits to implement the FFT/IFFT operations that are of high complexity and power consumption. It also requires the application of a high linear amplifier at the transmitter.

Research results presented in this thesis are related to the UWB-IR version of the UWB technology.

### 1.1.3 Distinctive properties of UWB

The UWB technology can be characterized by several distinct properties that differentiate it from the narrowband wireless communications technologies. By far the most important property is the use of very large bandwidth that is many times greater than the minimum

required to deliver information. This enables high data rate (up to hundreds of Mbit/s) support for multi-user network communication applications and very fine time and position resolution for non-communication applications such as localization and ranging. The radiated UWB signals are only permitted at very low power spectral density (PSD) levels that brings the ability to share the same spectrum with other (e.g. narrowband) systems due to the low interference, possibility of high device density, and low probability of detection and interception (LPD/I) being of particular importance for military applications. Due to the presence of low frequency components in the UWB frequency spectrum, the UWB signals have superior penetration properties in comparison to narrowband signals. This allows for through-the-wall imaging and radar applications. The use of narrow pulses in the order of a nanosecond leads to relative immunity to fading due to the possibility of exploiting many resolvable independent paths. Moreover, the UWB technology promises prospects for low-cost and long-life battery-operated devices mainly thanks to simple transceiver implementations. However, the same properties provide design challenges, such as scalability, synchronization and power control. Although UWB systems exhibit robustness to multipath effects, they are not entirely immune to them. In typical indoor applications, where the transmitted pulses undergo numerous reflections and when the channel duration is in the order of tens or hundreds of nanoseconds, multipath fading phenomena may cause significant inter-symbol interference severely limiting the maximum data rate that can be supported or degrading the link reliability. To mitigate the negative effects of these phenomena, efficient error control techniques that take into account specific time domain properties of the UWB propagation channel and can exploit its inherent temporal diversity, have to be designed. This is of particular importance when realizing that the costs of effective UWB equalizers, in terms of gate count and power consumption, may be prohibitive. Another challenging area is the the UWB antenna design. Portable communication devices put high requirements on the size and shape of the antenna which has to radiate effectively in a wide frequency band and under varying propagation conditions sometimes including the near-field, e.g. carried on the body or near objects. To ensure future development of UWB technology and wide presence of its products in the commercial market of tomorrow, these challenges must be properly addressed and resolved.

A comparison between contemporary short-range wireless communication standards that are suitable for Local-, Personal-, and Body- Area Networks (LAN, PAN and BAN, respectively) is presented in Table 1.1. The next generation of consumer electronics and mobile applications demand data rates beyond 1 Mbps offered by the Bluetooth technology used in PANs today. While IEEE 802.11.b technology, also known as Wi-Fi, or IEEE 802.11.g technology provide higher data rates than Bluetooth, they are still not optimized to effectively support multiple streaming of high-quality video or audio. For those applications, UWB, thanks to its high data rate capabilities, could clearly find the niche. On the other hand, a low data rate UWB transceiver is relatively less complex than its narrowband equivalent. This characteristic translates directly to lower power consumption and reduced costs of a final market product.

An important advantage of UWB over other wireless technologies is its flexibility. Since the operational range of UWB-IR systems is a function of the number of pulses transmitted over a period of time, by a simple software control one can dynamically trade the data rate and the power consumption for the range. This feature is of particular importance for the future power-constrained ambient computing applications.

#### 1.1.4 UWB cognitive radio

Another important characteristic of the UWB technology that stems from the wide bandwidth utilized, is the ability to adaptively assign certain portions of the bandwidth to the users. This can be done in a cognitive fashion as in cognitive radios, where the spectrum is sensed for the radio signal optimization, co-existence, and interference avoidance purposes. UWB cognitive radio systems may fully utilize the available radio resources by dynamically adapting to the available spectrum in real-time, which can be accomplished by changing pulse shape by means of application of a filter of a given transfer function or changing the carrier frequency in case of systems with frequency up-conversion. Furthermore, UWB cognitive radio systems are able to offer bandwidth on demand, dynamically choosing the most appropriate air interface, modulation, etc., based upon perception of the wireless channel, locations, spectrum rules, spectral occupancy and other parameters. The parameters that may be traded for include data rate, bit/packet error rate, Quality of Service (QoS), and cost of connection. These parameters can be varied by dynamically controlling frequency, power levels, modulation type, and its order (PAM, PPM, etc.), error control coding schemes, protocols, antenna beamforming, and timing. Finding the optimal values of the above parameters, given the set of conditions regarding, e.g. data rate, bit error rate, latency etc., in a UWB cognitive radio systems is at present an active research area. Examples of publications on the UWB cognitive radio include [8] and [91].

Table 1.1. Comparison Between Short-range Wireless Communication Standards [78].

Standard	ZigBee IEEE 802.15.4	Bluetooth	Wi-Fi IEEE 802.11b	Wi-Fi IEEE 802.11g	Wi-Fi IEEE 802.11a	UWB IEEE 802.15.3a <sup>†</sup>
Data Rate	250 kbps 40 kbps 20 kbps	1 Mbps	11 Mbps	54 Mbps	24 Mbps 54 Mps (opt.)	200 Mbps <sup>1</sup> 110 Mbps <sup>2</sup>
Max. Distance	30 m	10 m	100 m	100 m	50 m	10 m
Frequency	868-868.6 MHz <sup>3</sup> 902-928 MHz <sup>4</sup> 2400 MHz -2483.5 MHz <sup>5</sup>	2.4 GHz	2.4 GHz	2.4 GHz	5.15-5.35 GHz 5.725 GHz -5.825 GHz	3.1-10.6 GHz
Channel Bandwidth	0.3; 0.6 MHz 2 MHz	1 MHz	25 MHz	25 MHz	20 MHz	500 MHz
Number of Channels	1; 10; 16	79	3	3	12 <sup>†</sup> 8 <sup>‡</sup>	1-15
Modulation	BPSK OQPSK	GFSK	QPSK	OFDM	COFDM BPSK	BPSK QPSK
Spreading	DS-SS	DS-FH	CCK	OFDM	OFDM	OFDM
Max. Allowed RF Power	1 W <sup>†</sup> 25 mW <sup>‡</sup> 20 mW <sup>‡</sup>	1 mW <sup>†</sup> 0.1 W <sup>‡</sup>	1 W <sup>†</sup> 0.1 W <sup>‡</sup>	1 W <sup>†</sup> 0.1 W <sup>‡</sup>	50 mW 250 mW 1 W	-41.3 dBm /MHz
Approx.* PHY Layer Power Consum.	< BT	BT (~ 40-100 mW)	~ 4 BT	~ 4 BT	~ 6 BT	~ 2-3 BT
Approx.* Chip Cost	0.5 BT	BT (~ 5\$)	~ 4 BT	~ 4 BT	~ 5 BT	~ 1-2 BT

Acronyms used: BT - Bluetooth device, CCK - complementary code keying, COFDM - coded orthogonal frequency division multiplexing, ISM - industrial scientific and medical band.

<sup>1</sup> 4 m distance.

<sup>2</sup> 10 m distance.

<sup>3</sup> ISM EU.

<sup>4</sup> ISM USA.

<sup>5</sup> ISM.

<sup>†</sup> In the USA.

<sup>‡</sup> In Europe.

\* Values of these parameters highly depend on a design and the numbers provided here serve as rough indications.

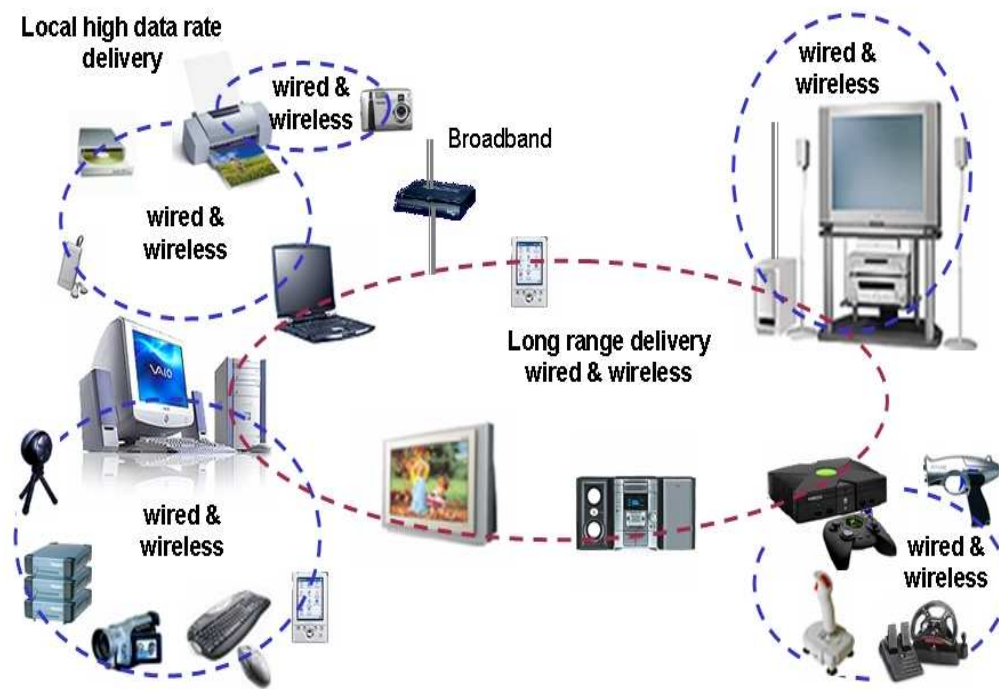


Figure 1.1. An example of UWB application - PAN. Source: Intel Research and Development.

### 1.1.5 Potential applications

The UWB technology has many potential applications supporting high as well as low data rate short range wireless personal and body area networking. As long as high data rate is considered, the very promising application is a USB cable replacement between a PC and associated peripherals such as handheld computers, printers, still cameras, web cams, and mobile phones just to mention a few. It is expected that wireless USB products based on the UWB technology will become in the coming years as popular as wired USB whose market is estimated to be nearly 2.5 billion USB connections worldwide [3]. The UWB technology can also enable high data rate ( $> 20$  Mbps) wireless video and audio streaming from camcorders to computers or TV sets. Emerging low data rate ( $< 100$  kbps) applications include sensor networks that are the focal point of mobile computing. An example of application of the UWB technology in PAN is shown in Fig. 1.1. The UWB technology makes it possible to introduce positioning and ranging capabilities into sensor networks due to the inherent centimeter accuracy that originates from the sub-nanosecond duration of UWB pulses. Simple UWB transceiver architecture may result in a very low price ( $< 1\$$ ) of a single UWB chip which may operate in strict power consumption conditions typical to mobile devices. The above mentioned features are crucial in medical applications (e.g. monitoring patients), search and rescue devices and logistics. The military and government applications include: tactical handheld and network-capable low probability of interception/detection (LPI/D) radios, data-links for unmanned aerial vehicles (UAVs), wireless intercom systems for se-

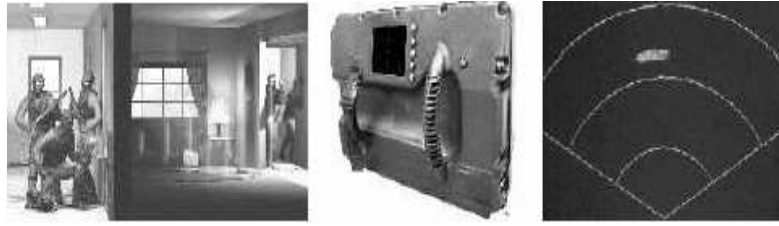


Figure 1.2. An example of UWB application - through wall surveillance radar. Source: Time Domain Inc.

cure, untethered communication onboard aircraft, LPI proximity fuses for smart munitions, through-wall imaging for fire-fighters, and precision geo-location systems. Since UWB signals can penetrate through walls, a whole range of new applications, including through-the-wall penetration radars which give the ability to detect personnel through several intervening walls, ground penetrating radars, intelligent transportation systems (ITS) with vehicle to vehicle and vehicle to roadside communications, collision and obstacle avoidance radars, can be supported. An example of UWB application as a through wall surveillance radar is shown in Fig. 1.2.

### 1.1.6 Regulatory issues

The UWB technology has been licensed in the USA when the FCC issued the First Report and Order on 14 February 2002 [67]. The UWB operation has been divided into three main categories:

- Communications and measurement systems
- Vehicular radar systems
- Imaging systems including ground penetrating radars, surveillance systems and medical imaging

with each category having a specific spectral mask with emission limits. It has been assumed that UWB systems may operate overlaid with the existing legacy systems and services, e.g. Global Positioning System (GPS), satellite receivers, cellular services, causing interference at low enough power levels that ideally would not cause significant performance degradation. The FCC intentionally did not specify techniques related to generation and detection of RF signals, e.g. modulation, receiver architecture etc., leaving them to the industry leaders and academia. The spectral masks for indoor UWB communication systems specified by the FCC in the USA and Electronic Communication Committee are shown in Fig. 1.3. In the USA, the modulated UWB signal for indoor communications in the frequency range from 3.1 GHz

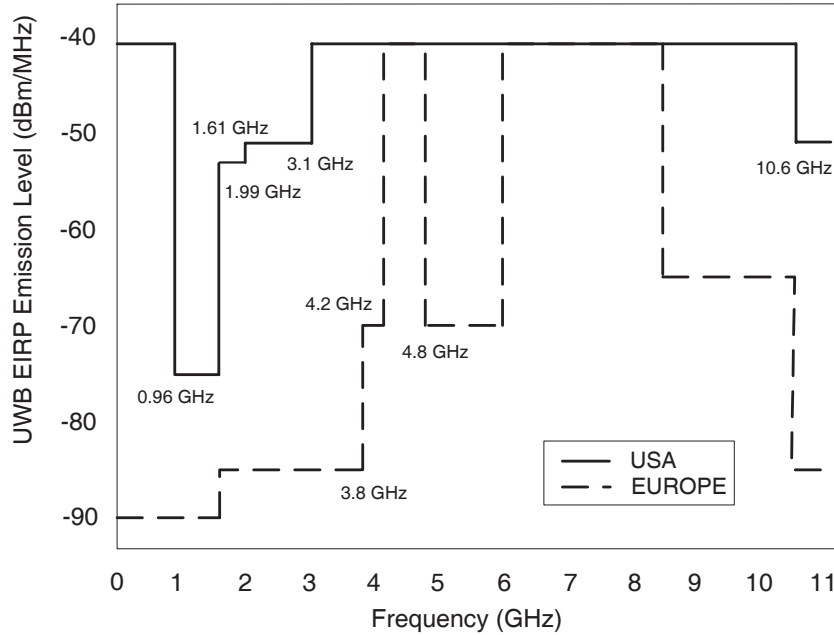


Figure 1.3. Spectral mask for indoor UWB applications mandated by the FCC in the USA and EC in Europe.

to 10.6 GHz (7.5 GHz-wide bandwidth) must satisfy a  $-41.3$  dBm/MHz equivalent isotropic radiated power (EIRP) density limit. In Europe, the UWB technology has been allowed to operate since 21 February 2007 when the EC has issued the Commission Decision [66]. The EC has been a somewhat conservative stating in [66] that "Although ultra-wideband signals are typically of extremely low power, the possibility of harmful interference with existing radiocommunication services exists and needs to be managed". As a consequence the UWB systems has been allowed to operate in the 6.0 GHz - 8.5 GHz band where interference to existing wireless infrastructure systems such as Broadband Fixed Wireless Access systems can be avoided. It is important to know the definitions of the mean and peak EIRP densities used by the EC.

The mean EIRP density is defined as mean power measured with a 1 MHz resolution bandwidth, a root-mean-square (RMS) detector and an averaging time of 1 ms or less. The peak EIRP density means the peak level of transmission contained within a 50 MHz bandwidth centered on the frequency at which the highest mean radiated power occurs.

The maximum EIRP density refers to the highest signal strength measured in any direction and at any frequency within the defined range [66]. When the appropriate mitigation techniques are applied, the limits are less strict and a maximum mean EIRP density of  $-41.3$  dBm/MHz is allowed in the 3.4 GHz - 4.8 GHz band under the condition that the duration of the sum of all transmitted signals is less than 5% of the time each second and less than

0.5% of the time each hour, and provided that the duration of each transmitted signal does not exceed 5 ms.

The ECC has proposed its own definition of the UWB technology stating that a UWB system is any radiocommunication system "involving the intentional generation and transmission of radio-frequency energy that spreads over a frequency range wider than 50 MHz" [66] as opposed to 500 MHz range according to the definition by the FCC.

## 1.2 Channel coding

In almost any wireless communication system there is a need for maintaining a certain level of reliability of transmission of information. It is often due to the requirements imposed by source encoding which may not work properly when the bit error rate is above a certain level. It is also required when the transmission takes place in harsh propagation conditions for which simple retransmission of messages proves to be insufficient. For these situations, by introducing an additional overhead to the original data messages, it is possible to cope with transmission errors.

Depending on the manner in which redundancy is added to the data messages, channel codes can be classified into two major categories, i.e., block and convolutional codes.

### 1.2.1 Block codes

There exist a vast number of different types of block codes with typical examples including Hamming codes [42], Bose Chaudhuri Hocquenghem codes (BCH codes) [12], and Reed Solomon codes (RS codes) [85]. However, the simplest block code is the repetition code.

A block encoder divides a data sequence into blocks and encodes each block independently from the others. The output sequence of the encoder of length  $n$  depends only on the current input sequence of length  $k$  and not on the previous sequences. Consequently, block encoding is a memoryless operation. The ratio  $k/n$  is called the code rate.

Optimum distance decoding (also known as maximum likelihood decoding) of a block code involves comparing the received code word with the possible code words and deciding in favor on the code word that is closest in Hamming distance to the received code word [80]. Although this method is simple in the concept, it is computationally inefficient. Examples of the most known and computationally efficient decoding methods of BCH codes (and RS codes as they belong to the BCH codes family) include the Berlekamp-Massey algorithm [9], [62], Euclidian algorithm [96], [59] and Direct solution proposed by Peterson [77].



### 1.2.2 Convolutional codes

Convolutional codes were first presented by Elias [23]. A convolutional code is produced by the encoder that maps  $k$  binary symbols onto  $n$  binary symbols, where the  $n$  output symbols are affected by a number of previous inputs or outputs, due to the presence of the memory in the encoder. In general, a memory element can be represented as a shift register that consists of  $K$  stages. The parameter  $K$  is called the constraint length of the convolutional code. A convolutional encoder is a finite state machine.

Convolutional codes were considered as very promising and to utilize their potential, proper decoding techniques had to be found. In 1961, Wozencraft and Reiffen proposed sequential decoding [106]. Improved sequential decoding algorithms were later proposed by Fano [24], Zigangirov [116], and Jelinek [49]. However, the most popular decoding technique to day is the Viterbi algorithm proposed in 1967 [101]. Optimum decoding of a convolutional code involves a search through the trellis (time representation of the state diagram) for the most probable sequence [80]. Depending on whether soft or hard decision decoding is to be performed, a Hamming or Euclidian metric in the trellis search is considered. The advantage of the Viterbi algorithm is that soft decision can be performed that enables for large coding gains for AWGN and fading channels [80].

### 1.2.3 Iteratively decodable codes

Iterative decoding dates back to 1954 when the work of Elias [22] on iterated codes was presented. Other important early contributions include works of Gallager [34] and Massey [61] in 1960.

Iterative decoding is based on application of a soft-output decoding algorithm that is performed in an iterative fashion in order to improve the error performance of a coding scheme. The goal is to maximize the a-posteriori probability of a symbol being sent given a noisy version of the coded sequence.

The iterative decoding algorithms can be divided into two categories, i.e. turbo codes and low-density parity-check (LDPC) codes.

#### Turbo codes

Turbo codes were first introduced in 1993 by Berrou, Glavieux and Thitimajshima [10]. In a later paper, Berrou gave credit to the work of J. Hagenauer and P. Hoeher on soft-output Viterbi algorithm (SOVA) [40]. Since 1993, when it was shown that they have the possibility to approach the Shannon limit, turbo codes have received a lot of attention from research community. Recently, the concept of turbo coding has been commercialized with applications present in the 3G and 3.5G mobile telephony standards.

By far the simplest parallel concatenated (turbo) code is composed of two recursive systematic convolutional encoders that are separated by an interleaver. This interleaver is a key element and should be of a large size to ensure that the component maximum a-posteriori (MAP) decoders receive independent estimates on the information symbols. The output of the encoder is multiplexed from the data input, and outputs of the component encoders. Decoding of such a code requires the use of interleavers and soft-input soft-output (SISO) MAP decoders for the component codes. It has to be pointed here that apart from parallel concatenation, there are also other configuration possible, including for instance serial concatenation.

The advantage of turbo codes is that they allow for improving the BER performance without increasing the transmitted signal power. The disadvantage lies in the increased complexity of the decoder and introduced latency. More information about turbo codes can be found in [102], [1], [2].

### **Low-density parity-check codes**

Originally proposed in 1992 by Gallager [34], LDPC codes, were for long time ignored due to the requirement for high complexity computation. In 1999, MacKay [58] shown that LDPC codes can allow for data transmission rates as close to the Shannon limit as turbo codes. Nowadays, LDPC codes are one of the hottest topics in coding theory with commercial applications in Digital Video Broadcasting (DVB) and Worldwide Interoperability for Microwave Access (WiMAX) telecommunication technologies.

LDPC codes are linear block codes defined by sparse parity-check matrices using bipartite graphs known as Tanner graphs. There are two general types of LDPC codes, namely regular and irregular. Regular LDPC codes have the same weight (number of ones) of the columns and rows of the parity check matrix. On the other hand, irregular LDPC codes have different weights in their parity check matrix. Encoding of LDPC codes comprises two tasks, i.e., construction of the sparse parity-check matrix and generation of codewords using this matrix. One of the most popular iterative decoding algorithm for LDPC codes is the iterative belief-propagation algorithm also known as Pearl's algorithm [76] and sum-product algorithm [104], [56] and [28].

Despite their large potential to achieve excellent performance on AWGN channels, little is known on performance of LDPC codes on more realistic channels. Moreover, the complexity of irregular LDPC codes that provide the best performance, poses, at present, a great challenge. Excellent work on LDPC codes is done by T. Richardson and R. Urbanke, e.g. in [87].

## 1.3 Prior research

Current literature on channel coding for UWB technology is very sparse. A most often considered coding scheme is the simplest frame repetition (FR) (also referred to as pulse repetition), whereas more sophisticated schemes include superorthogonal convolutional (SOC) coding or turbo coding. Although several papers investigate the BER performance improvement introduced by channel coding in UWB-IR systems on additive white Gaussian noise (AWGN) or simple multipath channels, the performance under realistic UWB channel conditions has not been well addressed. Moreover, in the available literature, the most often considered receiver type is a RAKE architecture which is of higher complexity than noncoherent differential autocorrelator used in this thesis.

In this section, an overview of the available literature related to channel coding and receiver architectures dedicated for UWB-IR systems is presented.

### 1.3.1 Channel coding schemes for UWB systems

#### Frame repetition

A study on random sign repetition in binary pulse position modulation (BPPM) time-hopping (TH) UWB systems is presented in [15]. The proposed scheme is a modification of TH-PPM signalling in which random sign repetition is imposed on top of originally proposed PPM. It is claimed that such a technique improves the performance of multi-user detection. To the certain extend, the sign repetition operation reflects frame repetition, although in our scenario, we deal with a differential modulation scheme. However, in [15], no inter-symbol interference nor inter-pulse interference is taken into account. Moreover, for the sake of simplicity, the effects of pulse distortion due to multipath are neglected.

A comparison of pulse repetition with a RAKE receiver vs. cyclic prefix (CP) technique applied in the frequency domain (FD) UWB detector is given in [71]. The redundancy due to the insertion of a cyclic prefix is shown as an alternative to the processing gain introduced by the pulse repetition. The investigated scenarios include 15.6 Mbit/s and 243.6 kbit/s data flows transmitted over the 802.15.3a UWB channel model. The considered modulation is PPM. The effects of ISI are taken into account. Simulation results presented in [71] indicate that the method based on CP insertion in the frequency domain detector performs better than a RAKE receiver for high data rate highly loaded UWB systems.

## Superorthogonal convolutional coding

Application of superorthogonal convolutional (SOC) coding to UWB-IR dates back to the year 2000 when Forouzan *et al.* published their paper [30]. The considered signalling was BPPM. A free space propagation channel was assumed that simplified presented derivations based on the Gaussian Approximation (GA) to model the multi-user interference. The use of superorthogonal convolutional codes was proposed due to near optimal performance and simple SOC decoder architecture. Low data rates of 5 Mbps, 312 kbps, and 19.5 kbps were considered. As shown in [30], the proposed SOC coded scheme significantly outperformed the scheme based on pulse repetitions.

In [31], a more precise analysis by the same authors is given. The UWB system setting is basically the same as in [30]. A difference is in the more precise method used to compute the probability density function (PDF) of the multi-user interference compared to the previously applied Gaussian Approximation. The results in [31], reveal that at high data rates, GA overestimates the number of users supported by the UWB system. A further extension of the considered system analysis to an unsynchronized case is presented in [29].

In all of the three papers, [30], [31], and [29], the investigations have been limited to the ideal free space propagation model, which does not correspond to the conditions in a typical indoor environment. Moreover, as a receiver, a correlator requiring a perfect template that is unfeasible in practical hardware implementations has been assumed. Furthermore, the considered modulation has been BPPM, whereas in this thesis, a simple differential autocorrelation signalling is investigated.

A UWB system employing the superorthogonal convolutional coding and pulse-shape modulation (PSM) using Hermite polynomial functions is proposed in [63]. The received signals are detected based on the output of correlators matched to all possible waveforms. The BER performance of 50 Mbps, 25 Mbps, and 12.5 Mbps data rate UWB systems is evaluated on AWGN and the IEEE 802.15.3a channel model [27]. Significant coding gains are reported when SOC coding is applied.

## Turbo coding

A combined solution for the UWB-IR system that shares the transmission bandwidth between frame repetition and turbo coding is proposed in [107]. The modulation considered is BPPM. The BER performance of UWB-IR systems with 10 active users and data rates ranging from 278 kbps up to 3.33 Mbps is evaluated in AWGN and Rayleigh fading channels. According to [107], for both types of channels and for the same data rates, it is advantageous to make the number of pulse repetitions smaller and dedicate the rest of the available bandwidth to the turbo code by lowering its code rate. An extension of the proposed method to higher data rate (up to 66.7 Mbps) UWB-IR systems based on Selective-Rake (SRake) with maximal ratio combining (MRC) receiver is proposed in [109]. Binary Phase Shift Keying

(BPSK) is considered with an SRake receiver of 10 fingers. The BER simulation results performed for CM3 scenario of the IEEE 802.15.3a multipath fading channel suggest optimal values of the number of pulse repetitions and code rate depending on the data rate.

### 1.3.2 UWB receiver architectures

There are several architectures proposed for UWB application. They can be generally classified into coherent and noncoherent architectures.

#### Coherent architectures

When there is no intersymbol interference, the optimum architecture in multipath fading channels is the RAKE receiver [79], [92], [83]. This receiver is optimum under the condition of perfect knowledge of the channel, i.e., amplitudes and delays of the multipath components. Its application is considered in the majority of the performance analyses of coded UWB-IR systems, e.g. in [35]. Such a receiver can exploit channel frequency diversity, however, it requires large number of fingers. Considering UWB channels with many multipath components, and the fact that per multipath component, there is one correlator, these pose a real implementation challenge. A RAKE receiver also requires to operate at a rate of several GSample/s which may lead to high power consumption. Simplifications of the RAKE receiver include Partial-RAKE receiver and the Selective-RAKE receiver. A difference between the two is that the former collects the energy from a given number of the first multipath components, whereas the latter collects the energy only from several strongest multipath components. Although these modifications may lead to the reduction of number of considered paths, still the complexity of a this type of receiver is prohibitive.

Time Reversal is one of the proposed RAKE techniques for UWB systems that has recently received attention by researchers [37], [72], [115]. It is based on shifting the receiver complexity to the transmitter and as such is called "Pre-RAKE". In this scheme, the reversed channel impulse response is used as a filter at the transmitter. The transmitted time-reversed signal retraces its path through the channel resulting in the auto-correlation of the channel impulse response [81]. In the time reversal scheme, a signal is pre-coded so that it may focus in time or/and in space on the particular receiver. Temporal focusing enables simple receiver architecture as the receiver power can be concentrated within a few paths, whereas spacial focusing reduces the interference to other co-existing systems [95]. In [99] and [113] it has been found that the BER performance of time reversal and traditional RAKE schemes operating on the IEEE 802.15.3a channel model is comparable.

## Noncoherent architectures

Noncoherent receivers are receivers that operate without the knowledge of the channel, which may lead to simple architectures and low power consumption. They are best suited for orthogonal signalling schemes. However, the price for these benefits is degradation of the performance due to noise enhancement introduced by their non-linear square device. Autocorrelation receivers belong to the family of noncoherent receivers, where detection is based, as the name indicates, on the autocorrelation of the received signal. Recently, autocorrelation receivers with the transmitted-reference (TR) scheme has gained a lot of attention, starting with the works of Hoor, Thomlinson [46] and Choi, Stark [16]. The idea behind the TR scheme, originally proposed in the 1960s [90], [45], is to transmit, in addition to the modulated signal, a reference signal for sounding the channel. This reference signal can be used in a correlation receiver as a template for data demodulation. In the UWB context, the TR idea boils down to transmission of two pulses, so called doublets, of which one is used as a reference, and the other conveys useful information. These pulses are separated in time with a lag enabling them to undergo the same channel distortion. The disadvantage inherent in TR receivers, i.e., the transmission of two pulses of which only one carries useful information, is omitted in autocorrelation receivers with differential modulation. We call them here differential autocorrelation receivers and they are considered in this thesis. A differential autocorrelation receiver correlates the received signal with its symbol delayed version. Such a suboptimal solution has numerous implementation advantages compared to the RAKE receivers for which the required number of fingers can be unaffordable. Among the benefits are lower synchronization requirements, no channel estimation requisites and as a result significantly lower implementation complexity. However, the main drawback of the autocorrelation receiver is the performance degradation due to employing a noise-corrupted signal as a reference in the demodulation process. Moreover, since correlation is performed on a pair of symbols, i.e., the symbol of interest and its predecessor, single delay branch differential autocorrelation modulation requires that the pulse positions for every modulation symbol must be the same. The above results in a BER performance degradation, especially if we consider a high data rate transmission in a severe multipath environment, when the mean frame time is small (e.g. a few pulse widths) and much shorter than the channel duration. Excellent work on autocorrelation receivers is done by Pausini in [74].

## 1.4 Aim and outline of the thesis

### 1.4.1 Aim of the thesis

Error control coding is an essential part of UWB systems, especially for systems operating in harsh propagation environments, e.g. non-line-of-sight indoor residential and industrial

halls, where the multipath phenomena may significantly limit the supported data rate or the link quality. In UWB systems, the requirements related to efficiency of error control coding schemes are being somewhat relaxed comparing to the narrowband systems, due to the UWB bandwidth abundance that can be dedicated to methods introducing additional overhead to the transmitted source information. However, a proper selection of suitable channel coding schemes for a UWB application proves to be difficult. Moreover, theoretical characterization of the bit error rate performance of coded UWB-IR systems based on differential autocorrelation receiver and operating on multipath fading channels has been relatively unexplored and a very challenging task. This is what constitutes the main motivation in this thesis: to assess the performance of feasible coded UWB-IR systems under a realistic channel propagation model when most of the major and important phenomena, i.e., ISI, IFI, and IPI effects, RF-front-end aspects, and antenna's characteristics, often neglected by other researchers in their works, are taken into account. (We call IFI the interference caused by pulses belonging to different UWB frames, and IPI the interference caused by pulses corresponding to the same UWB frame.) The performance evaluation studies include theoretical analyzes based on bounds on BER, including bounds based on the Poisson distribution, as well as extensive Monte-Carlo simulations. A particular focus is laid on single-user and scarcely populated multi-user scenarios.

### 1.4.2 Thesis outline

This thesis is organized as follows. Chapter 1 provides an introduction to the UWB technology, including its history, technical basics and distinctive properties that distinguish it from other wireless technologies. Moreover, a list of potential applications and a summary of current standardization developments is given. Additionally, in Chapter 1, a short introduction to channel coding and review of the channel coding schemes and receiver architectures considered for UWB systems and related to the thesis is provided.

A UWB-IR system model that is considered in this thesis is described in detail in Chapter 2. It starts with a description of a transmitter with the proposed interleaved-coding modulation and polarity randomization (ICM+PR) techniques. Four levels of operation of ICM+PR methods are distinguished, namely, information bit, code bit, UWB frame, and chip level. The particular focus is laid on frame and chip levels as they yield the greatest performance enhancements. Next, the considered channel models, i.e., AWGN channel and IEEE 802.15.3a multipath fading channel model are described in detail. The following is the consideration of different UWB pulse shapes together with a motivation for the use of the Gaussian monocycle. Next, aspects of modeling of the effects of RF-front-end and real antenna characteristics on the pulse shape are discussed. Then, details of a feasible UWB receiver architecture utilizing a single delay branch differential autocorrelator are provided. Moreover, related hardware implementation challenges are being addressed.

Chapter 3 provides a description of channel coding schemes suitable for UWB systems,

including frame repetition, bit repetition and superorthogonal convolutional coding, along with the criteria for their selection. Furthermore, selected aspects of the hardware implementation of a decoding algorithm available in the literature are reviewed.

Chapter 4 provides performance characterization of UWB-IR systems based on theoretical- and Monte-Carlo-simulation-based analyzes. The bit error rate performance of single-user coded UWB-IR systems operating on AWGN and multipath fading channels with or without the proposed interleaving techniques is studied in detail. The main research contribution here is the analysis considering ISI, IFI, and IPI effects, RF front-end and real antenna characteristics that are often neglected by the researchers. This chapter also includes performance evaluations of the proposed methods for different system parameter configurations and under different environmental conditions.

The extension of the UWB-IR system model and performance analysis considering a multi-user scenario is presented Chapter 5. The main contributions here include a novel design of a deterministic chip interleaver that is based on time-hopping hyperbolic congruence sequences. This scheme together with superorthogonal convolutional coding or frame repetition constitutes an effective method of protection against errors in scarcely populated UWB-IR systems operating in severe multipath interference prone environments. In this chapter, the bit error rate performance of UWB-IR systems operating on multipath fading channels with and without the proposed scheme is evaluated by referring to bounds based on the Poisson distribution and intensive Monte Carlo simulations. This is a novel approach considering lack of studies on the ISI, IFI, and IPI effects in coded UWB-IR systems and with the majority of the existing work on the Gaussian approximation that gives inaccurate and overoptimistic BER results. The presented results indicate that a deterministic interleaver based on hyperbolic congruence sequences may perform similarly to the random interleavers with the advantage of simple implementation.

Chapter 6 presents the study of application of UWB-IR technology in body area networks (BANs). It starts with an introduction to the BAN concept. Next, a description of several considered scenarios, system and body area radio propagation channel models is given. Performance of BANs based on UWB-IR technology is evaluated by Monte-Carlo simulations.

Finally, a summary of original contributions and directions for future research is presented in Chapter 7.

### 1.4.3 Framework

This work was supported by the Dutch Min. Econ. Affairs/Min. Education within the confines of the Freeband Airlink (Ad-hoc Impulse Radio: Local Instantaneous Networks) project. Airlink was a national research project carried out at the Delft University of Technology and with the consortium including TNO and industry partners. The aim of the



---

project was to investigate the potential of the UWB-IR technology for high data rate wireless communications.



# Chapter 2

## UWB-IR system model

In this chapter, a detailed UWB-IR single-user system model description used throughout the thesis is given. A novel interleaved coding-modulation with polarity randomization scheme is proposed. This scheme together with superorthogonal convolutional coding or frame repetition constitutes an effective method of protection against errors for UWB-IR systems operating in severe multipath interference prone environments.

This chapter is organized as follows. Section 2.1 presents a single-user UWB-IR system model architecture. Principles of the ICM-PR technique, pulse shape, antenna characteristics and modulation format are provided. Moreover, channel models on which the considered UWB-IR systems are evaluated in Chapter 4, namely AWGN and IEEE 802.15.3a model are given in detail. Finally, Section 2.3 summarizes this chapter.

### 2.1 System model

In this section, a single-user UWB-IR system model is presented. The transmitter and receiver architecture is discussed in detail. Moreover, characteristics of the UWB multipath radio channel model and pulse shape are given.

#### 2.1.1 Principle of ICM+PR – UWB-IR transmitter

The proposed interleaved coding-modulation with polarity randomization method exploits the temporal diversity brought by the UWB channels through multipaths and as a result allows for the alleviation of destructive effects of inter-symbol and inter-pulse interfer-

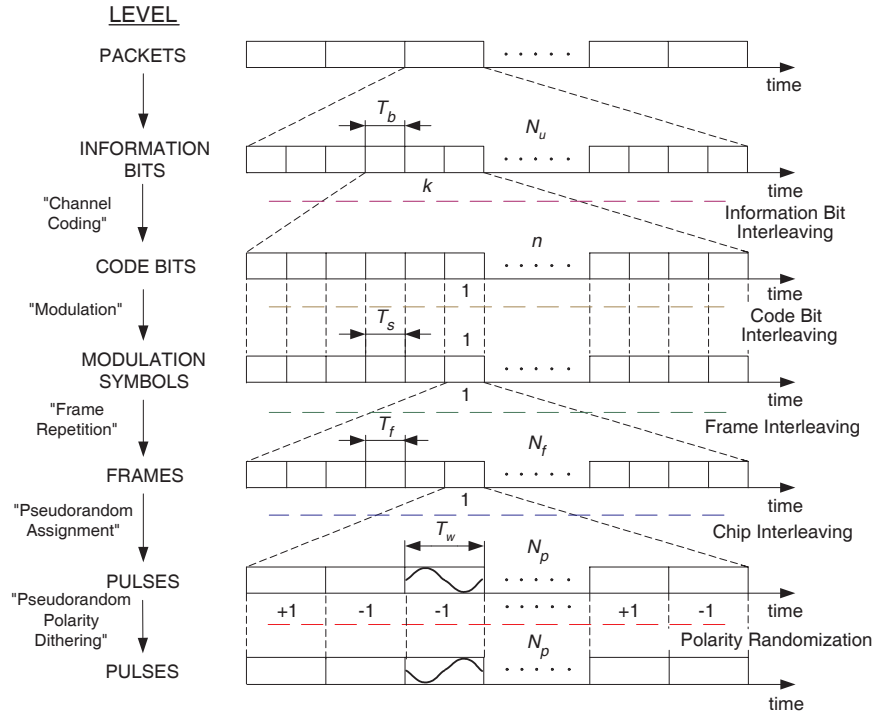


Figure 2.1. Interleaved coding-modulation scheme with polarity randomization in a UWB-IR system.

ence. As it will be shown in Chapter 4, rearranging the order of UWB chips or UWB frames results in a bit error rate performance improvement.

The concept of interleaved coding-modulation with polarity randomization for the UWB-IR transmitter is shown in Fig. 2.1. There are several signal processing steps that include channel coding, modulation, frame repetition, pseudorandom assignment and pseudorandom polarity dithering that will be described in detail below. Although the description provided here is general and valid for any channel coding scheme and modulation format, what will be considered in the following chapters are superorthogonal convolutional coding and frame and bit repetition combined with differential autocorrelation modulation. These coding schemes are described in Chapter 3. As it will be presented in detail below, a differential autocorrelation modulation format considered in this thesis involves transmission of information in relative polarity between modulation symbols that are later represented by pulses. Logical "0" means repeating the polarity of a preceding modulation symbol, whereas logical "1" results in reverting the polarity in comparison to the preceding modulation symbol. Polarity randomization implies changing the polarity of every pulse in a sequence of pulses according to the known at the receiver pseudorandom sequence. Regarding interleaving, we distinguish four levels on which interleaving may be applied, namely, the information bit, code bit, frame, and chip level. The notation used to describe the interleaving operation is summarized in Table 2.1. According to the level of interleaving, a sequence  $\mathbf{x}$  of information

Table 2.1. Interleaving Notation.

Level	Name	Size
Information Bits	$\Pi_u$	$L_u$
Code Bits	$\Pi_d$	$L_d$
Frames	$\Pi_f$	$L_f$
Chips	$\Pi_p$	$L_p$

bits, code bits, frames or chips is interleaved using a mapping  $\Pi : x \rightarrow \Pi(x)$  such that

$$\bigcup_{i=0}^{L_j-1} \{\Pi(i)\} = \bigcup_{i=0}^{L_j-1} \{i\}, \quad (2.1)$$

where  $L_j$  denotes the size of the corresponding interleaver and  $j \in \{u, d, f, p\}$ . For a special case, when  $L_j = 1$ , there is no interleaving.

In this section, we describe how the generation of the transmitted signal waveform is performed when interleaving might be applied on every level. However, in the following sections, we focus on frame and chip interleaving only since they yield the best performance enhancement.

A sequence of  $N_u$  information bits  $\mathbf{u} = (u_0, u_1, \dots, u_{N_u-1})$ , each of a duration of  $T_b$ , might be interleaved by  $\Pi_u : x \rightarrow \Pi_u(x)$ . In general, a sequence  $\Pi_u(\mathbf{x})$  is obtained by partitioning sequence  $\mathbf{x}$  into subsequences of length  $L_u$  and applying  $\Pi_u$  on every subsequence. As a result of applying  $\Pi_u$  on the sequence  $\mathbf{u}$ , a sequence of interleaved information bits  $\mathbf{u}' = \Pi_u(\mathbf{u}) = (u'_0, u'_1, \dots, u'_{N_u-1})$  is obtained. The following operation is encoding that is performed according to the selected encoding function  $\varphi$  resulting in a code bit sequence  $\mathbf{d} = \varphi(\mathbf{u}') = (d_0, d_1, \dots, d_{N_d-1})$ , where  $N_d$  denotes the number of code bits in a packet and can be calculated as  $N_d = \frac{n}{k} N_u$ . A bijection  $\varphi$  transforms a block of  $k$  bits into a block of  $n$  bits. In general,  $\varphi(\mathbf{x})$  is a sequence obtained by partitioning sequence  $\mathbf{x}$  into subsequences of length  $k$  and applying  $\varphi$  on every subsequence. For a special case, when  $k = n (= 1)$ ,  $\varphi(\mathbf{x}) = \mathbf{x}$  and hence there is no channel coding. Code bits  $d_i$  may then be interleaved according to the mapping  $\Pi_d : x \rightarrow \Pi_d(x)$ . A sequence of interleaved code bits  $\Pi_d(\mathbf{d}) = (d'_0, d'_1, \dots, d'_{N_d-1})$  is obtained by partitioning sequence  $\mathbf{d}$  into subsequences of length  $L_d$  and applying  $\Pi_d$  on every subsequence. Next, a differential autocorrelation modulation is performed, i.e.,  $b_i = b_{i-1}(1 - 2d'_i)$ ,  $\forall 0 \leq i \leq N_d - 1$  resulting in a sequence of modulated symbols  $\mathbf{b} = (b_0, b_1, \dots, b_{N_d-1})$ , with the duration of each symbol equal to  $T_s$ . The considered modulation is of order one.

Next, for all values of  $i \in \{0, 1, \dots, N_d-1\}$ , a repetition  $\mathbf{f}_i = (f_{i,0}, f_{i,1}, \dots, f_{i,N_f-1})$ , with  $f_{i,j} = b_i$ ,  $\forall j$  is performed, resulting in a frame sequence  $\mathbf{f} = (\mathbf{f}_0, \mathbf{f}_1, \dots, \mathbf{f}_{N_d-1}) = (f_0, f_1, \dots, f_{N_d N_f-1})$ , where the number of frames representing one code bit is denoted by  $N_f$  and the frame duration is  $T_f$ . The following step may be frame interleaving  $\Pi_f : x \rightarrow \Pi_f(x)$ . As a result of

applying frame interleaving  $\Pi_f$ , a sequence of interleaved frames  $\Pi_f(\mathbf{f}) = (f'_0, f'_1, \dots, f'_{N_d N_f - 1})$  is obtained. Next operation is pseudorandom chip assignment  $s_{i,j,m} = f'_{i N_f + j} \delta_{m,c_j}$ ,  $\forall 0 \leq i \leq N_d - 1$ ,  $\forall 0 \leq j \leq N_f - 1$ , and  $\forall 0 \leq m \leq N_p - 1$ , where  $\delta_{i,j} = 1$  if  $i = j$ , and  $\delta_{i,j} = 0$  if  $i \neq j$ . The pseudorandom assignment code is defined as  $\mathbf{c} = (c_0, c_1, \dots, c_{N_f - 1})$  with values  $c_i \in \{0, 1, \dots, N_p - 1\}$ ,  $\forall i$ , where the number of chips in a frame is denoted by  $N_p$ . The resulting chip sequence is

$$\begin{aligned} \mathbf{s} &= (s_{0,0,0}, s_{0,0,1}, \dots, s_{0,0,N_p-1}, s_{0,1,0}, s_{0,1,1}, \dots, s_{N_d-1,N_f-1,N_p-1}) \\ &= (s_0, s_1, \dots, s_{N-1}), \end{aligned} \quad (2.2)$$

where  $N$  is the total number of chips in a data packet and can be calculated as  $N = N_d N_f N_p$ . The following step may be chip interleaving  $\Pi_p : x \rightarrow \Pi_p(x)$ .  $\Pi_p$  is applied on the sequence  $\mathbf{s}$  yielding a sequence of interleaved chips  $\Pi_p(\mathbf{s}) = (s'_0, s'_1, \dots, s'_{N-1})$ . Next, polarity randomization  $\mathbf{p} = (p_0, p_1, \dots, p_{N-1})$  with  $p_i$  being a uniformly distributed discrete random variable  $p_i \in \{-1, 1\}$ ,  $\forall i$ , may be applied. For the non-polarity case,  $p_i = 1$ ,  $\forall i$ . The resulting sequence is  $\mathbf{v} = (p_0 s'_0, p_1 s'_1, \dots, p_{N-1} s'_{N-1}) = (v_0, v_1, \dots, v_{N-1})$ . The transmitted signal waveform for one data packet is thus given by

$$s_{tr}(t) = \sum_{i=0}^{N-1} v_i w(t - iT_w), \quad (2.3)$$

where  $w(t)$  denotes the transmitted pulse of duration  $T_w$ .

### 2.1.2 Channel models

A realistic channel model, which captures the important characteristics of the radio communication medium, is a vital prerequisite for system design. It is desirable that the channel model should be simple and yet reflective of actual channel measurements. For more than 50 years, the wireless propagation channels have been thoroughly investigated and currently there are numerous channel models available for the narrowband communication systems. However, there are distinct differences between UWB and narrowband wireless channels, especially with respect to fading statistics and time of arrivals of multipath components. The most common is the assumption of flat fading which is used when the signal bandwidth is small enough that the delays of the individual multipath components do not impact the system performance. However, when the signal bandwidth becomes larger, the different delays of multipath components may influence the system performance. For a wideband signal of bandwidth that is larger than the coherence bandwidth of the channel, the channel becomes frequency-selective. If there is interference between the multipath components that fall within each delay bin, the amplitude statistics of the delay bins can be modeled as Rayleigh or Rice. For UWB systems characterized by extremely large bandwidth, only few or even no multipath components fall or/and overlap in each resolvable delay bin, and as a result the central limit theorem is no longer applicable in predicting the fading statistics.

The IEEE 802.15.3a Task Group has evaluated a number of popular indoor channel models to determine which model best fits the channel characteristics obtained from realistic UWB channel measurements. In particular, the channel measurements showed that multipath components arrive in clusters rather than in a continuum. The UWB channel measurements also indicated that the fading amplitudes follow a lognormal distribution.

In this thesis, for the case of simulations, two particular types of channel models are considered, namely additive white Gaussian noise (AWGN) channel and the IEEE 802.15.3a multipath fading channel. The AWGN channel is simple and often used as a reference. The IEEE 802.15.3a multipath fading channel is based on real channel measurements and is used for closer-to-reality evaluation of the performance of UWB-IR systems. In Chapter 4, we refer to bounds on the BER performance of UWB-IR systems operating on uncorrelated multipath fading channels. Channels, like for instance, the IEEE 802.15.3a channel, can be considered as uncorrelated when the memory that results in packet errors during the transmission is removed. In this way there is no correlation between the faders in every UWB frame (compare with [114]). One way to accomplish this may be application of the proposed ICM techniques.

### AWGN channel model

We assume that the channel through which the signal is transmitted corrupts the signal by addition of noise, denoted as  $n(t)$  that is a sample function of a white Gaussian process with the power spectral density (power spectrum) equal to  $N_0/2$  (W/Hz). Such a channel is called an additive white Gaussian noise (AWGN) channel [80].

### IEEE 802.15.3a channel model

We consider the IEEE 802.15.3a UWB channel model which is a modified Saleh-Velenzuela (S-V) model taking into account the clustering phenomena observed in several UWB channel measurements [57]. The channel impulse response is given by [27]

$$h(t) = X \sum_{l=1}^L \sum_{m=1}^M \alpha_{m,l} \delta(t - T_l - \tau_{m,l}), \quad (2.4)$$

where  $L$  is the number of clusters,  $M$  is the number of paths within a cluster, and  $\alpha_{m,l}$  is the multipath gain coefficient of the  $m$ -th path corresponding to the  $l$ -th cluster.  $T_l$  is the delay of the  $l$ -th cluster and  $\tau_{m,l}$  is the delay of the  $m$ -th path relative to the  $l$ -th cluster arrival time  $T_l$ . The multipath channel coefficients are defined as  $\alpha_{m,l} = p_{m,l} \xi_l \beta_{m,l}$ , where  $p_{m,l}$  denotes the sign of the coefficient and takes values  $\pm 1$  with equal probability to account for signal inversions due to reflections, and  $\beta_{m,l}$  corresponds to the fading associated with the  $m$ -th ray of the  $l$ -th cluster and satisfies

Table 2.2. IEEE UWB Channel Model Parameters.

Model Parameter	CM1	CM2	CM3	CM4	Unit
(Non-)line-of-sight	LOS	NLOS	NLOS	NLOS	n/a
Tx-Rx Separation	0-4	0-4	4-10		m
$\Lambda$	0.0233	0.4	0.0667	0.0667	(ns) <sup>-1</sup>
$\lambda$	2.5	0.5	2.1	2.1	(ns) <sup>-1</sup>
$\Gamma$	7.1	5.5	14	24	n/a
$\gamma$	4.3	6.7	7.9	12	n/a
$\sigma_1$	3.3941	3.3941	3.3941	3.3941	dB
$\sigma_2$	3.3941	3.3941	3.3941	3.3941	dB

$$20 \log(\xi_l \beta_{m,l}) \propto \text{Normal}(\mu_{m,l}, \sigma_1^2 + \sigma_2^2),$$

$$\text{or } |\xi_l \beta_{m,l}| = 10^{(\mu_{m,l} + n_1 + n_2)/20},$$

where  $n_1 \propto \text{Normal}(0, \sigma_1^2)$  and  $n_2 \propto \text{Normal}(0, \sigma_2^2)$  are independent and correspond to the fading on each cluster and ray, respectively. Fading associated with the  $l$ -th cluster is represented by  $\xi_l$ . One can write

$$E[|\xi_l \beta_{m,l}|^2] = \Omega_0 \exp(-T_l/\Gamma) \exp(-\tau_{m,l}/\gamma), \quad (2.5)$$

where  $\Omega_0$  is the mean energy of the first path of the first cluster.  $\Gamma$  and  $\gamma$  are the cluster and ray decay factors, respectively. The  $\mu_{m,l}$  is given by

$$\mu_{m,l} = \frac{10 \ln(\Omega_0) - 10T_l/\Gamma - 10\tau_{m,l}/\gamma - (\sigma_1^2 + \sigma_2^2) \ln(10)}{\ln(10)}. \quad (2.6)$$

The inter-arrival times of clusters and rays follow Poisson distributions

$$p(T_l|T_{l-1}) = \Lambda \exp[-\Lambda(T_l - T_{l-1})], \quad l > 0, \quad (2.7)$$

$$p(\tau_{m,l}|\tau_{(m-1),l}) = \lambda \exp[-\lambda(\tau_{m,l} - \tau_{(m-1),l})], \quad m > 0, \quad (2.8)$$

where  $\Lambda$  is the cluster arrival rate, and  $\lambda$  is the ray arrival rate. Total received local-mean multipath energy fluctuations about a certain area-mean energy due to the blockage of the line-of-sight path, known as shadowing, can be modeled by the lognormal term  $X$ , where  $20 \log(X) \propto \text{Normal}(0, \sigma_x^2)$ . Here, however, we do not model shadowing, focusing mainly on the multipath phenomena, i.e., local-mean energy effects, thus  $X = 1$ . As in [27], we also use the terms ray, path, and multipath component interchangeably.

For most of the simulations, we consider two out of four different propagation scenarios covering indoor residential environments as proposed in [27], namely line-of-sight CM1 and



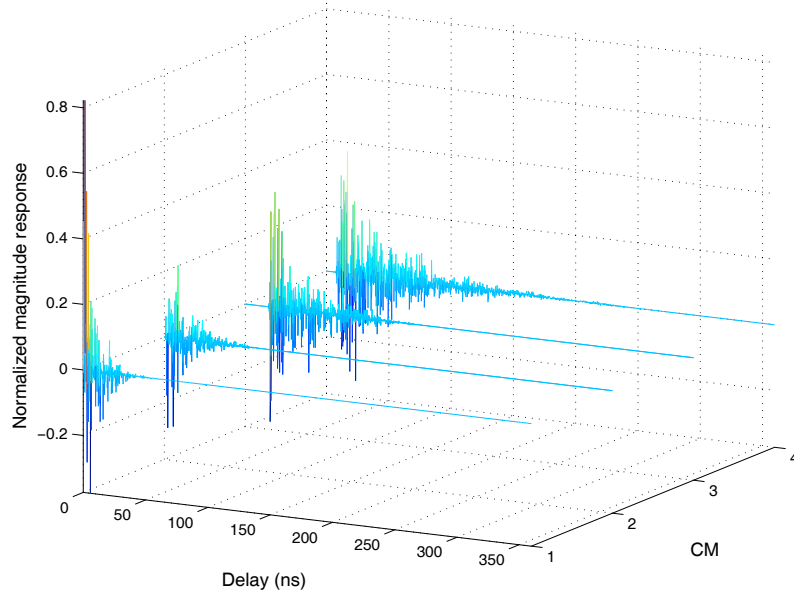


Figure 2.2. Snapshots of channel impulse responses for CM1-CM4.

non-line-of-sight CM3. Information on the definitions of the channel statistics and their influence on the BER of UWB-IR systems, is provided in Section 4.2.4, Chapter 4.

Fig. 2.2 presents channel impulse responses in the CM1-CM4 scenarios. We notice longer channel duration and higher number of multipath components in non-line-of-sight scenarios comparing to the line-of-sight scenario. Moreover, with the increase of distance between the transmitter and the receiver, the channel becomes sparse, i.e., not every resolvable delay tap carries significant energy.

Fig. 2.3 provides motivation for the use of a differential autocorrelation receiver instead of a RAKE receiver in the UWB-IR system. Our results indicate that more than 20 RAKE fingers are required to capture 60% of the energy in the NLOS scenario CM3 with TX-RX distance larger than 4 m. The high number of paths that needs to be resolved results in increased computational complexity of the receiver. Note that since the IEEE 802.15.3a UWB channel model is a double exponential model, it can happen that some of the subsequent multipath arrivals may carry more energy than the earlier ones. Taking this into account, in Fig. 2.3, the multipath components are sorted out in ascending order of their energy.

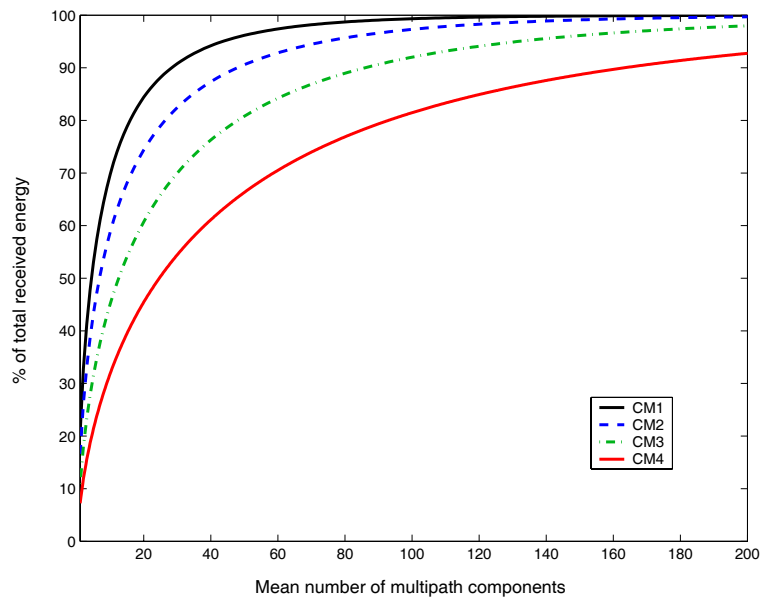


Figure 2.3. The mean number of significant multipath components required to capture a given amount of energy for CM1-CM4. Multipath components are sorted out in ascending order of their energy.

### 2.1.3 Pulse shape

Ultra-wideband Impulse Radio is based on transmission of very short pulses of the length of a fraction of a nanosecond. For such short pulses the energy is spread over frequency bandwidth of several GHz. Various waveforms with complex mathematical formats have been proposed including Gaussian monocycle [19], second derivative of the Gaussian pulse [105], [19] and Hermite pulses [69].

A fundamental characteristic of a UWB-IR monopulse signal is that it must not have a DC content to allow it to radiate effectively [19]. It is also important that the pulse frequency spectrum satisfies a mask imposed by the FCC on the power emission levels [FCC], especially for frequencies below 2 GHz where the Global Positioning Systems (GPS), mobile telephony and military systems operate. For this reason, Manchester, Return-to-zero (RZ) Manchester, and rectangle monocycles, although proposed in [14], are discarded. In our UWB-IR system, we model the transmitted pulse as a distorted Gaussian monocycle.

The Gaussian pulse has its mathematical definition similar to the Gauss function given by

$$x(t) = \frac{1}{\sqrt{2\pi\sigma'}} e^{-\left(\frac{t-\mu}{2\sigma'}\right)^2}, \quad (2.9)$$

where  $\mu$  and  $\sigma'^2$  denote the mean and variance, respectively. Knowing that an  $1/\sqrt{2\pi}\sigma'$  term represents the pulse amplitude and that for UWB-IR applications the mean  $\mu = 0$ , the Gaussian pulse has the form

$$\tilde{x}(t) = Ae^{-\left(\frac{t}{\sigma}\right)^2}, \quad (2.10)$$

where  $A$  is the pulse amplitude and  $\sigma$  is the time-scaling parameter also referred to as the pulse temporal width. The Fourier transform of the Gaussian pulse is

$$\tilde{X}(f) = \mathcal{F}[\tilde{x}(t)] = \int_{-\infty}^{+\infty} \tilde{x}(t) e^{-j2\pi ft} dt = \sqrt{\pi}\sigma A e^{-(\pi\sigma f)^2}. \quad (2.11)$$

The Gaussian monocycle is the first derivative of a Gaussian pulse and can be expressed as

$$w(t) = \frac{d}{dt}(\tilde{x}(t)) = \frac{2At}{\sigma^2} e^{-\left(\frac{t}{\sigma}\right)^2}. \quad (2.12)$$

Based on a differentiation property of the Fourier transform

$$\mathcal{F}\left[\frac{d^n}{dt^n} \tilde{x}(t)\right] = (j2\pi f)^n X(f), \quad (2.13)$$

the Fourier transform of the Gaussian monocycle can be found as

$$\Omega_1(f) = j2\pi f \sqrt{\pi}\sigma A e^{-(\pi\sigma f)^2}. \quad (2.14)$$

The energy spectrum of the Gaussian monocycle is

$$|\Omega_1(f)|^2 = 4\pi^3 f^2 \sigma^2 A^2 e^{-2(\pi\sigma f)^2}. \quad (2.15)$$

Fig. 2.4 shows the Gaussian monocycles in time and frequency domains with their normalized energy spectra for different values of the time-scaling parameter  $\sigma$ . The practical advantage of the Gaussian monocycle over the Gaussian pulse, is that it does not contain a DC component, allowing for simplified transmitter architecture. Gaussian monocycles have single zero crossing and increasing central frequency with the decrease of  $\sigma$  value. For our system model,  $\sigma = 0.037$  ns and the center frequency equals circa 6 GHz. This results in the pulse duration of 0.167 ns. When the value of  $\sigma$  is fixed, by taking the further derivatives of the Gaussian pulse i.e., second, third, etc., the value of the center frequency increases and the fractional bandwidth decreases. Moreover, further derivatives have more zero crossings.

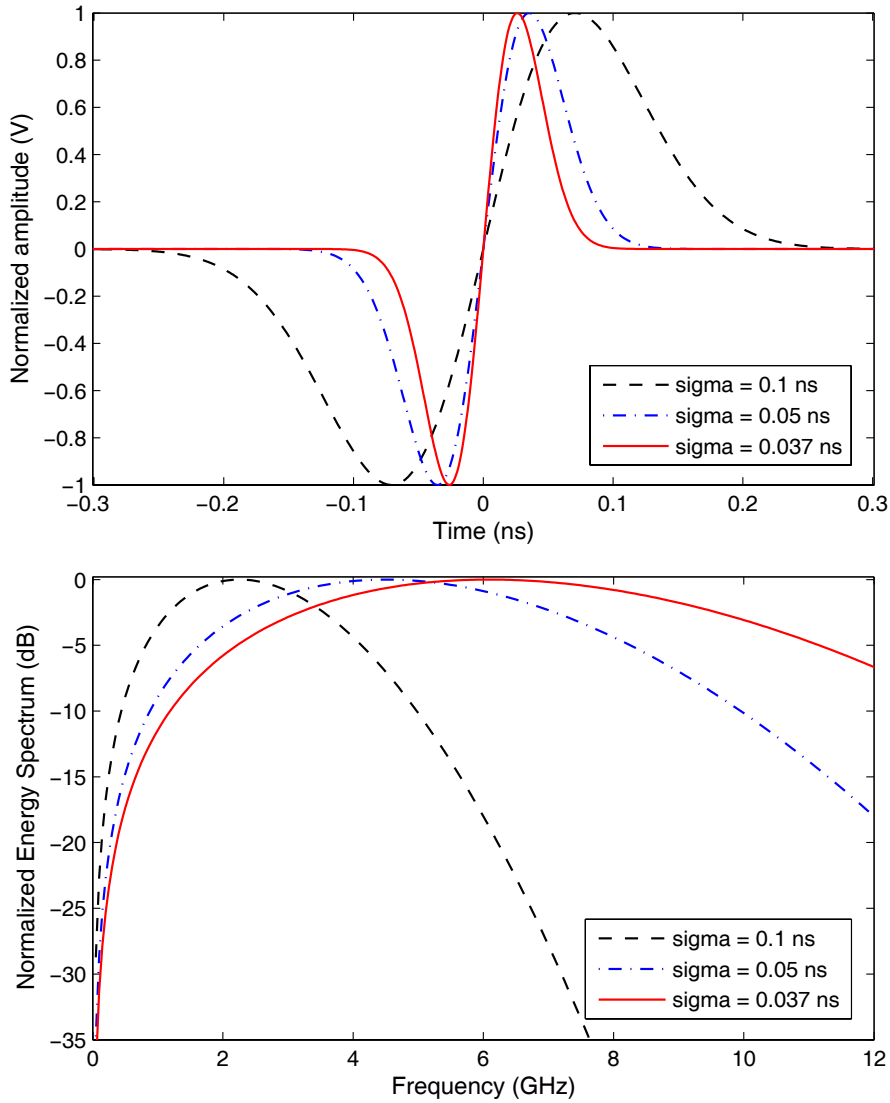


Figure 2.4. The Gaussian monocycle in time and frequency domains for different values of the time-scaling parameter  $\sigma$ . In our system model  $\sigma = 0.037$  ns.

In order to characterize the UWB-IR system as accurate as possible, we model distortions introduced by the bandpass filter and amplifier by a third-order passband Chebyshev filter with the cutoff frequencies  $f_1 = 2$  GHz and  $f_2 = 8$  GHz, on which the magnitude response of the filter equals -0.2 dB. The choice for this type of an infinite impulse response filter (also known as a recursive filter) is mainly due to the possibility of modeling the ripple in the passband which is commonly present in type I Chebyshev filters. This type of filters is also characterized by the fast roll-off in the frequency domain. The cutoff frequencies refer to the IEEE 802.15.3a UWB channel model considered in this thesis which is based on measurements in the 2-8 GHz band. The transfer function of the filter,  $G_2(f)$ , is found by numerical methods using Matlab since polynomials greater than the second order, here - the third, cannot generally be factored using algebra.

The general formula for the transfer function of a filter in the  $s$ -domain,  $s = \sigma \pm j\omega$ ,  $\omega = 2\pi f$  is

$$H(s) = \frac{B(s)}{A(s)} = \frac{b(1)s^n + b(2)s^{n-1} + \dots + b(n+1)}{s^n + a(2)s^{n-1} + \dots + a(n+1)}. \quad (2.16)$$

For our filter, (2.16) has the following form

$$H(s) = \frac{0.00056977s^6 - 0.0017093s^4 + 0.0017093s^2 - 0.00056977}{s^6 - 5.6774s^5 + 13.485s^4 - 17.153s^3 + 12.326s^2 - 4.7439s + 0.76405}. \quad (2.17)$$

The transfer function of this filter in the frequency domain, (also known as the magnitude spectrum or frequency response),  $G_2(f)$ , may be found by setting  $\sigma = 0$ , i.e.

$$G_2(f) = H(s)|_{s=j\omega}. \quad (2.18)$$

The magnitude and phase spectra of the modeled Chebyshev filter are presented in Fig. 2.5. We observe the non-linear phase which translates to the non-symmetrical impulse response of the filter and also left and right edges of the signal being different. This is generally a disadvantage of the Chebyshev filters but for the purpose of modeling distortions in a communication system we exploit this property.

#### 2.1.4 Antenna characteristics

We take into account the effects of the transmitter and receiver biconical antennas on the pulse shape by employing the actual measured frequency response collected in [47]. This is a more accurate way of modeling of the influence of the antennas than just a simple differentiator, what can be found in the UWB literature [41].

The main antenna parameter determining the influence on the pulse shape is its transfer function,  $G_1(f)$ , which is shown in Fig. 2.6. The resulting transfer function of the receiver's front-end including the antenna is given by  $G(f) = G_1(f)G_2(f)$ . The transfer function and the impulse response of the transceiver's front-end are mutually related, i.e.,  $G(f) = \mathcal{F}(g(t))$ , where  $\mathcal{F}(x)$  denotes the Fourier transform.

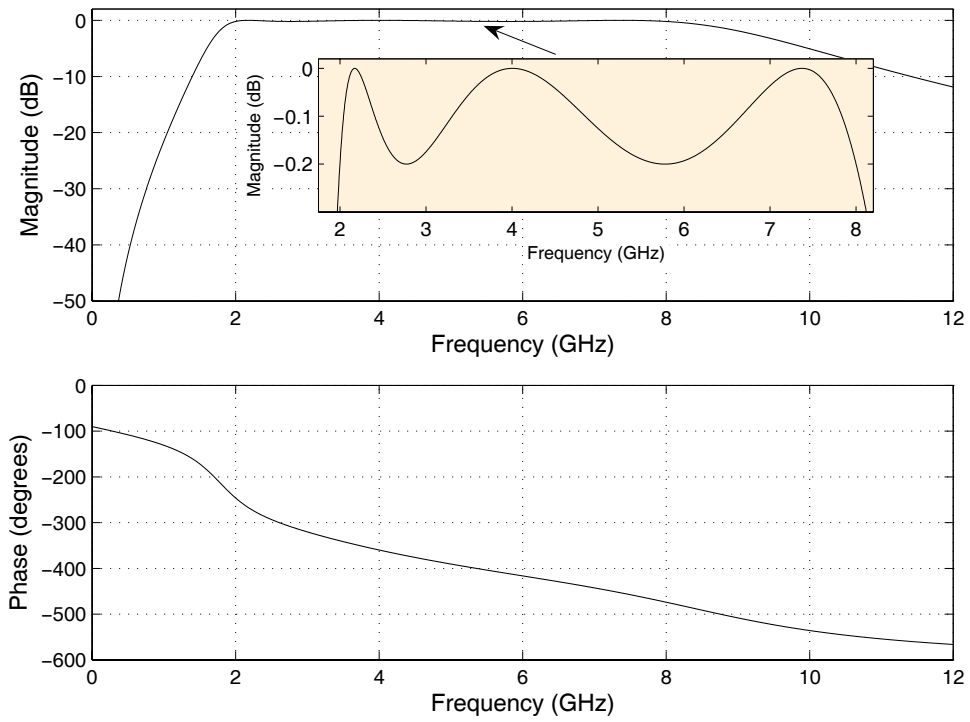


Figure 2.5. The magnitude and phase spectra of the modeled Chebyshev filter.

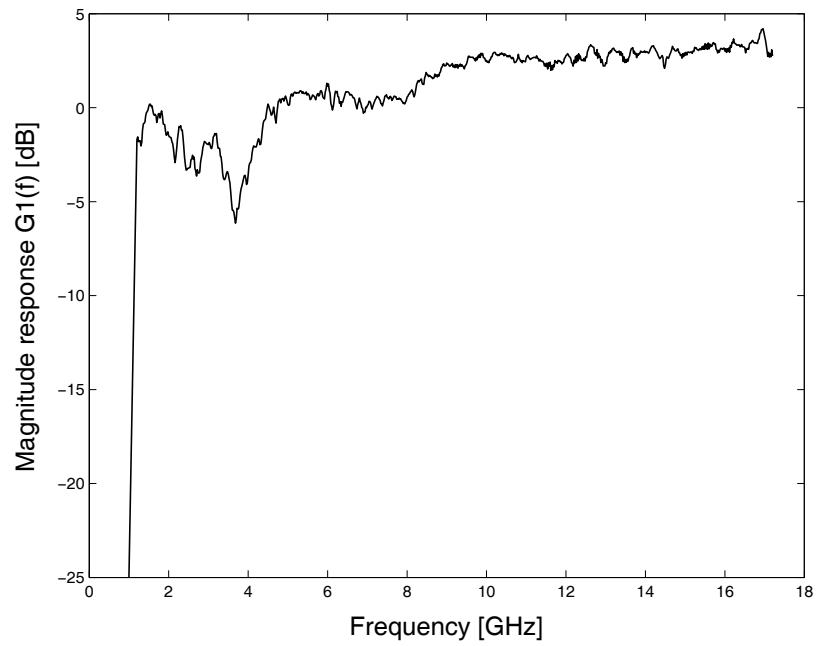


Figure 2.6. The antenna transfer function obtained from measurements [47].

The original and modeled received pulses are depicted in Fig. 2.7.

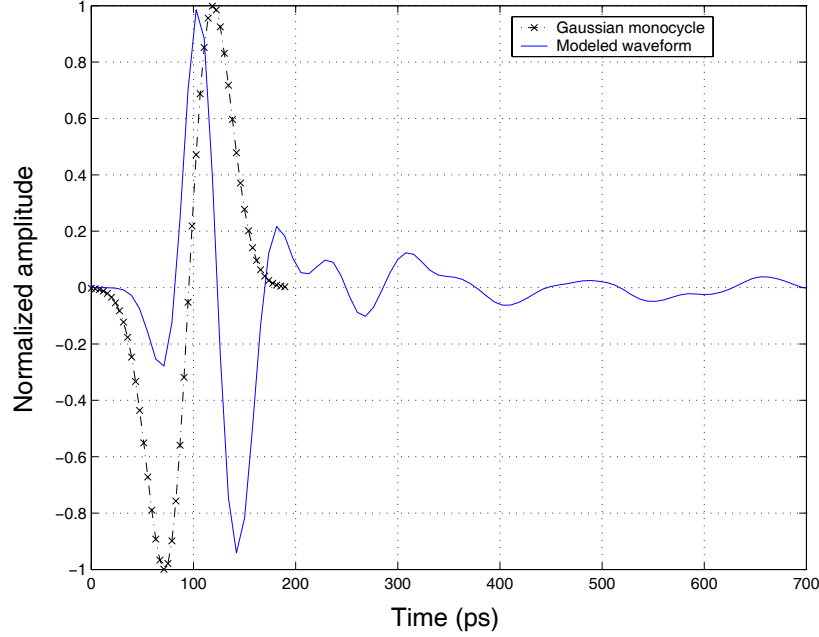


Figure 2.7. The Gaussian monocycle and the modeled received waveform.

### 2.1.5 Principle of ICM+PR – UWB-IR receiver

The structure of a UWB-IR receiver is presented in Fig. 2.8. The received signal waveform  $r(t)$ , after passing through an antenna and amplifier, can be expressed mathematically as

$$r''(t) = s_{tr}(t) * g(t) * h(t) + n(t), \quad (2.19)$$

where  $g(t)$  is the impulse response of the transceiver's front-end,  $h(t)$  is the channel impulse response,  $n(t)$  is zero mean additive white Gaussian noise, and  $*$  denotes convolution. The received sequence for one data packet may be expressed as  $\mathbf{r}'' = (r''_0, r''_1, \dots, r''_{N-1})$ , where  $r''_i$  is the waveform  $r''(t)$  on the interval  $[iT_w, (i+1)T_w]$ . The first operation upon receiving the signal is pulse-based polarity derandomization. The elements of the sequence of pseudorandom values  $\mathbf{p}$  are multiplied by the elements of  $\mathbf{r}''$  resulting in a sequence  $\boldsymbol{\theta}' = (p_0 r''_0, p_1 r''_1, \dots, p_{N-1} r''_{N-1}) = (\theta'_0, \theta'_1, \dots, \theta'_{N-1})$ . Next, chip deinterleaving  $\Pi_p^{-1}(\boldsymbol{\theta}')$  might be applied yielding a sequence  $\boldsymbol{\theta} = (\theta_0, \theta_1, \dots, \theta_{N-1})$ . The following operation might be frame deinterleaving  $\Pi_f^{-1}(\boldsymbol{\theta})$ . The resulting frame sequence  $\mathbf{z} = (z_0, z_1, \dots, z_{N-1})$  is fed to the demodulator that correlates the signal with its symbol-delayed version as

$$\hat{y}'_i = \int_{iT_s}^{iT_s+T_s} \tilde{z}(t) \tilde{z}(t - T_s) dt, \quad (2.20)$$

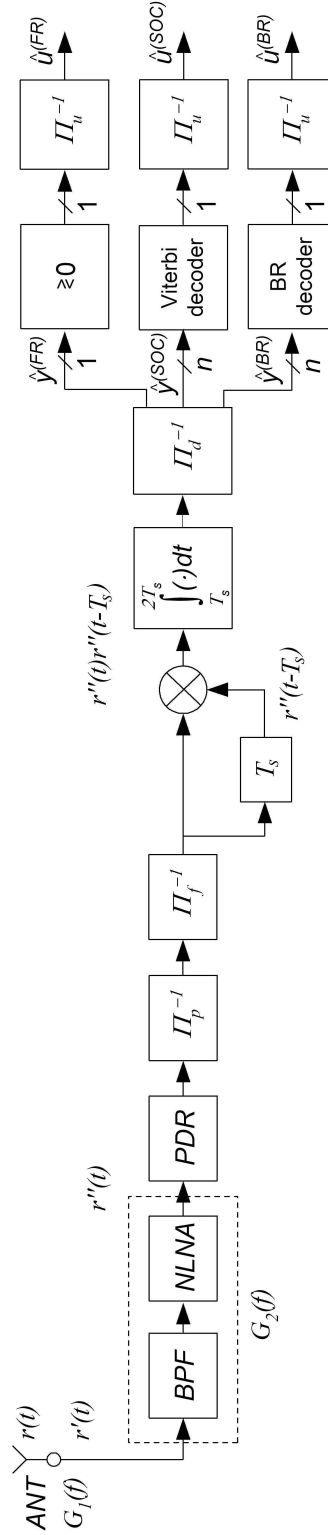


Figure 2.8. Diagram showing the modeled UWB-IR receiver architecture and considered in a single-user scenario. The acronyms BPF, NLNA, and PDR, stand for a bandpass filter, non-linear low noise amplifier, and pulse polarity derandomizer, respectively.



where  $i$  is the symbol index and  $\tilde{z}$  is a subsequence of  $\mathbf{z}$  with length  $N_f N_p$  corresponding to one symbol of duration  $T_s$ . In our system setup, for the case of FR, a resulting sequence of real values, written as  $\hat{\mathbf{y}}' = (\hat{y}'_0, \hat{y}'_1, \dots, \hat{y}'_{N_d-1})$ , might be deinterleaved according to the demapping  $\Pi_d^{-1}(\hat{\mathbf{y}}')$ . Next, the resulting sequence  $\hat{\mathbf{y}} = \Pi_d(\hat{\mathbf{y}}') = (\hat{y}_0, \hat{y}_1, \dots, \hat{y}_{N_d-1})$ , is passed through a threshold detector yielding a sequence of binary values  $\hat{\mathbf{y}}_b = [-\mathbf{1} \cdot \hat{\mathbf{y}}]$ , where  $[x]$  is equal to 1 for  $x > 0$  or 0 for  $x \leq 0$ . For the case of SOC coding, the sequence of real values  $\hat{\mathbf{y}}$  might be deinterleaved according to the demapping  $\Pi_d^{-1}(\hat{\mathbf{y}}')$  and then fed to the soft-input Viterbi decoder. In general, the sequence  $\hat{\mathbf{y}}_b$  is decoded with a decoding function  $\psi(\hat{\mathbf{y}}_b)$  yielding a decoded bit sequence  $\hat{\mathbf{u}}' = (\hat{u}'_0, \hat{u}'_1, \dots, \hat{u}'_{N_u-1})$ . The following operation might be bit deinterleaving applied for FR and SOC coding according to the demapping  $\Pi_u^{-1}(\hat{\mathbf{u}}')$  and resulting in a sequence of deinterleaved decoded bits  $\hat{\mathbf{u}} = (\hat{u}_0, \hat{u}_1, \dots, \hat{u}_{N_u-1})$ .

## 2.2 Hardware implementation issues

### 2.2.1 General issues

Although the UWB technology is a very promising solution for short range wireless communications and ranging, it has many implementation challenges that stop it from the wide presence in a commercial market of today. One of them is the requirement for high sampling rate of order of several tens or hundreds of Gsamples for pulses of sub-nanosecond duration. Presently, only the most advanced Field Programmable Gate Arrays (FPGAs) and Application Specific Integrated Circuits (ASICs) are capable of handling such sampling rates. This is also why researchers and designers focus currently on non-coherent autocorrelation or transmitted-reference receiver architectures that, due to the integration time of the order of several nanoseconds, do not require such high sampling rates. Another challenge is the so-called analog input bandwidth limitation present in the Analog-to-Digital Converters (ADCs). Regardless of the sampling clock frequency, the analog input bandwidth represents the bandwidth of the signal that will be converted into the digital format. The analog input bandwidth of most of the mass produced ADC converters produced today is less than one GHz. It is clear, that for the frequency range as standardized by the FCC in the USA, i.e. 3.1 GHz - 10.6 GHz, the analog input bandwidth of 1 GHz is far too insufficient. Moreover, the use of highly integrated ADCs in FPGA or DSP are somehow contradicting the promise of having a low complexity and low cost UWB transceiver. Ensuring establishment and maintenance of highly accurate synchronization between the UWB-IR devices poses another challenge. Most of UWB receiver techniques today require highly accurate synchronization and stable oscillators to ensure precise timing of the pulse and/or precision positioning. Another difficulty lies in the pulse distortion caused by antennas. In a real UWB-IR communication system, the shapes of transmitted pulses are far from the original Gaussian or Gaussian monocycle pulses. It is also difficult to decouple the effect of antennas from propa-

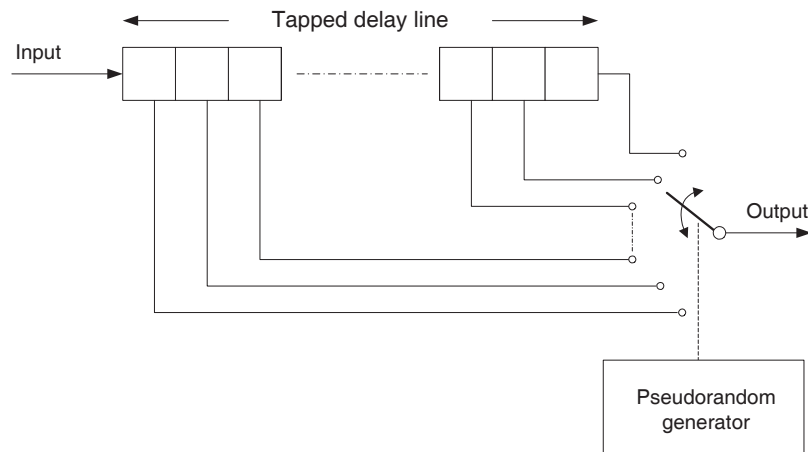


Figure 2.9. An example of hardware implementation of the ICM technique.

gation environments. However, the pulse distortion effects have to be included in the system model. The design of low cost and low size omni-directional antennas specifically dedicated for UWB systems, i.e., having flat propagation characteristics in the frequency domain, is very challenging. The latest developments in this area include co-design with other parts of baseband.

### 2.2.2 A view on hardware realization of the ICM technique

A view on a possible hardware realization of the ICM technique is shown in Fig. 2.9. A switch selects the output of a tapped delay line according to the selected (pseudorandom) sequence. In this way, a partitioned signal is read in a deterministic manner. Depending on the minimum delay of the tapped delay line, it is possible to realize chip, frame, code bit or information bit interleaving. As an analog delay line, a microstrip transmission line on a printed circuit board (PCB) can be used. However, for a PCB of the size of a matchbox, the maximum achievable delay may not exceed 1 or 2 ns, as the delay is proportional to the line length with a signal propagation speed lower than the speed of light and dependent on the substrate permittivity. Passive delays introduce attenuation which increases with the delay and frequency. Accurate delay lines in the order of a few nanoseconds have been presented [6], and [39]. Recently, a concept of a quantized time-interleaved analog delay has been proposed [112]. According to simulations, such a concept allows for introduction of a delay in the range from 100 ps to 900 ps with a step of 100 ps. Another solution, at least on the transmitter side, may be the use of programmable delay lines, e.g. 3D3438 from Data Delay Devices or MC100EP195 from ON Semiconductor. The former allows for an increment of 50 ps, whereas the latter allows for 10 ps resolution.

Other approaches to time interleaving, although not directly related to differential autocorrelation modulation, consider operation on time interleaved samples of ADCs [36] or DACs [55]. The former deals with the successive approximation register (SAR) topology enabling for very low power operation of 7.8 mW. The latter enables to generate oversampled signals that can be interleaved and allows for the use of low-complexity analog filters.

## 2.3 Summary

This chapter presents a single-user UWB-IR system model architecture that is considered in this thesis. A particular focus has been given to the description of the interleaved coding-modulation with polarity randomization concept.

Our contribution includes the design of the interleaved coding-modulation scheme which, when applied in combination with frame repetition or superorthogonal convolutional coding, allows to alleviate the problem of inter-symbol and inter-pulse interference commonly present in high data rate UWB-IR systems. Moreover, in order to characterize the UWB-IR system as accurate as possible, we model distortions introduced by a bandpass filter and amplifier and the effects of the transmitter and receiver antennas on the pulse shape. Simple yet feasible differential autocorrelation modulation is considered. The channel models studied in this thesis are the model suggested by the IEEE 802.15.3a committee and the AWGN channel.



# Chapter 3

## Channel coding

High data rate UWB-IR systems operating on multipath fading channels are susceptible to the destructive effects of inter-symbol and inter-pulse interference. By introducing channel coding in a communication system one may overcome destructive effects of such phenomena and simultaneously maintain a certain performance level.

In this chapter, a detailed description of channel coding schemes considered throughout this thesis is given. This chapter starts with a discussion on channel coding selection criteria which is given in Section 3.1. Next, in Section 3.2 details on superorthogonal convolutional coding, frame repetition and bit repetition schemes are presented. Finally, in Section 3.3, review of the existing literature on a high data rate hardware implementation of the Viterbi algorithm is given.

### 3.1 Channel coding selection criteria

When considering channel coding schemes, the most important and distinctive property of UWB technology is its very large bandwidth. The latest FCC definition describes an UWB system as any communication system with the total bandwidth larger than 0.5 GHz. Most often, in typical narrowband communication systems, bandwidth expansion due to the application of channel coding is seen as a constraint. From a designers point of view, selection of appropriate coding scheme is primarily based on the information of how much bandwidth is available in combination with the desired data rate and reliability level. The redundancy that lies behind any coding scheme implies the need to increase the transmission bandwidth or to decrease the data rate. In this respect, UWB differs from the narrowband techniques; a larger part of the available bandwidth can be dedicated to apply a particular channel coding scheme. This fact results in the application of channel codes characterized by low

or very low code rates, e.g., superorthogonal convolutional or superorthogonal turbo codes. For a communication system with channel coding applied, the desired bit error performance must be determined. Typically, it is characterized by a range of BER that is acceptable for a particular type of service, e.g. video, voice or data. Channel coding introduces computational complexity to the communication system, particularly in the decoder at the receiver side. Such complexity results in an additional delay and energy consumption. Considering the introduced delay in a high data-rate UWB system, an appropriate selection of the channel coding scheme might be critical. The decoder must have enough time to perform the decoding operations. Additionally, the decoder startup delay may be an important factor in a UWB system design. For UWB-based ad hoc sensor networks or wearable UWB devices, the energy consumption and associated with it operational time is of paramount importance. Regarding the above, the application of the channel codes of rather low or moderate level of complexity has been proposed. Another important consideration is synchronization. The information of how the receiver establishes synchronization with the transmitter at the beginning of a transmission or at the beginning of a particular data block may play an important role. The above considerations give some view of driving factors in the choice of particular channel coding schemes for an UWB system.

Finally, the ultimate selection of the coding scheme is a trade-off between the desired BER characteristics and delay/complexity constraints depending on the selected application.

## 3.2 Investigated channel coding schemes

In this thesis, three particular system setups are investigated, one further referred to as a UWB-IR system with SOC coding, the second, further referred to as a UWB-IR system with frame repetition, in which there is no coding scheme applied, and the third further referred to as a UWB-IR system with bit repetition with no FR nor SOC coding scheme applied.

In order to allow a fair comparison between the three schemes, we choose the  $n$  of the SOC and BR code equal to the  $N_f$  of the FR scheme. In this way, an equal number of transmitted pulses per information bit is guaranteed. In the following subsections, each system setup will be described in detail.

### 3.2.1 Frame repetition

For the case of UWB-IR systems with frame repetition, one can write that  $k = n = 1$  and  $N_f > 1$ . Decoding operation is based on integration over a duration of a modulation symbol time and threshold detection and is shown in Fig. 2.8. Although being simple, frame repetition does not constitute good method of protection against errors, as shown in Chapter 4. We mention it in this thesis mainly as a reference to SOC codes and due to the fact that

it is commonly considered by researchers, e.g. [15], [71], [92], [105], [82], [17], [26], [13], [68], [111], working in the UWB area.

### 3.2.2 Bit repetition

For the case of UWB-IR systems with bit repetition, the following holds:  $k = 1$ ,  $n = N_b > 1$ ,  $d_1 = d_2 = \dots = d_n$ , and  $N_f = 1$ , where  $N_b$  is the number of code bits that represent one information bit.

Bit repetition decoding boils down to majority decoding, i.e., the channel decoder makes a decision based on the number of zeros  $N_0$  and ones  $N_1$  in the subsequence of  $\hat{\mathbf{y}}_{\mathbf{b}}$  corresponding to the  $i$ th information bit, so that  $\hat{u}_i = 0$  if  $N_0 > N_1$  and  $\hat{u}_i = 1$  if  $N_0 < N_1 \forall i$ .

Similarly to frame repetition, although being relatively simple, bit repetition does not ensure good protection against errors especially on multipath fading channels. BR is treated in this thesis as a reference to the performance of the SOC codes.

### 3.2.3 Superorthogonal convolutional coding

The availability of excess bandwidth common in UWB techniques allows to construct redundant signalling schemes in order to establish an asynchronous and robust multi-access communication system link. The redundant signalling scheme may be achieved by using part of the available excess bandwidth to introduce frame repetition. Another approach may be based on application of various error-correcting codes to enhance the UWB-IR system performance. In this thesis, we consider low rate superorthogonal convolutional codes as error-correcting schemes [100]. In conventional narrowband communication systems, the bandwidth expansion due to the application of low rate channel coding schemes is generally an undesired feature. However, in UWB applications, similarly to CDMA and fiber-optic CDMA systems [5], there is no penalty associated with applying very low rate codes. In fact, deft application of such codes can be advantageous to spreading and error correction properties of the communication system [93].

Superorthogonal convolutional codes have desirable properties, i.e. good autocorrelation properties due to the Hadamard-Walsh transform employed, and a simple decoder architecture with processing complexity growing only linearly with the constraint length of the code,  $K$ , and thus making the decoder feasible even for high values of  $K$  [100]. The main parameters of the SOC code, i.e. the code rate  $R$  and free distance  $d_f$ , are  $R = 1/n$ , where  $n = 2^{K-2}$  and  $d_f = 2^{K-3}(K+2)$ , respectively. In our system model, for the case of UWB-IR systems with superorthogonal convolutional coding, the following holds:  $k = 1$ ,  $n > 1$ , and  $N_f = 1$ . The structure of the SOC encoder is shown in Fig. 3.1. The SOC encoder consists of a  $K$ -stage shift register, a bit orthogonal block encoder, and a modulo-2 adder with 3

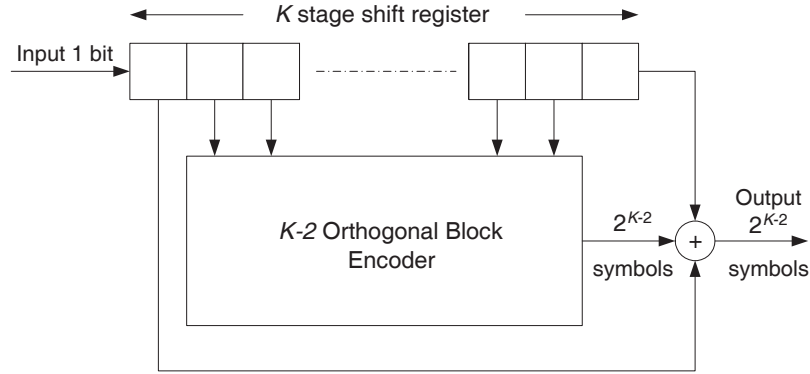


Figure 3.1. Diagram showing a superorthogonal convolutional encoder architecture.

inputs. The block encoder is a Hadamard-Walsh encoder with length  $K - 2$ . For every input bit  $2^{K-2}$  coded bits are generated by the Hadamard-Walsh encoder and the contents of the first and last stages of the shift register are added modulo-2 to added generating a final codeword. The codewords of the superorthogonal convolutional code are pair-wise orthogonal, i.e., they are similar in  $2^{K-3}$  code bits and different in the other  $2^{K-3}$  code bits. Superorthogonal convolutional codes differ from orthogonal convolutional codes in the number of shift register outputs that fed the Walsh-Hadamard block encoder, namely all the outputs of the shift register drive the block encoder. There is also no modulo-2 adder and the output of the block encoder constitutes the output of the code. As a result, the code rate of orthogonal convolutional codes equals to  $1/2^K$ . It should be noted that SOC codes yield better performance than orthogonal convolutional codes.

Since convolutional encoders have memory and as a result comprise finite state machines, it is convenient to represent the encoding operation by a state diagram. The state diagram consists of a number of states with the relation between the input, the previous and current state, and the current output. The state of the encoder is defined as the contents of the memory. By splitting the all-zero state into an initial state and a final state and labeling the branches of the diagram by terms  $D^\omega \beta^l$  we obtain a modified state diagram. A modified state diagram of a rate  $1/2^{K-2}$  superorthogonal convolutional code is shown in Fig. 3.2. The exponent of  $D$  denotes the Hamming weight of the coded output sequence, whereas the exponent of  $\beta$  is the Hamming weight of the input sequence. For the notational convenience, as in [100], we denote  $W = D^\omega = D^{2^{K-3}}$ . In Fig. 3.2, we notice interior states labeled by integers starting from 0 to  $K - 2$ , corresponding to the number of successive zeros following the initial 1 in the input stream that caused divergence from the all-zero state. The shortest path from the initial state to the final state has length  $K$  and corresponds to a "1" followed by  $K - 1$  zeros. The modified state diagram is useful in determining the transfer function of the code, which is also known as the weight enumerating sequence (WES), and bounds on the bit error rate.



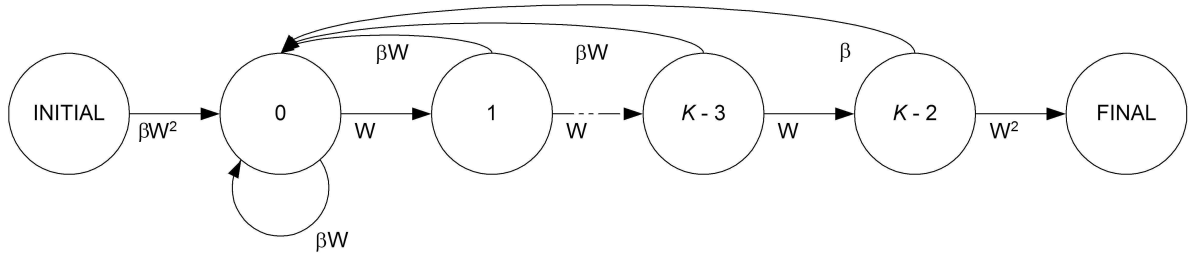


Figure 3.2. A modified state diagram of a constraint length- $K$  rate  $1/2^{K-2}$  superorthogonal convolutional code.

As visible from Fig. 3.2 and also noted from Fig. 3.1, in case of there is a single "1" in the first stage, the orthogonal block encoder generates an all-zero sequence, and hence the output of the SOC encoder after modulo-2 addition is an all-one sequence. As a result, the weight of the first branch is  $2\omega = 2^{K-2}$ , where  $\omega = 2^{K-3}$  is the distance accumulated of each branch traversed. Similarly, the last branch just before remerging to the all-zero state has the weight  $2\omega$ , because for the only "1" in the last stage, the output of the modulo-2 adder is again an all-one sequence. The weight of the branch leading from the state 100...0 (last from possible remerging) to the state 000...01 (same as same as first after diverging) is zero since when the first and last stages have zeros, the output of the block encoder is an all-zero sequence, and it remains zero until each symbol is added modulo-2 successively to two ones [100].

The decoding operation is performed with the use of the Viterbi algorithm with  $2^{K-1}$  states. Generally, decoding of the SOC codes is simpler than ordinary low rate convolutional codes. Each branch metric is a correlation or a scalar product of the received code word and the corresponding Walsh or its complementary sequence. Such correlations may be computed with the inverse Walsh-Hadamard transformation (IWHT), for which fast algorithms can be used [54]. An example of implementation of a decoder is presented in Fig. 3.3. The branch metrics are calculated according to the soft output of the differential autocorrelation receiver. For the  $K = 5$  SOC code, eight metrics needs to be determined. This can be obtained in  $K - 2 = 3$  steps, which can be implemented by the  $K - 2$  - stage processor at the top of Fig. 3.3. Each metric generated by this processor represent branch metrics that are added to or subtracted from  $2^{K-1}$  state metrics of the convolutional code by the add-compare-select (ACS) unit. For  $K = 5$  SOC code, the metric  $m_x$ , corresponding to the 3-bit input  $x$ , must be added to and subtracted from both the state metrics  $M_{0x}$  and  $M_{1x}$  (see Fig. 3.3). The result of comparison, i.e., the surviving path at each branch is selected. It should be noted that  $2^{K-2}$  ACS pairs are needed for a rate- $1/2^{K-2}$  SOC code. At each step, two updated state metrics are placed in the appropriate registers of the  $2^{K-1}$  state metric memory. The decisions are fed to the path memory containing  $2^{K-1}$  registers, one for each of the states, each of the length on the order of  $5K$  (decoding depth). The information bits are decoded by

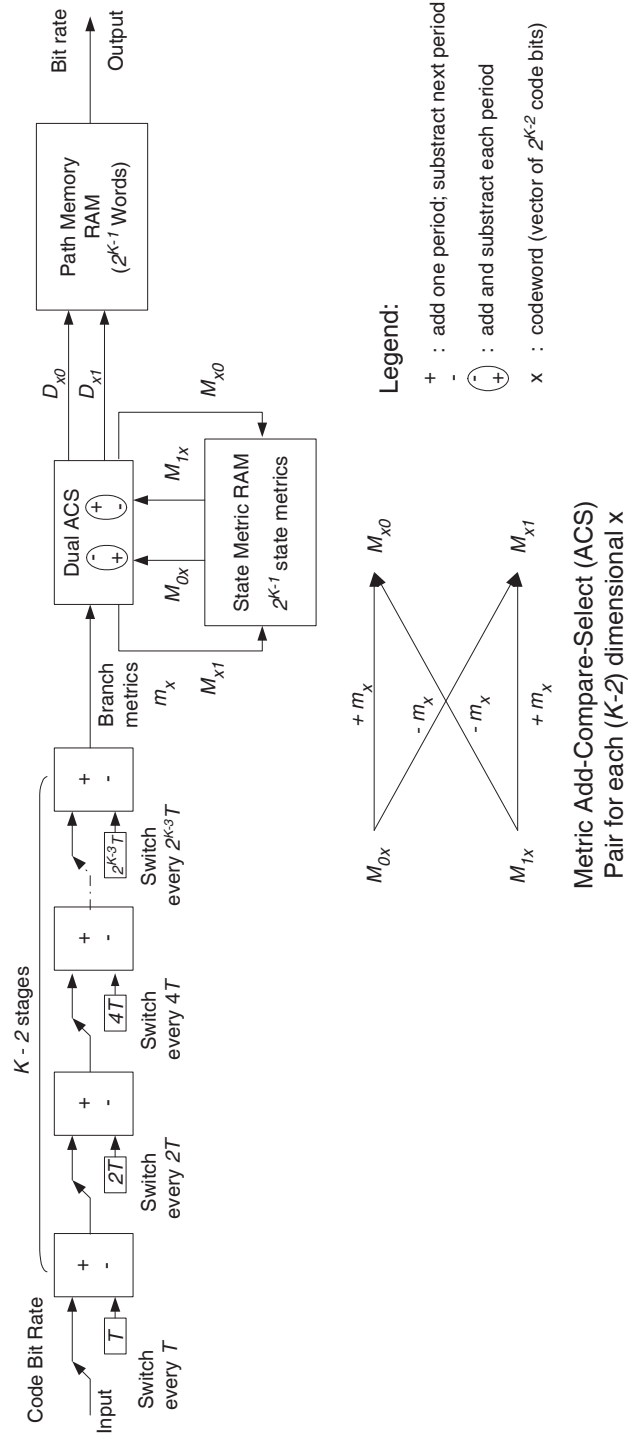


Figure 3.3. Superorthogonal convolutional decoder implementation [100].

reading in reverse order the state transitions from the last state to the first. It is important to append  $K$  dummy bits at the end of every input sequence in order to force the decoder to the all-zero state. This procedure is called "tailing-off". With the price of little performance degradation due to suboptimality, it is, however, possible to make a final decision without tailing-off. This process is called "memory truncation" [100].

It is imperative to point out that all decoder operations are performed at the code bit clock speed and, counting the dual ACS as four adders and subtractors, there are  $K + 2$  additions and subtractions per code bit time. As a result, the processing complexity (or speed requirement) of the SOC decoder grows only linearly with  $K$ , although the metrics and path memories grow exponentially. This is different than for the case of standard convolutional codes for which the decoding process complexity grows exponentially with the number of memory elements making the decoder unfeasible for high values of  $K$ .

Interestingly, the processing complexity of the SOC decoder is greater than the processing complexity of the encoder only in the fact that the real number addition (or subtraction) is needed to replace the modulo-2 addition performed at the encoder.

The above mentioned features are of high value to UWB-IR systems, where the overall system process complexity is an issue.

### 3.3 Hardware implementation of a Viterbi decoder

In this section, a review of the available literature on hardware implementation of a Viterbi decoder is given.

Although this thesis deals with UWB-IR, the only proposed high data rate hardware implementations for UWB communications refer to the MB-OFDM version of this technology. In an MB-OFDM UWB system, the input to the decoder is soft information from the frequency domain equalizer. Several different data rates are proposed ranging from 53.3 Mbps to 480 Mbps [7]. As a channel coding scheme, a rate 1/3 convolutional code with constraint length,  $K = 7$ , punctured to provide 1/2, 5/8, and 3/4 rate codes, is applied. Due to large variation in the data rates and code rates, it is advantageous to design a Viterbi decoder architecture able to support the highest rate with high hardware efficiency and reduced power consumption at lower rates. In [98], a Viterbi decoder architecture that can achieve the above mentioned goals is proposed. This architecture combines three main techniques developed to increase the decoding speed with a relatively low clock frequency, namely, *lookahead*, *parallelism*, and *the sliding block*. All of these methods solve the bottleneck problem on the decoding speed of the Viterbi decoder imposed by the add-compare-select (ACS) unit. However, the application of the first two methods, increases the complexity of the architecture, namely, as the level of the lookahead increases, the complexity grows exponentially, and for *parallel processing* the complexity grows linearly with the level of parallelism. The increase

in complexity results in higher power consumption. As a result, the level of lookahead and parallelism must be limited [98]. The *sliding block* technique can be used to increase the data rate of the decoder by performing the decoding process simultaneously in forward and backward directions [98]. However, with the increase in the number of states, the constraint length and track back length, the number of the required ACS units and buffer registers becomes prohibitively high. As stated in [98], for the 480 Mbps decoding speed, it is possible to replace the fully parallel ACS architecture by a serial architecture by utilizing the *folding technique*. The proposed Viterbi decoder architecture in [98] combines 2-step *lookahead*, 2-level *parallelism* and *serialized sliding block* techniques. The decoder is divided into 3 blocks, from which some are enabled or disabled depending on the required data rate. The trace memory and the minimum state estimate unit are shared by both parallel branches to reduce hardware complexity.

Another approach in the design of a Viterbi decoder architecture for MB-OFDM UWB is proposed in [18]. For the same as previously considered convolutional code, it is based on one-stage *lookahead technique* and the use of radix-4 instead of radix-2 ACS units. As a result, two symbols are processed at half rate of conventional architecture allowing for the support of high speed decoding. For the data rate of 200 Mbps, the clock speed equals 100 MHz. The proposed in [18] architecture was implemented in an FPGA Xilinx x2v6000 ff1152-5 occupying 15 % of the total number of its components. For the support of data rates above 100 Mbps, it is suggested in [18] to refer to the Application Specific Integrated Circuits (ASIC) technology that is known to be much faster than FPGA.

### 3.4 Summary

This chapter presents three channel coding schemes that are considered in this thesis, namely superorthogonal convolutional coding, frame repetition and bit repetition. Special attention has been given to the description of superorthogonal convolutional coding as it yields the best performance results. All of the three schemes have been implemented in the UWB-IR system model in a way ensuring a fair comparison so that an equal number of transmitted pulses per information bit is always guaranteed. Additionally, in this chapter, information on practical implementation issues and architectures for the Viterbi algorithm has been provided.

# Chapter 4

## Performance analysis

Theoretical analysis of the performance of UWB-IR systems with a differential autocorrelation modulation operating on multipath fading channels is generally cumbersome. Adding channel coding on top of this signalling scheme makes it even more difficult. These are the reasons why researchers, e.g. [48], [29], [107], [11], although some of them considering other signalling schemes, in order to simplify their performance analyzes, commonly consider AWGN channels and primitive scenarios with no ISI nor IPI effects. In this chapter, we evaluate the bit error rate performance of UWB-IR systems operating on additive white Gaussian noise and multipath fading channels with and without the proposed schemes by referring to bounds and intensive Monte Carlo simulations.

This chapter is organized as follows. In Section 4.1, bounds on the bit error probabilities of single-user UWB-IR systems operating on AWGN and multipath fading channels are derived. To do so, we rely on the transfer function and spectral properties of the superorthogonal convolutional code. In Section 4.2, the results of Monte Carlo simulations for single-user UWB-IR systems are provided. All of the UWB-IR system parameters and assumptions made during the simulations are listed. Several scenarios depending on the presence of the proposed techniques, i.e., interleaved coding-modulation and polarity randomization, are considered. Furthermore, in this section, the effects of the influence of system parameters and channel parameters on the bit error rate are thoroughly studied. Section 4.3 concludes this chapter.

### 4.1 Bounds on the bit error probabilities

In this section, the performance of coded UWB-IR systems is evaluated by using bounds on the bit error probabilities. The analysis starts with a single-user scenario and AWGN

channels. Next, UWB-IR systems operating on multipath fading channels are considered. The data rates of the considered systems are the same and the bandwidth expansions introduced by SOC coding, the FR and BR schemes are equal. Table 4.1 presents the parameters of the UWB-IR system models examined in this chapter.

#### 4.1.1 Bounds on the bit error probabilities on AWGN channels

An upper bound on the bit error probability of the UWB-IR system with superorthogonal convolutional coding is derived from the transfer function of the code that is given by [100]

$$T(W, \beta) = \frac{\beta W^{K+2}(1-W)}{1 - W[1 + \beta(1 + W^{K-3} - 2W^{K-2})]}, \quad (4.1)$$

where  $W = Z^{K-3}$ .

By expanding (4.1), we get a polynomial in which the exponent of  $W$  gives the Hamming weight of the coded sequence (the weight of the branch) and the exponent of  $\beta$  gives the Hamming weight of the input sequence, as defined in Section 3.2.3. The parameter  $\beta$  denotes the information error weight. The parameter  $Z$  can be calculated from the Bhattacharyya bound as

$$Z = \int_{-\infty}^{\infty} \sqrt{p_0(y)p_1(y)} dy, \quad (4.2)$$

where  $p_0(y)$  and  $p_1(y)$  are the density functions of the receiver/channel output conditioned on the input symbol being 0 and 1, respectively. The upper bound on the bit error probability of the UWB-IR system is expressed as

$$P_b < \left. \frac{\partial T(W, \beta)}{\partial \beta} \right|_{\beta=1} = \frac{W^{K+2}}{(1-2W)^2} \left( \frac{1-W}{1-W^{K-2}} \right)^2. \quad (4.3)$$

For an AWGN channel, the parameter  $W$  can be calculated as  $W = \exp(-\gamma_{out})$  [100], where  $\gamma_{out}$  denotes the output signal-to-noise ratio of the autocorrelator. Since the relationship binding the input and output signal-to-noise ratio of the differential autocorrelation receiver for the Gaussian monocycle is compound, for simplicity, as in [75], we consider a rectangular pulse shape having

$$\gamma_{out} \cong \frac{G_p \gamma_{in}}{1 + (2\gamma_{in})^{-1}}, \quad (4.4)$$

where  $\gamma_{in}$  can be calculated from

$$\gamma_{in} = \frac{E_b}{N_0} G_p^{-1}. \quad (4.5)$$

The parameter  $G_p$  denotes the processing gain of the UWB-IR system and is defined as

$$G_p = \frac{B}{R_b} = B N_f N_p T_w \frac{n}{k}, \quad (4.6)$$

Table 4.1. UWB-IR System Parameters.

Bandwidth		$B = 6$ GHz
Modulation		Differential Autocorrelation
Pulse Width		$T_w \simeq 0.167$ ns
Bit Rate		$R_b = 125$ Mbps
Processing Gain		$G_p = 48$
SOC	Coding Scheme	SOC
Channel	Constraint Length	$K = 4, 5, 6$
Coding	Code Rate	$R = 1/4, 1/8, 1/16$
	Decoding Algorithm	Soft-Input Viterbi Algorithm
Frame	Coding Scheme	None
Repetition	Number of Frame Repet.	$N_f = 4, 8, 16$
Interleaving	Chip Interleaving	$L_p = 400$ , Random
Number of Chips in a Frame		$N_p = 12, 6, 3$
Channel Model		CM1, CM3

where  $B$  is the bandwidth and  $R_b$  is the bit rate. From (4.1) we can also compute the free distance of the SOC code with the constraint length  $K$  as  $d_f^{(SOC)} = 2^{K-3}(K+2)$ . Comparing this value with the free distance of the simple frame repetition scheme  $d_f^{(FR)} = 2^{K-2}$ , it can be easily observed that SOC coding enables substantially better performance compared to frame repetition.

The lower bound on the bit error probability of the UWB-IR system incorporating the SOC code can be calculated as [29]

$$P_b \geq Q \left( \left( \frac{\mu^2}{\sigma^2} d_f \right)^{1/2} \right), \quad (4.7)$$

where  $\mu$  and  $\sigma^2$  are the mean and the variance of the autocorrelation receiver output conditioned on the input symbol being zero. The  $Q(x)$  function refers to the area under the tail of the Gaussian PDF and is defined as

$$Q(x) = \frac{1}{\sqrt{2\pi}} \int_x^\infty e^{-t^2/2} dt, \quad x \geq 0. \quad (4.8)$$

A comparison of bounds and simulation results will be presented in Section 4.2.1.

### 4.1.2 Bounds on the bit error probabilities on multipath fading channels

We start our analysis by rewriting the formula for the channel impulse response, given in (2.4), without the shadowing term as

$$h(t) = \sum_{i=1}^{M_t} \alpha'_i \delta(t - \tau'_i), \quad (4.9)$$

where  $M_t = LM$  is the total number of multipath components,  $\alpha'_i$  and  $\tau'_i$  are the gain and delay of the  $i$ -th multipath component. The continuous time Fourier transform of  $h(t)$  in (4.9) is

$$H(f) = \sum_{i=1}^{M_t} \alpha'_i \exp(-j2\pi f \tau'_i), \quad (4.10)$$

where  $f$  denotes the frequency. As shown in [103], the magnitude  $|H(f)|$  and the phase  $\angle H(f)$  are Rayleigh and uniformly distributed, respectively. This, together with the fact that ICM+PR makes the channel uncorrelated, allows us to determine the BER performance by using the union upper bound given by [80]

$$P_b < \frac{1}{k} \sum_{d=d_f}^{\infty} \varsigma_d P_2(d), \quad (4.11)$$

where  $d_f$  is the free distance of the code and  $k$  is the number of information bits. Since we consider SOC codes here,  $k = 1$ . The weighting coefficients  $\varsigma_d$  in the summation, also referred to as a distance spectrum of the code, are the sums of bit errors for paths of distance  $d$ . The pairwise error probability  $P_2$  refers to the probability that the channel decoder erroneously selects a specific sequence with the Hamming distance  $d$  from the transmitted sequence. The pairwise error probability depends primarily on the channel and modulation, and is given by [80]

$$P_2(d) = p^d \sum_{k=0}^{d-1} \binom{d-1+k}{k} (1-p)^k, \quad (4.12)$$

where  $p$  is the error probability for binary signalling. Since we consider a differential auto-correlation modulation and noncoherent detection on a Rayleigh fading channel,  $p$  is [80]

$$p = \frac{1}{2 + E/N_0}, \quad (4.13)$$

where  $E/N_0$  is the average signal-to-noise-ratio and  $E$  is the energy per component of the code (energy per dimension) and is derived from the energy per information bit,  $E_b$ , by

$$E = RE_b. \quad (4.14)$$



Table 4.2. Distance Properties of the Considered SOC Codes.

K	$d_f$	$R$	Distance spectrum $\{(\varsigma_d, d)\}$
4	12	1/4	$\{(1,12), (2,14), (7,16), (16,18), (41,20), (94,22), (219,24), (492,26), (1101,28), (2426,30), (5311,32), (11528,34)\}$
5	28	1/8	$\{(1,28), (2,32), (5,36), (14,40), (32,44), (74,48)\}$
6	64	1/16	$\{(1,64), (2,72), (5,80), (12,88), (30,96)\}$

Fig. 4.1 shows the calculated upper union bounds on the BER performance of UWB-IR systems with superorthogonal convolutional codes of the constraint lengths  $K = 4, 5$ , and  $6$  on uncorrelated multipath fading channels. As observed, increasing the value of the constraint length results in better BER performance. For the constraint length  $K = 6$  and  $E_b/N_0$  values lower than 10 dB, the calculated bound is loose. The reason for that is a relatively small number of non-zero terms used in calculation of bit error probability in (4.11).

In general, a transfer function of a convolutional code can be expressed as [80]

$$T(D, \beta) = \sum_{d=d_f}^{\infty} a_d D^d \beta^{f(d)}, \quad (4.15)$$

where  $a_d$  is the number of paths of distance  $d$  from the all-zero path that merge with the all-zero path for the first time. The exponent of  $D$  denotes the distance of the sequence of encoded (output) bits corresponding to each branch and the sequence of output bits corresponding to the all-zero branch. The exponent of  $\beta$  indicates the number of 1s in the information sequence corresponding to a given branch. Taking the derivative of  $T(D, \beta)$  with respect to  $\beta$  and setting  $\beta = 1$ , we obtain

$$\left. \frac{\partial T(D, \beta)}{\partial \beta} \right|_{\beta=1} = \sum_{d=d_f}^{\infty} \varsigma_d D^d. \quad (4.16)$$

For the case of a SOC code (4.16) becomes

$$\begin{aligned} \left. \frac{\partial T(D, \beta)}{\partial \beta} \right|_{\beta=1} &= \frac{W^{K+2}}{(1-2W)^2} \left( \frac{1-W}{1-W^{K-2}} \right)^2 \\ &= \frac{D^{(K+2)2^{K-3}}}{(1-2D^{2^{K-3}})^2} \left( \frac{1-D^{2^{K-3}}}{1-D^{(K-2)2^{K-3}}} \right)^2 \end{aligned} \quad (4.17)$$

with  $W = D^{2^{K-3}}$ . By expanding the above equation using Taylor's series, we get a polynomial from which we can determine the code's distance spectrum  $\varsigma_d$ . Table 4.2 presents the calculated distance spectra  $\varsigma_d$ , and free distances  $d_f$ , for SOC codes of the constraint lengths  $K = 4, 5$ , and  $6$ . True bound given in (4.11) needs inclusion of infinitely many terms. In Table 4.2, we consider 23 terms for  $K = 4$  and  $K = 5$ , and 33 terms for  $K = 6$ , although 15 terms yield a good estimate of the true bit error rate [33].

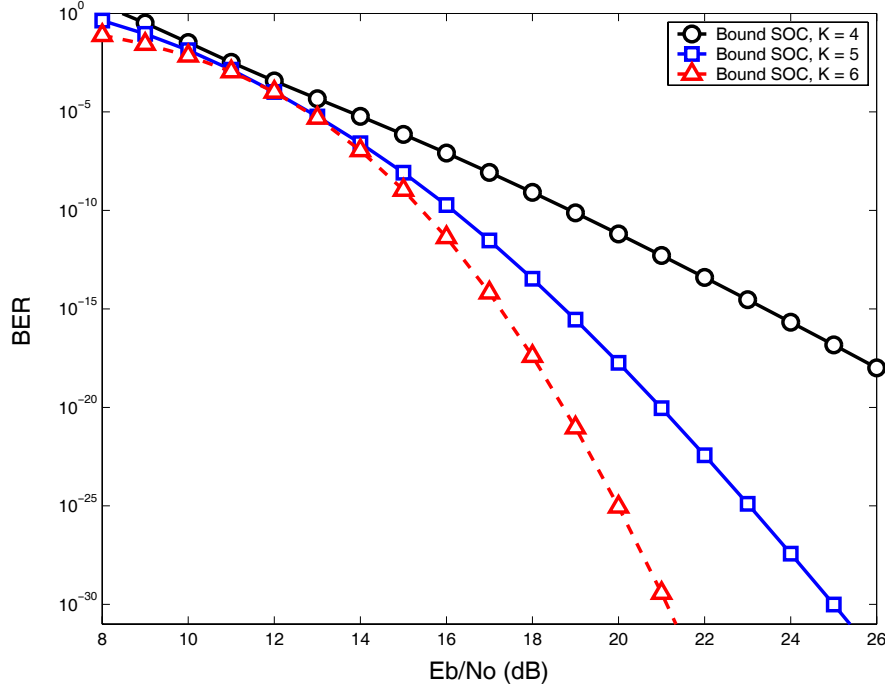


Figure 4.1. Upper union bounds on the bit error rate of UWB-IR systems with SOC coding on uncorrelated multipath fading channels.

### 4.1.3 Bit error probabilities of a RAKE receiver on multipath fading channels

In the following, we provide a mathematical approach in the bit error rate performance characterization of UWB-IR systems with a RAKE receiver [94]. Our motivation here is to have a reference that may serve for rough comparisons of the BER performance between UWB systems based on a differential autocorrelator and a RAKE receiver. Maximal Ratio Combining (MRC) is chosen as a strategy for exploiting channel diversity. As a modulation scheme, binary pulse amplitude modulation (BPAM) signaling is considered. An idealization in the analysis is that no ISI nor IPI is considered and the channel is slow fading. The instantaneous signal-to-noise ratio per information bit is

$$\gamma_b = \frac{2E_b}{N_0} \sum_{l=1}^{M_f} \alpha_l^2, \quad (4.18)$$

where  $M_f$  is the number of fingers of a RAKE receiver and  $\alpha_l$  is the  $l$ -th fading coefficient. The conditional BER for a fixed set of fading coefficients is

$$p(\gamma_b) = \frac{1}{2} \operatorname{erfc} \sqrt{\frac{\gamma_b}{2}}. \quad (4.19)$$

The complementary error function is defined as

$$\operatorname{erfc}(x) = \frac{2}{\sqrt{\pi}} \int_x^\infty e^{-t^2} dt \quad (4.20)$$

and is related to the Q-function defined in (4.8) as

$$Q(x) = \frac{1}{2} \operatorname{erfc} \left( \frac{x}{\sqrt{2}} \right). \quad (4.21)$$

The approximated pdf of  $\gamma_b$  can be calculated using the Wilkinson's method and is given

$$f(\gamma_b) = \frac{1}{\gamma_b \sqrt{2\pi\sigma_x^2}} \exp \left[ -\frac{(\ln(\gamma_b) - \mu_x)^2}{2\sigma_x^2} \right], \quad (4.22)$$

where  $\mu_x$  and  $\sigma_x$  are the parameters of a normal RV that is used in the Wilkinson's method [94]. The average BER is calculated by averaging the conditional BER  $p(\gamma_b)$  over  $f(\gamma_b)$  as

$$P_b = \int_0^\infty p(\gamma_b) f(\gamma_b) d\gamma_b. \quad (4.23)$$

## 4.2 Simulation results

In this section the performance of UWB-IR systems using SOC coding, FR, or BR is evaluated by using Monte Carlo simulations. The BER performance is examined with 80 independent channel realizations and 2000 bits in every packet. It is assumed that the channel is invariant throughout the duration of a single data packet and that synchronization is ideal. In the following subsections, we consider several scenarios depending on the presence of the proposed techniques, i.e., interleaved coding-modulation and polarity randomization.

### 4.2.1 Results - no interleaving nor PR case

Fig. 4.2 shows Monte Carlo simulation results together with the derived lower and upper bounds on the performance of the UWB-IR systems with SOC coding operating on the AWGN channel. The bounds are represented by dotted lines without markers. Moreover, simulation results for the line-of-sight (LOS)-CM1 scenario are included. The obtained simulation results are in good agreement with derived upper and lower bounds on the BER. Fig. 4.3 illustrates a comparison between the BER performance of the UWB-IR systems incorporating SOC coding or FR scheme in two environments, namely AWGN and LOS-CM1 scenario. Additionally, as a reference, performance of a RAKE receiver with MRC, two paths resolved and BPAM signaling is presented. As can be seen from this figure, the performance of a UWB-IR system in a LOS environment is noticeably worse than that in AWGN. The

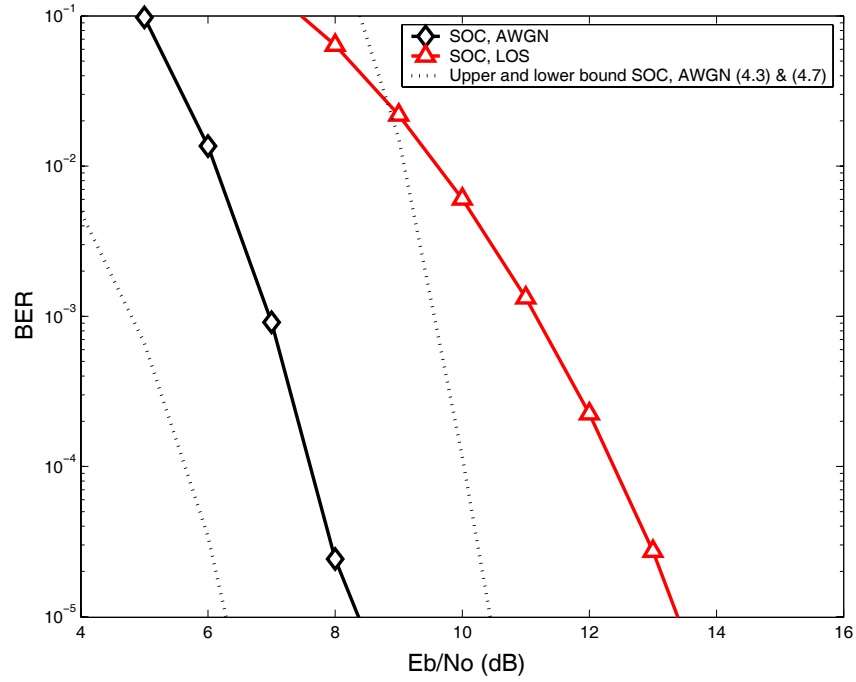


Figure 4.2. The bit error rate performance of the UWB-IR systems with SOC coding,  $K = 5$ ,  $n = 8$ ,  $N_f = 1$ ,  $N_p = 6$  in AWGN and LOS (CM1) scenarios; simulation results and bounds.

difference in the bit energy between the UWB-IR systems with SOC coding on a  $\text{BER} = 10^{-3}$  level, for AWGN and the case of LOS scenario, equals circa 4 dB. Comparing the performance of the UWB-IR systems based on SOC coding and FR in the LOS environment only, we notice the reduction of 1 dB in the bit energy on the  $\text{BER} = 10^{-3}$  level that is introduced by the SOC coding scheme. Similarly, Fig. 4.4 presents the previous comparison of the BER performance with the exception that the AWGN and non-line-of-sight (NLOS)-CM3 environments are considered here. As can be observed, SOC coding introduces a substantial performance gain over FR in NLOS environments. As can be observed from Fig. 4.3 and 4.4, the RAKE receiver yields better performance than the differential autocorrelation receiver with channel coding operating on the AWGN channel. The reason for that is in the PAM signaling used which is more power efficient than differential autocorrelation modulation. At the  $\text{BER} = 10^{-5}$  level the difference in  $E_b/N_0$  is about 3 dB. However, a clear disadvantage of a RAKE receiver is that it requires channel estimation.

#### 4.2.2 Results - interleaving and/or PR case

Fig. 4.5 and Fig. 4.6 show the BER performance improvement introduced by the interleaved coding-modulation, pulse-based polarity randomization, and a combination of the above for SOC coding, frame, and bit repetition. The interleaver size is  $L_p = 400$  chips.

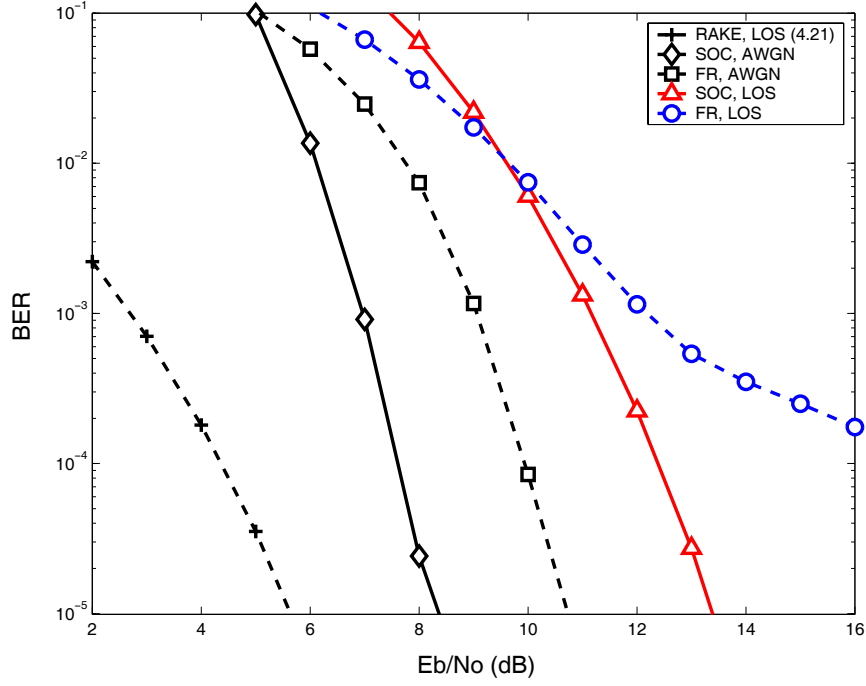


Figure 4.3. The bit error rate performance of the UWB-IR systems with a RAKE receiver or differential autocorrelation receiver with SOC coding,  $K = 5$ ,  $n = 8$ ,  $N_f = 1$ ,  $N_p = 6$  and FR,  $N_f = 8$ ,  $n = 1$ ,  $N_p = 6$  in AWGN and LOS (CM1) scenarios.

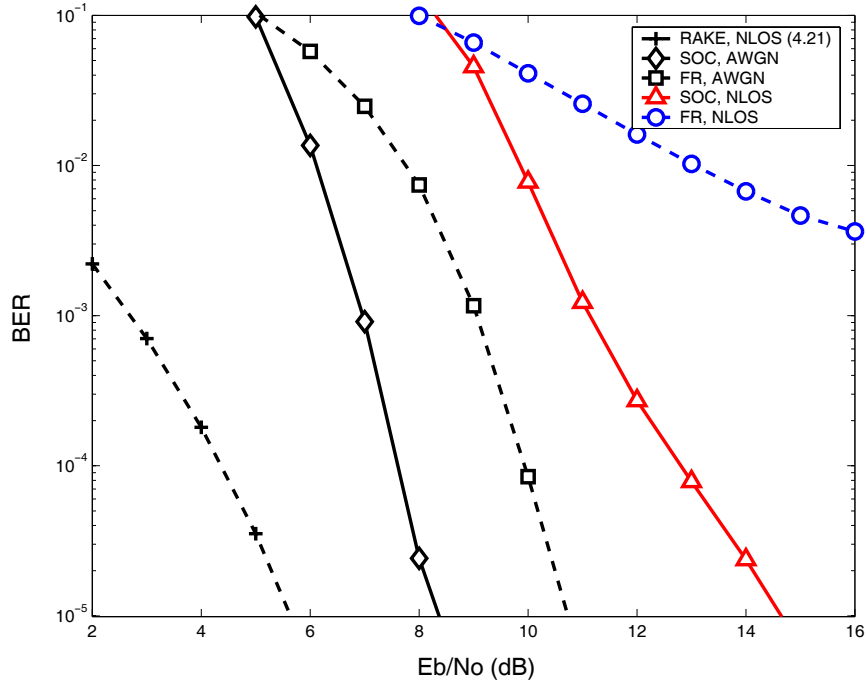


Figure 4.4. The bit error rate performance of the UWB-IR systems with a RAKE receiver or differential autocorrelation receiver with SOC coding,  $K = 5$ ,  $n = 8$ ,  $N_f = 1$ ,  $N_p = 6$  and FR,  $N_f = 8$ ,  $n = 1$ ,  $N_p = 6$  in AWGN and NLOS (CM3) scenarios.

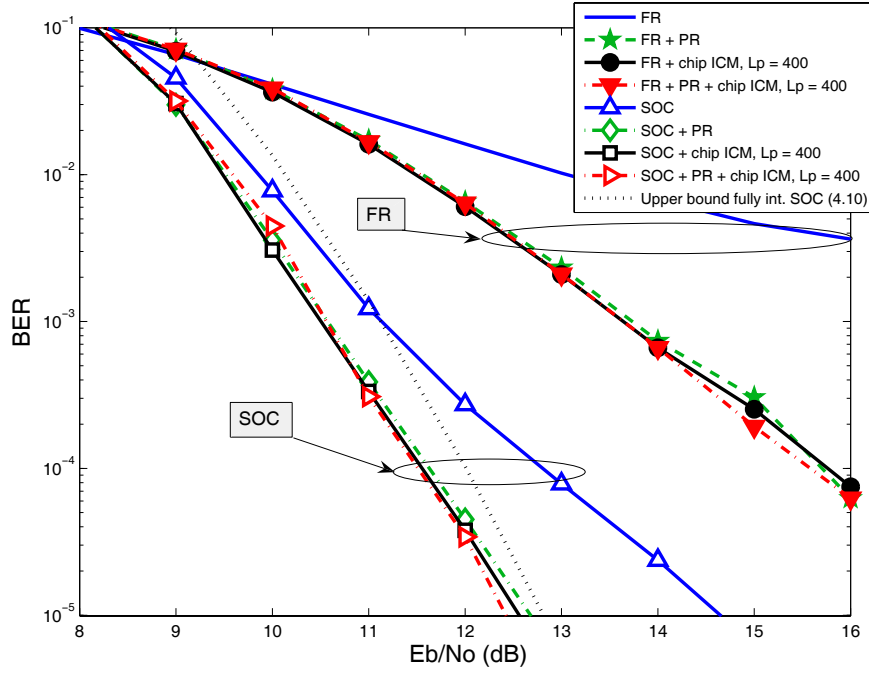


Figure 4.5. The effect of PR and ICM on the bit error rate of UWB-IR systems with SOC coding,  $K = 5$ ,  $n = 8$ ,  $N_f = 1$ ,  $N_p = 6$ , or FR,  $N_f = 8$ ,  $n = 1$ ,  $N_p = 6$  in the CM3 channel scenario.

We observe that the highest coding gain can be achieved for FR. The reason for that may lay in the fact that SOC coding may also be seen as a source of diversity, whereas FR is not. We notice that a difference in the BER performance of ICM, PR, and ICM with PR is small, making pulse-based polarity randomization a sort of alternative to ICM, without introducing any delay. For the cases of ICM, PR, and ICM + PR, the obtained simulation results are in good agreement with the derived upper bound on the BER. As indicated in Section 4.1.2, the calculated upper bound on the BER holds for uncorrelated channels and this is the reason why the bound crosses with the curve corresponding to the pure UWB-IR system with SOC coding applied only. The effects of the interleaving level choice on the BER performance are shown in Fig. 4.7. Chip interleaving yields superior performance compared to frame interleaving. Moreover, random interleaving offers higher performance gain than block interleaving. This is explained in terms of the higher level of time diversity introduced by the random chip interleaving over other types of interleaving making the channel fully uncorrelated.

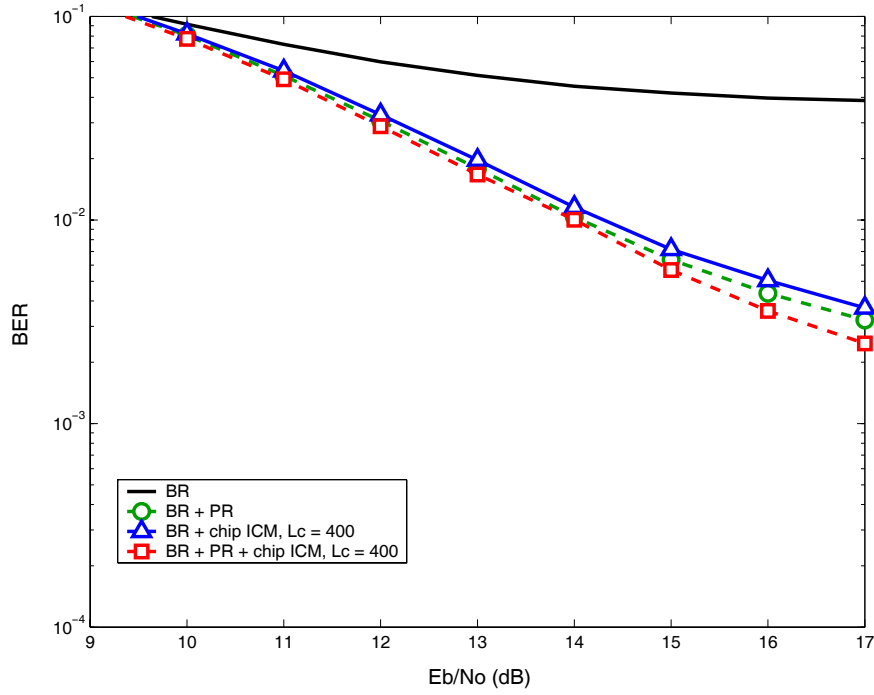


Figure 4.6. The effect of PR and ICM on the bit error rate of UWB-IR systems with BR,  $n = 8$ ,  $N_f = 1$ ,  $N_p = 6$  in the CM3 channel scenario.

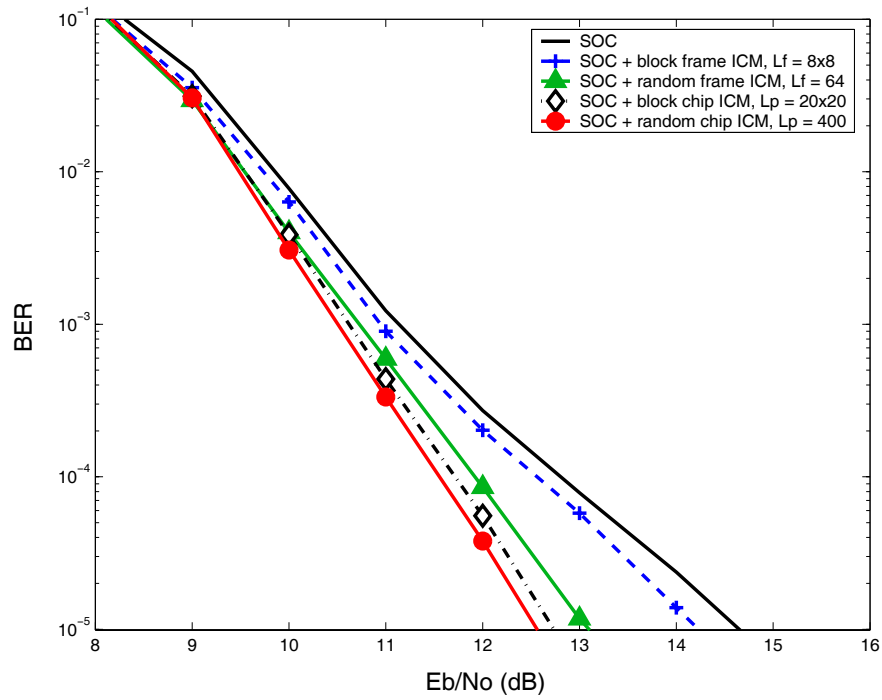


Figure 4.7. The effect of the interleaving level choice on the bit error rate of UWB-IR systems with SOC coding in CM3 channel scenario,  $K = 5$ ,  $n = 8$ ,  $N_f = 1$ ,  $N_p = 6$ .

### 4.2.3 Results - influence of the system parameters

Fig. 4.8 presents the influence of the interleaver size on the BER performance. As expected, a tendency for the BER improvement along with the increase of the size of an interleaver is observed. The oscillations of BER performance for small interleaver sizes have their root in the concatenation of the periodic fades whenever the size of the interleaver is a multiple of the period. This concatenation may produce a long sequence of faded receiver outputs that exceeds the ability of the code to correct errors. As a result, the interleaved BER performance is worse than without interleaving. A similar phenomenon is also observed in [86]. The cut off value of the size of a chip interleaver is  $L'_p \simeq 200$  chips that is an equivalent of a time period  $\tau = 33.4$  ns, whereas the channel delay spread equals  $\tau_{rms} = 15$  ns. Thus the interleaver size ensuring the channel to be fully uncorrelated is  $L'_p \simeq 200$  chips.

Fig. 4.9 shows the impact of UWB-IR system parameters on the BER performance for the case of interleaved coding-modulation with polarity randomization with FR or SOC coding. For the case of FR, decreasing the number of chips,  $N_p$ , and at the same time increasing the number of frames,  $N_f$ , to maintain the same data rate does not affect the BER performance much. However, for the case of SOC coding, decreasing the number of chips, and simultaneously increasing the number of code bits,  $n$ , leads to a BER performance improvement. These phenomena can be explained by the fact that the free distance of a SOC code increases faster along with the increase of  $n$  comparing to free distance of FR when the number of frames per symbol,  $N_f$ , is increased. Hence, despite that for a lower number of chips the destructive effects of multipath fading are enhanced (pulses are placed closer to each other), the SOC code can correct more errors.



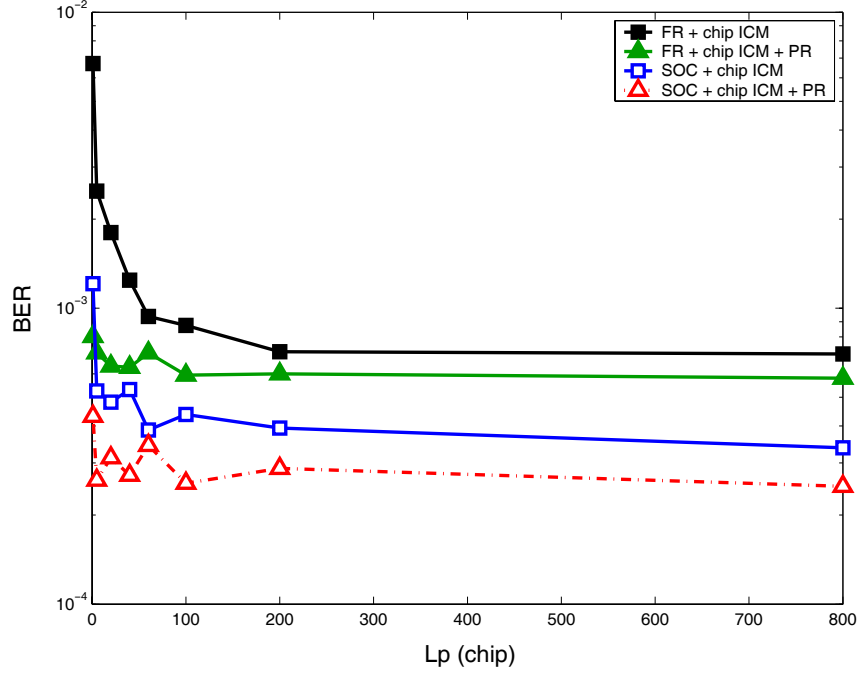


Figure 4.8. The effect of interleaver size  $L_p$  on the bit error rate of UWB-IR systems with SOC coding and FR in CM3 channel scenario. The values of  $E_b/N_0$  for SOC coding and FR equal 11 dB and 14 dB, respectively.

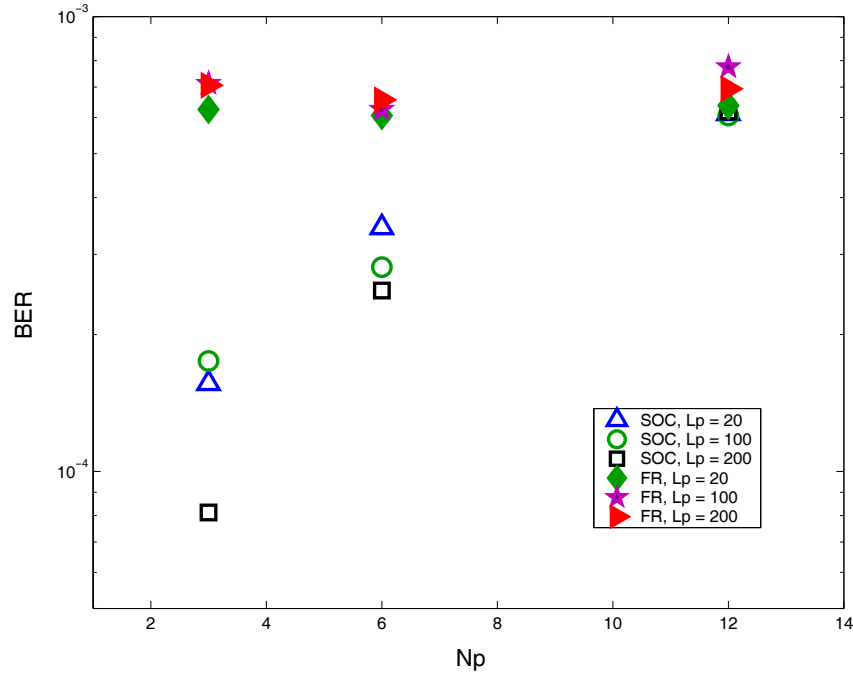


Figure 4.9. The effect of number of chips per frame on the bit error rate of UWB-IR systems with chip level ICM + PR and SOC coding with  $N_p n = \text{const.}$  or FR with  $N_p N_f = \text{const.}$  in CM3 channel scenario. The values of  $E_b/N_0$  for SOC coding and FR equal 11 dB and 14 dB, respectively.

#### 4.2.4 Results - influence of the channel parameters

In order to investigate the effects of the channel parameters on the BER performance of the UWB-IR systems, we estimate the main channel statistics. Their values averaged over an ensemble of 500 channel realizations are given in Table 4.3.

Table 4.3. IEEE UWB Channel Model Statistics.

Channel Metric	CM1	CM2	CM3	CM4	Unit
Est. mean $\bar{\tau}$	5.2	9.6	15.4	28.6	ns
Est. mean $\tau_{rms}$	5.5	8.4	14.5	25.3	ns
Est. mean $NP_{10dB}$	13.4	16.4	25.7	39.9	n/a
Est. mean $NP_{15dB}$	27.4	36.3	61.4	102	n/a
Est. mean $NP_{85\%}$	21.9	34.6	63.4	119.9	n/a
Est. mean $NP_{90\%}$	29.3	47.4	85.7	161.5	n/a
Est. mean IAT	0.34	0.31	0.19	0.17	ns

The mean number of multipath components that are within 10 dB and 15 dB of the peak multipath arrival are denoted by  $NP_{10dB}$  and  $NP_{15dB}$ , respectively. Similarly, the mean numbers of multipath components required to capture 85% and 90 % of the total channel energy are denoted by  $NP_{85\%}$  and  $NP_{90\%}$ , respectively. By rewriting (2.4), without the shadowing term  $X$ , as

$$h(t) = \sum_{i=1}^{M_t} \alpha'_i \delta(t - \tau'_i), \quad (4.24)$$

where  $M_t$  is the total number of multipath components,  $\alpha'_i$  and  $\tau'_i$  are the gain and delay of the  $i$ -th multipath component, we can determine the inter-arrival time, IAT, as  $\tau'_i - \tau'_{i-1}$ . We can also define the power decay profile that is the expected value of the magnitude squared of  $h(t)$  in (4.24) and is

$$P(t) = E[|h(t)|^2] = \sum_{i=1}^{M_t} |\alpha'_i|^2 |\delta(t - \tau'_i)|^2. \quad (4.25)$$

The RMS delay spread is the second central moment of the power decay profile and is defined as

$$\tau_{rms} = \sqrt{\overline{\tau^2} - (\bar{\tau})^2}, \quad (4.26)$$

where

$$\bar{\tau}^n = \frac{\sum_{i=1}^{M_t} \tau_i'^n |\alpha'_i|^2}{\sum_{i=1}^{M_t} |\alpha'_i|^2}; \quad n = 1, 2, \quad (4.27)$$

and the mean excess delay is  $\bar{\tau}$ . Using (4.27) in (4.26) we obtain

$$\tau_{rms} = \sqrt{\frac{\sum_{i=1}^{M_t} \tau_i'^2 |\alpha_i'|^2}{\sum_{i=1}^{M_t} |\alpha_i'|^2} - \left( \frac{\sum_{i=1}^{M_t} \tau_i' |\alpha_i'|^2}{\sum_{i=1}^{M_t} |\alpha_i'|^2} \right)^2}. \quad (4.28)$$

Fig. 4.10 and 4.11 show the BER performance improvement introduced by the ICM + PR technique in combination with FR and SOC coding, respectively. As can be observed from both figures, for the case of no ICM + PR, the BER performance is worst in the extreme NLOS scenario, CM4, that is characterized by the largest values of the mean excess delay, RMS delay spread, and mean number of significant paths, and the smallest value of the IAT (see Table 4.3). The reason lies in the fact that for high data rate transmissions, where pulses are placed close to each other, larger values of the RMS delay spread give rise to ISI and thus increase the BER. Furthermore, smaller values of the IAT indicate that multipath components are nigher which, in turn, contributes to higher IPI, and hence higher BER. The ICM + PR technique exploits the temporal diversity brought by the UWB channel through multipaths. The performance of the ICM + PR in the four channel scenarios is mutually comparable, which is mainly due to the size of the random interleavers that was chosen to ensure sufficient interleaving. In particular, in our system model, the size of the interleavers equals  $L = 400$  chips, which corresponds to a time period  $\tau_L = 66.8$  ns, whereas the maximum value of the estimated mean excess delay, among the evaluated scenarios, CM1-CM4, is  $\bar{\tau} = 28.6$  ns. We also notice that the BER performance of FR with ICM + PR in CM1 case, for values of  $E_b/N_0 < 12.5$  dB, is slightly worse ( $< 1.5$  dB difference at high BER) than that of no ICM + PR case. The reason for that is the vulnerability of FR to spreading of high energy chips, related to the earliest and strongest multipath components in the CM1 (LOS) scenario (see Fig. 2.2 and 4.15), over several frames, when the noise is high. In other words, instead of affecting only a few frames so that the FR could cope with the error correction, the errors are spread over a larger number of frames.

Fig. 4.12 and 4.13 show the cumulative distribution functions (CDFs) of the RMS delay spread and the number of significant paths,  $NP_{10dB}$ , respectively. As expected, for the case of NLOS scenarios, the mean and variance values of the statistics are larger than that of the LOS cases. Moreover, the CDFs of the RMS delay spread and the number of significant paths can be well fit by the Gaussian distribution.

Fig. 4.14 presents the received energy carried by multipath components in CM1-CM4. We observe that for the LOS scenario CM1, the first multipath component carries substantial amount energy. This phenomena does not occur in NLOS scenarios for which the energy is spread over many paths with the earliest ones carrying little energy.

Fig. 4.15 illustrates the average power decay profiles, showing, among others, that in CM1 the -10 dB energy is concentrated in the first several ns, while in CM4 the energy is

spread over the first 100 ns. Fig. 4.15 also constitutes an incentive, apart from the Fig. 2.2 and 2.3, for the use of a differential autocorrelation receiver instead of a RAKE receiver in the UWB-IR system for which many fingers are required to capture significant amount of energy, particularly in the NLOS scenarios with TX-RX distance larger than 4 m.

#### 4.2.5 Results - comparison with other systems

Performance of oversampled weighted autocorrelation receivers operating on multipath fading channels with the presence of ISI is presented in [88]. The presented systems with 800 MHz bandwidth and 40 Mbps data rate achieve BER value of  $10^{-4}$  at  $E_b/N_0 = 20$ -25 dB depending on the method for weighted sum combining, i.e., the maximum ratio and minimum mean square error combining. No channel coding is considered.

An uncoded UWB system with a perfect RAKE receiver operating on dense multipath fading channels with  $M$ -ary PPM is studied in [82]. It is shown that for  $M=2$  and  $SNR = 13.5$  dB, the  $BER = 10^{-4}$  can be achieved. The BER performance improves with the increase of modulation order so that for  $M = 16$  to achieve the same BER level of  $10^{-4}$  only 8.5 dB of  $SNR$  is required.

Application of equalization to frequency-domain UWB receiver is proposed in [71]. It has been shown that for uncoded UWB systems with a data rate of 15.6 Mbps, the BER of  $10^{-3}$  can be achieved at  $E_b/N_0 = 30$  dB. In the same paper, the performance of a reference UWB system with a RAKE receiver is presented. The results indicate that for the same data rate, the RAKE receiver with 100 fingers introduces significant performance improvement resulting in the 20 dB coding gain at  $BER = 10^{-3}$  level.

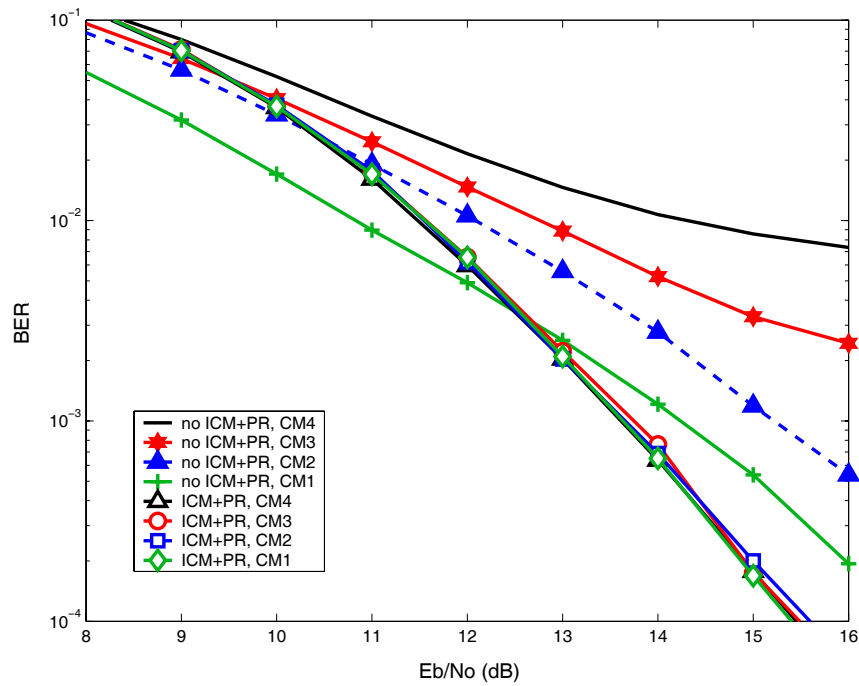


Figure 4.10. The bit error rate of UWB-IR systems with FR and with or without ICM + PR in different channel scenarios, CM1-CM4.

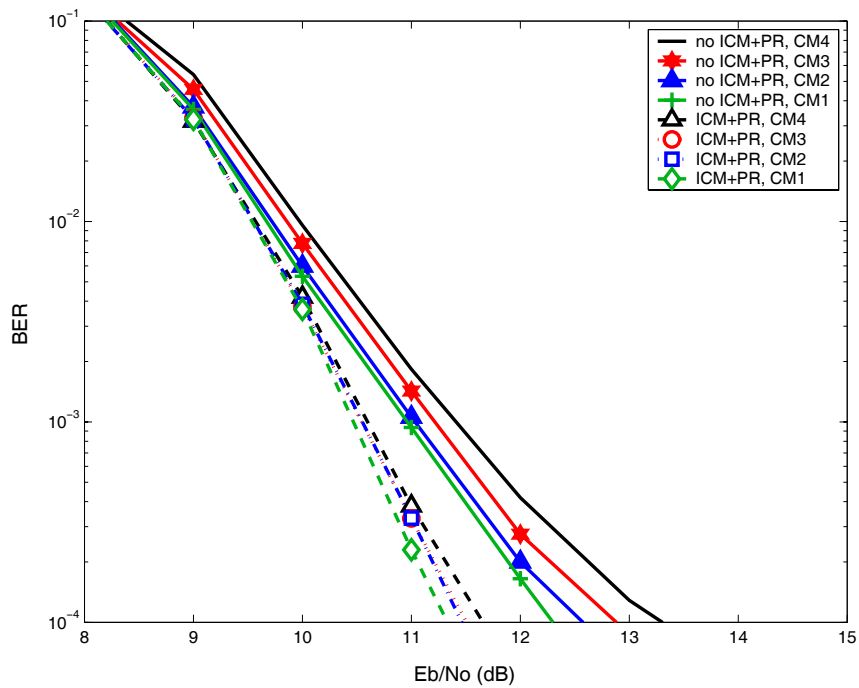


Figure 4.11. The bit error rate of UWB-IR systems with SOC coding and with or without ICM + PR in different channel scenarios, CM1-CM4.

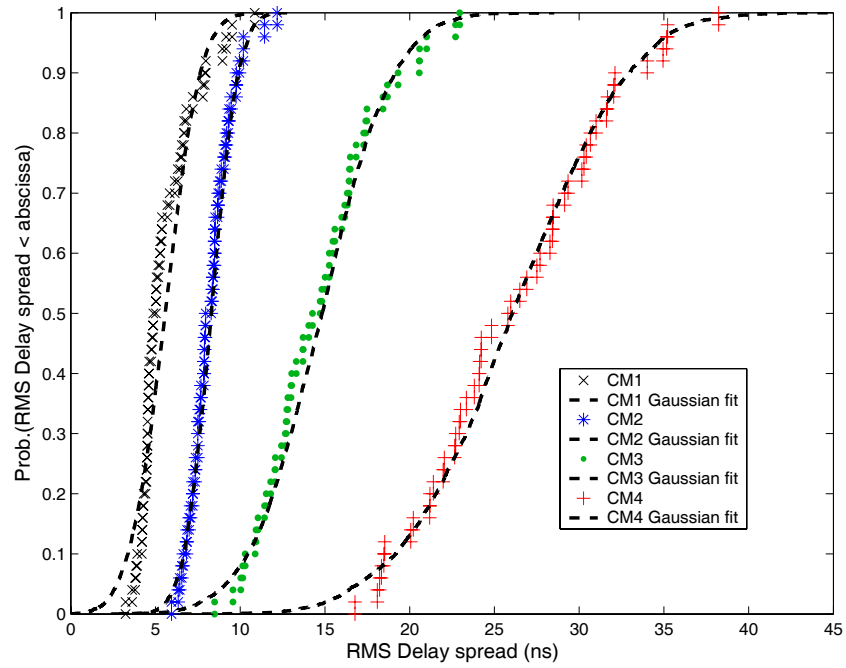


Figure 4.12. CDFs of the RMS delay spread for CM1-CM4.

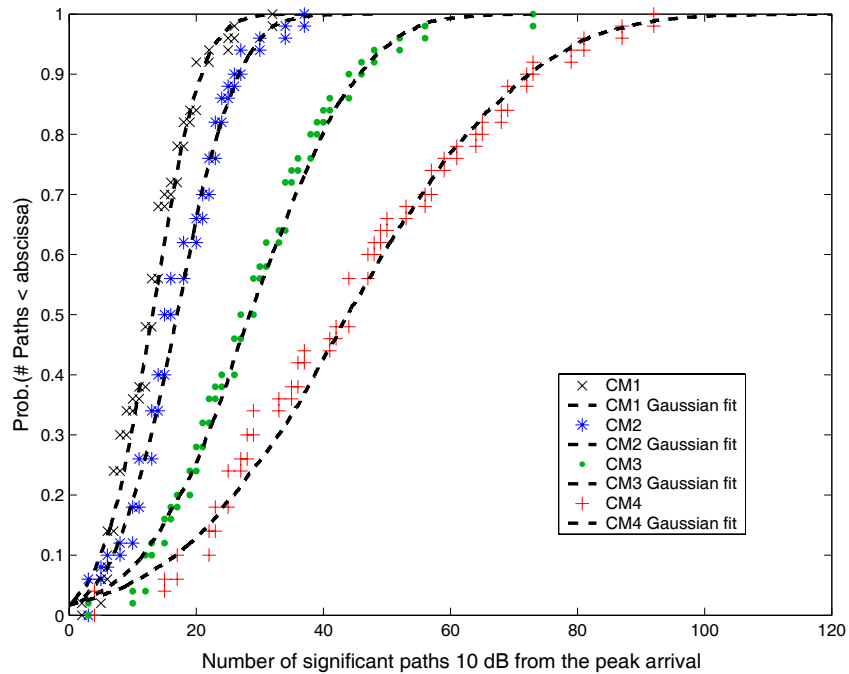


Figure 4.13. CDFs of the number of significant paths (10 dB from the peak arrival) for CM1-CM4.

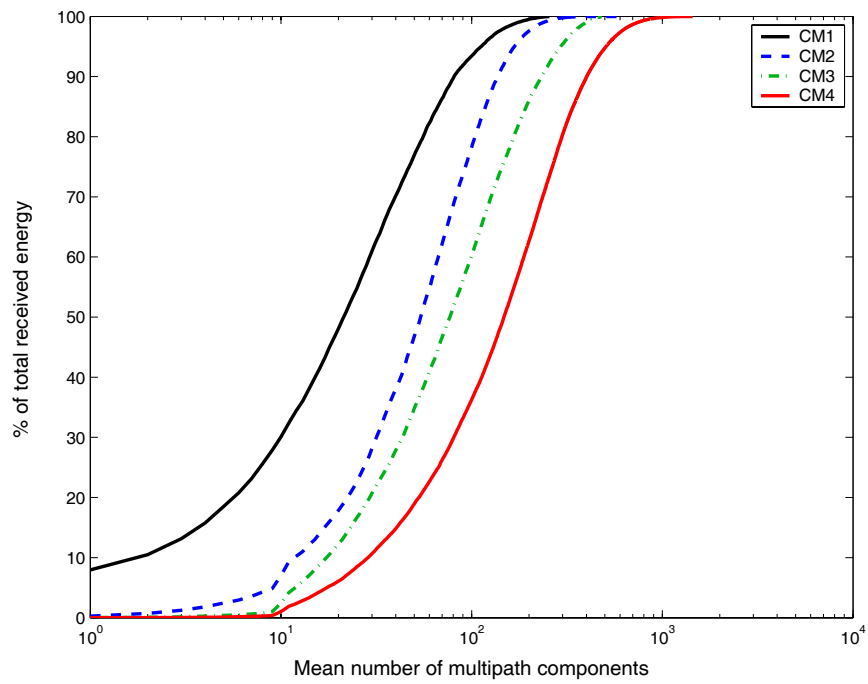


Figure 4.14. The received energy as a function of number of multipath components for CM1-CM4.

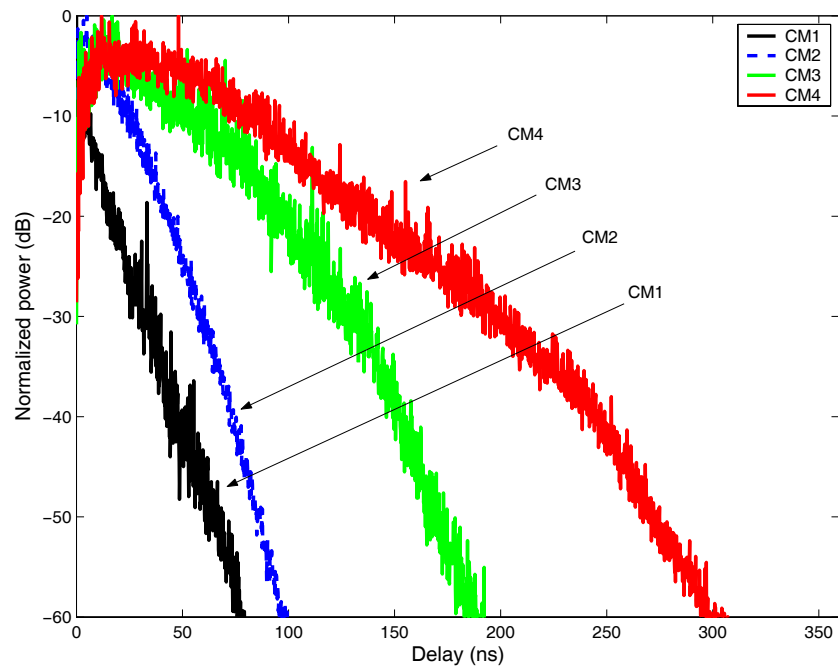


Figure 4.15. Average power decay profiles for CM1-CM4.

### 4.3 Summary

In this chapter, the bit error rate performance of UWB-IR systems operating on AWGN, IEEE 802.15.3a multipath fading, and uncorrelated multipath fading channels has been analyzed by means of theoretical bounds on the BER and intensive Monte Carlo simulations. Several scenarios have been evaluated (no ICM nor PR, ICM, PR, ICM + PR) for both single-user UWB-IR systems. It has been shown that the performance of the evaluated UWB-IR systems can be significantly enhanced if the proposed ICM or PR techniques are used. The best performing methods include chip interleaving and pulse based polarity randomization. As illustrated, altering the system parameter settings (within the considered values) does not entail major changes in the BER performance of FR-based UWB-IR systems. However, visible influence favoring low code-rate codes takes place for the case of SOC coding.

The obtained results demonstrate robustness of the ICM + PR method against multipath fading, yielding comparable BER performance irrespective of the channel scenarios under examination. On the contrary, the channel statistics have considerable influence on the BER performance of coded UWB-IR systems without ICM + PR.



# Chapter 5

## Multi-user UWB-IR systems

In this chapter, a detailed UWB-IR multi-user system model description is given. A novel design of a deterministic chip interleaver based on time-hopping hyperbolic congruence sequences is proposed. This scheme together with superorthogonal convolutional coding or frame repetition constitutes an effective method of protection against errors in scarcely populated UWB-IR systems operating in severe multipath interference prone environments. In this chapter, we evaluate the bit error rate performance of UWB-IR systems operating on multipath fading channels with and without the proposed scheme by referring to bounds based on the Poisson distribution and intensive Monte Carlo simulations.

This chapter is organized as follows. Section 5.1 presents a multi-user UWB-IR system model architecture. In Section 5.2 design of a chip interleaver based on time-hopping hyperbolic congruence sequences is presented. Furthermore, the main parameters of the random and hyperbolic interleavers are reviewed. In the next sections, the bit error rate performance of considered the scarcely populated UWB-IR systems is evaluated. In Section 5.3, bounds on the bit error probabilities of scarcely populated UWB-IR systems are derived. In Section 5.4, the results of Monte Carlo simulations are presented. Section 5.5 concludes this chapter.

### 5.1 System model

In this section, a multi-user UWB-IR system model is presented. In the subsequent sections, we refer to the description of the UWB-IR system model presented in Section 2.1 with the following exceptions:

- Before the application of chip interleaving  $\Pi_p$ , pulses are grouped at the beginning of every modulation symbol  $b_i$ . This insures orthogonality of the users' signals since

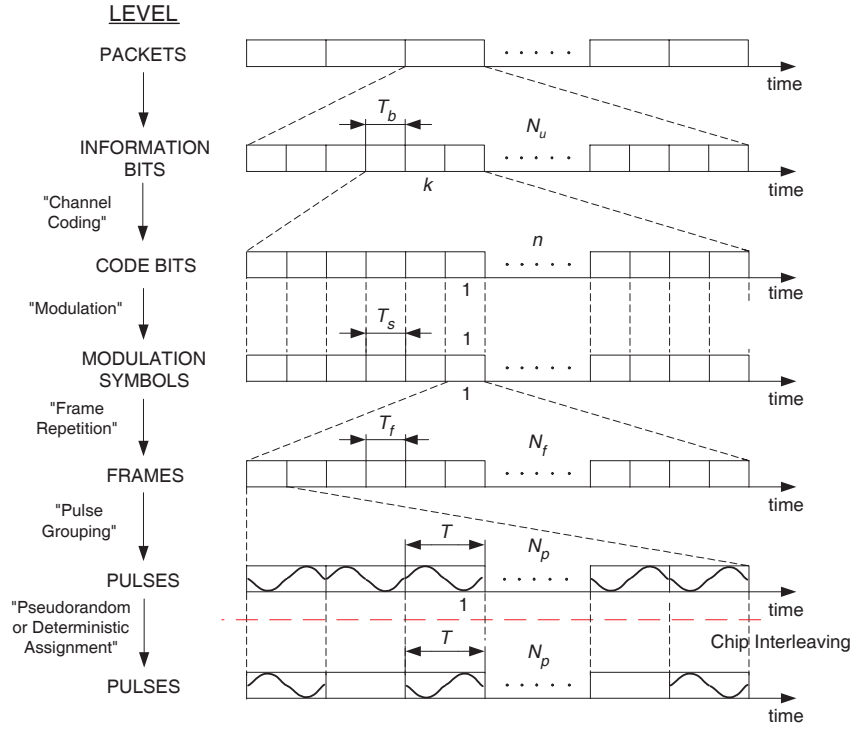


Figure 5.1. Interleaved coding-modulation scheme in a multi-user UWB-IR system.

TH-based chip interleaving will be operating on the same initial conditions for every user.

- Polarity randomization is not considered here, thus  $p_i = 1, \forall i \in \{0, 1, \dots, N-1\}$ , where  $N$  is the total number of chips in the data packet.
- Bit repetition is not considered here, thus only frame repetition and superorthogonal convolutional coding schemes are evaluated and compared. The reason for that is the poor BER performance of BR scheme even for single-user UWB-IR systems.
- Information bit, code bit, and frame interleaving schemes are not considered here. Our intention is to provide the highest level of time diversity that can be obtained by application of chip interleaving.
- At the receiver side, in order to further improve the BER performance, a time-filtering operation is performed.

### 5.1.1 UWB-IR Transmitter

The interleaved coding-modulation together with a pulse grouping operation concept are shown in Fig. 5.1.

Generation of the transmitted signal waveform for one data packet is performed in the following way. A sequence of  $N_u$  information bits  $\mathbf{u} = (u_0, u_1, \dots, u_{N_u-1})$  is encoded according to the selected encoding function  $\varphi$  resulting in a code bit sequence  $\mathbf{d} = \varphi(\mathbf{u}) = (d_0, d_1, \dots, d_{N_d-1})$ , where  $N_d$  denotes the number of code bits/modulation symbols in a packet. The considered modulation is of order one. A bijection  $\varphi$  transforms a block of  $k$  bits into a block of  $n$  bits. In general,  $\varphi(\mathbf{x})$  is a sequence obtained by partitioning the sequence  $\mathbf{x}$  into subsequences of length  $k$  and applying  $\varphi$  on every subsequence. For a special case, when  $k = n (= 1)$ ,  $\varphi(\mathbf{x}) = \mathbf{x}$  and hence there is no channel coding. Code bits  $d_i$  are fed into a differential autocorrelator  $b_i = b_{i-1}(1 - 2d_i)$ ,  $\forall i \in \{0, 1, \dots, N_d - 1\}$  which delivers a sequence of modulated symbols  $\mathbf{b} = (b_0, b_1, \dots, b_{N_d-1})$ , where  $N_d$  can be calculated as  $N_d = \frac{n}{k} N_u$ .

The next operation is pulse grouping that results in a sequence  $\tilde{\mathbf{s}} = (\tilde{s}_0, \tilde{s}_1, \dots, \tilde{s}_{N-1})$ , where  $\tilde{s}_l = b_i$ , if  $iN_f N_p \leq l \leq iN_f N_p + N_f - 1$ ,  $\forall i \in \{0, 1, \dots, N_d - 1\}$ , and  $\tilde{s}_l = 0$  otherwise. The number of frames per modulation symbol is  $N_f$ , whereas the number of chips per frame is denoted by  $N_p$ . The pulse grouping operation boils down to placing pulses at the beginning of every modulation symbol  $b_i$ . This insures orthogonality of the users' signals before passing them through the channel since chip interleaving will be operating on the same initial conditions for every user.

The following step is chip interleaving  $\Pi_p : x \rightarrow \Pi_p(x)$ , where the size of the interleaver is denoted by  $L_p$ . The mapping  $\Pi_p$  is user-dependent. In general, a sequence  $\Pi_p(\mathbf{x})$  is obtained by partitioning sequence  $\mathbf{x}$  into subsequences of length  $L_p$  and applying  $\Pi_p$  on every subsequence. Here,  $\Pi_p$  is applied on the sequence  $\tilde{\mathbf{s}}$  yielding a sequence of interleaved chips  $\tilde{\mathbf{v}} = \Pi_p(\tilde{\mathbf{s}}) = (\tilde{v}_0, \tilde{v}_1, \dots, \tilde{v}_{N-1})$ . As compared with Section 2.1, polarity randomization is not considered here. The transmitted signal waveform for one data packet from user  $\kappa$  is thus given by

$$s_t^{(\kappa)}(t) = \sum_{i=0}^{N-1} \tilde{v}_i^{(\kappa)} w(t - iT_w), \quad (5.1)$$

where  $w(t)$  denotes the transmitted pulse of duration  $T_w$ .

### 5.1.2 UWB-IR Receiver

The modeled UWB-IR receiver architecture is shown in Fig. 5.2. The received signal over a multipath fading channel in an  $U$  multi-user system can be expressed as

$$r''(t) = r''^{(1)}(t) + I(t) + n(t), \quad (5.2)$$

where  $r''^{(1)}(t)$  is the useful signal corresponding to the user 1 and is given by

$$r''^{(1)}(t) = A_1 s_t^{(1)}(t) * g^{(1)}(t) * h^{(1)}(t) \quad (5.3)$$

and  $I(t)$  is the multi-user interference term expressed as

$$I(t) = \sum_{\kappa=2}^U A_{\kappa} s_t^{(\kappa)}(t) * g^{(\kappa)}(t) * h^{(\kappa)}(t), \quad (5.4)$$

and  $n(t)$  is additive white Gaussian noise. The channel impulse response of user  $\kappa$  is denoted by  $h^{(\kappa)}(t)$ . In our system model, we assume perfect power control, i.e., the signal amplitudes satisfy  $A_1 = A_2 = \dots = A_{\kappa} = \dots = A_U$ . Furthermore, we assume that the impulse responses of the front-ends of every user's transceiver are the same, i.e.,  $g^{(1)}(t) = g^{(2)}(t) = \dots = g^{(\kappa)}(t) = \dots = g^{(U)}(t)$ .

The received sequence for one data packet may be expressed as  $\mathbf{r}'' = (r''_0, r''_1, \dots, r''_{N-1})$ , where  $r''_i$  is the waveform  $r''(t)$  on the interval  $[iT_w, (i+1)T_w]$ . The first operation upon receiving the signal is chip deinterleaving,  $\Pi_p^{-1}(\mathbf{r}'')$  yielding a sequence  $\mathbf{z} = \Pi_p^{-1}(\mathbf{r}'') = (z_0, z_1, \dots, z_{N-1})$ . Next, pulse de-grouping and time-filtering operations are performed resulting in the sequence  $\check{\mathbf{z}} = (\check{z}_0, \check{z}_1, \dots, \check{z}_{N-1})$ , where  $\check{z}_l = z_{iN_f N_p + m} \delta_{m, c_j}$ ,  $\forall 0 \leq l \leq N-1$ ,  $\forall 0 \leq i \leq N_d-1$ , and  $\forall 0 \leq m \leq N_p-1$ , where  $\delta_{i,j} = 1$  if  $i = j$ , and  $\delta_{i,j} = 0$  if  $i \neq j$ . The pseudorandom assignment code used to distinguish the users and known at the receiver is  $\mathbf{c} = (c_0, c_1, \dots, c_{N_f-1})$  with values  $c_i \in \{0, 1, \dots, N_p-1\}$ ,  $\forall i$ . It is important to notice that the time-filtering operation boils down to selecting these chips from the sequence  $\mathbf{z}$  that originally carried pulses at the transmitter side. The rest of the chips in the sequence  $\mathbf{z}$  are zero padded. The result of deinterleaving is fed to the demodulator that correlates the signal with its symbol-delayed version as

$$\hat{y}_i = \int_{iT_s}^{iT_s+T_s} \tilde{z}(t) \tilde{z}(t - T_s) dt, \quad (5.5)$$

where  $i$  is the symbol index and  $\tilde{z}$  is a subsequence of  $\check{\mathbf{z}}$  with length  $N_f N_p$  corresponding to one symbol of duration  $T_s$ . In our system setup, for the case of FR, a resulting sequence of real values written as  $\hat{\mathbf{y}} = (\hat{y}_0, \hat{y}_1, \dots, \hat{y}_{N_d-1})$  is passed through a threshold detector yielding a sequence of binary values  $\hat{\mathbf{y}}_{\mathbf{b}} = [-\mathbf{1} \cdot \hat{\mathbf{y}}]$ , where  $[x]$  is equal to 1 for  $x > 0$  and 0 for  $x \leq 0$ . For the case of SOC coding, the sequence of real values  $\hat{\mathbf{y}}$  is fed directly to the soft-input Viterbi decoder. In general, the sequence  $\hat{\mathbf{y}}_{\mathbf{b}}$  is decoded with a decoding function  $\psi(\hat{\mathbf{y}}_{\mathbf{b}})$  yielding a decoded bit sequence  $\hat{\mathbf{u}} = (\hat{u}_0, \hat{u}_1, \dots, \hat{u}_{N_u-1})$ .

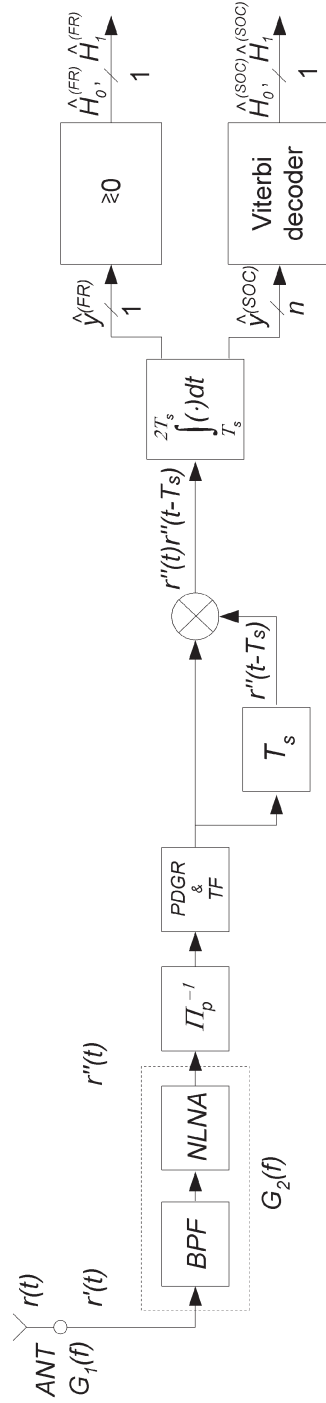


Figure 5.2. Diagram showing the modeled UWB-IR receiver architecture considered in a multi-user scenario. The acronyms PDGR and TF denote pulse de-grouping and time filtering operations, respectively.

## 5.2 Chip interleaver design based on TH sequences

Orthogonal sequencing is employed in the design of the chip interleaver whose purpose is to intersperse the pulses corresponding to all users for all the symbols transmitted. A unique sequence indicating the reordering mapping of the chips periodically repeated for the whole data packet is assigned to each user. However, unlike in conventional time-hopping applications, pulses dispersed through interleaving are generally not in time consecutive order. This introduces time diversity allowing for spreading of bursty errors caused by fading over several code words. Both time and frequency hopping codes may be used for this application, provided that they adhere to the following constraints:

- Each sequence consists of unique values required for the interleaver's one-to-one mapping operation.
- High level of orthogonality between the sequences is ensured to avoid catastrophic collisions and minimize the multi-access interference.

For the purpose of our analysis, we have chosen hyperbolic congruence and random sequences. The former are known to have very good auto- and cross-correlation properties [70] and a defined structure that can be easily implemented in the system. Interleavers based on the latter, however, provide good BER performance but lack of compact representation.

### 5.2.1 Hyperbolic congruence sequence design

The placement operator is defined as [60]

$$\Upsilon(i) = \frac{a}{i} \pmod{p'}, \quad 1 \leq a, i \leq p' - 1, \quad (5.6)$$

where  $p'$  is a prime number,  $a$  is the sequence index, and  $i$  is the sequence element index. The cardinality of the set of sequences equals  $p' - 1$ .  $1/i$  is the unique inverse of  $i$  in the Galois field  $\text{GF}(p')$  and can be calculated as [50]

$$\frac{1}{i} = i^{p'-2} \pmod{p'}. \quad (5.7)$$

### 5.2.2 Interleaver properties

In the following, we review the main interleaver parameters. We distinguish key parameters determining time diversity introduced by the interleaver, i.e., delays, dispersion, and the input-output separation spectrum. The error spreading properties of the interleaver are represented by spread, whereas cross-correlation properties between any two sequences are characterized by the Hamming correlation.

Table 5.1. Example of Operation of an Interleaver.

i	1	2	3	4	5	6	...	400
$\Pi(i)$	5	1	8	10	3	2	...	100
$\Delta(i)$	-4	1	-5	-6	2	4	...	300

### Delays

The delay function of an interleaver,  $\Delta(i)$ , is defined as

$$\Delta(i) = i - \Pi(i), \quad \forall i \in \mathbf{Z}, \mathbf{Z} = \{1, 2, \dots, L_p\}. \quad (5.8)$$

The interleaver operation can thus be described as

$$y(i) = x(i - \Delta(i)). \quad (5.9)$$

An example of operation of an interleaver is shown in Table 5.1. The minimum delay is defined as

$$\Delta_{min} = \inf_{i \in \mathbf{Z}} \Delta(i), \quad (5.10)$$

whereas the maximum delay is

$$\Delta_{max} = \sup_{i \in \mathbf{Z}} \Delta(i). \quad (5.11)$$

The characteristic delay is given by

$$\tilde{\Delta} = \Delta_{max} - \Delta_{min}. \quad (5.12)$$

### Dispersion

The randomness of an interleaver can be measured by the dispersion parameter. The normalized dispersion is given by [97]

$$\begin{aligned} \gamma = & |\{(\Delta_x, \Delta_y) | \Delta_x = j - i, \Delta_y = \Pi(j) - \Pi(i), \\ & 1 \leq i < j \leq L_p\}|(L_p(L_p - 1)/2), \end{aligned} \quad (5.13)$$

where the cardinality of a set is denoted by  $|\cdot|$ . A low value of dispersion means that the interleaver is very regular. The smallest value of the dispersion is achieved by the identity permutation. The maximum dispersion value of  $\gamma = 1$  is achieved by interleavers based on Costas arrays [97].

## Spread

The spread of an interleaver is a measure of the distance between interleaved symbols that were "close" to each other before interleaving. The design of an interleaver characterized by the square spread parameter  $S$  guarantees that if two input symbols to the interleaver  $\Pi$  are within a distance  $S_1$ , they cannot be mapped in such a way that a distance between the output symbols is less than  $S_2$ , and usually  $S_1 = S_2 = S$  [21]. Thus considering two indices  $i$  and  $j$  such that

$$0 < |i - j| \leq S \quad (5.14)$$

the design imposes that

$$|\Pi(i) - \Pi(j)| \geq S. \quad (5.15)$$

Recently, a slight modification of the above definition was proposed that refers to the triangular spread. Since spread parameters of the interleavers considered here equal 1, we will not introduce the new definition here. An interested reader is advised to study [20].

## Hamming Correlation

The Hamming cross-correlation returns the number of coincidences or hits, between the sequences for relative time delay  $\tau$  and is given by

$$\lambda_{\tilde{a}, \tilde{b}}(\tau) = \sum_{i=0}^{L_p-1} \tilde{a}_i \circ \tilde{b}_{i+\tau}, \quad (5.16)$$

where  $\tilde{a}$  and  $\tilde{b}$  are two sequences of an interleaver and

$$\tilde{a}_i \circ \tilde{b}_{i+\tau} = \begin{cases} 0, & \text{if } \tilde{a}_i \neq \tilde{b}_{i+\tau} \\ 1, & \text{if } \tilde{a}_i = \tilde{b}_{i+\tau}. \end{cases} \quad (5.17)$$

Please note that in (5.16) and (5.17), the sequence  $\tilde{b}$  is being circularly shifted with a relative time delay  $\tau$ . For hyperbolic and random sequences the normalized Hamming cross-correlation is given by

$$\bar{\lambda} = \frac{1}{L_p} \sum_{\tau=0}^{L_p-1} \lambda_{\tilde{a}, \tilde{b}}(\tau). \quad (5.18)$$

The mean value of normalized Hamming cross-correlation of the sequences examined here equals  $\bar{\lambda} \simeq 2.5 \cdot 10^{-3}$  indicating on average one hit for the whole sequence length  $L_p = 400$ . We have also calculated the average mean square aperiodic correlation functions defined in [73] and for all of the sequences investigated here, the values were similar.



Table 5.2. Interleaver Parameters.

Interleaver	$L_p$	$\overline{\Delta_{min}}$	$\overline{\Delta_{max}}$	$\overline{\tilde{\Delta}}$	$\bar{S}$	$\bar{\gamma}$
Random	400	-372.4	384.6	757	1	0.81
Hyperbolic	400	-367.8	382.8	750.6	1	0.65

### Input-Output Separation Spectrum

Fig. 5.3 and 5.4 present the input-output separation spectra (IOSS) of a random and hyperbolic interleaver, respectively. These graphs represent two-dimensional histograms with the axes being the separation for all possible element-pairs at the input and output of the interleaver. The IOSS indicates the level of randomness of an interleaver since the fewer the possible combinations of the element-pairs, the more structured the interleaver is. As can be observed from Fig. 5.3 and 5.4, the IOSS of the two considered interleavers look similar, however, with slight superiority with respect to the randomness level of the random interleaver. The parameters of interleavers under examination averaged over five realizations are gathered in Table 5.2. We observe small differences in values of the delay functions. Furthermore, the value of the dispersion of a random interleaver is larger indicating the higher level of randomness of this type of interleaver. This fact is also visible when comparing Fig. 5.3 with 5.4. The spread of the two considered types of interleavers equals one.

In the following sections, we evaluate the bit error rate performance of multi-user UWB-IR systems operating on IEEE 802.15.3a multipath fading channels by referring to bounds based on the Poisson distribution and intensive Monte Carlo simulations.

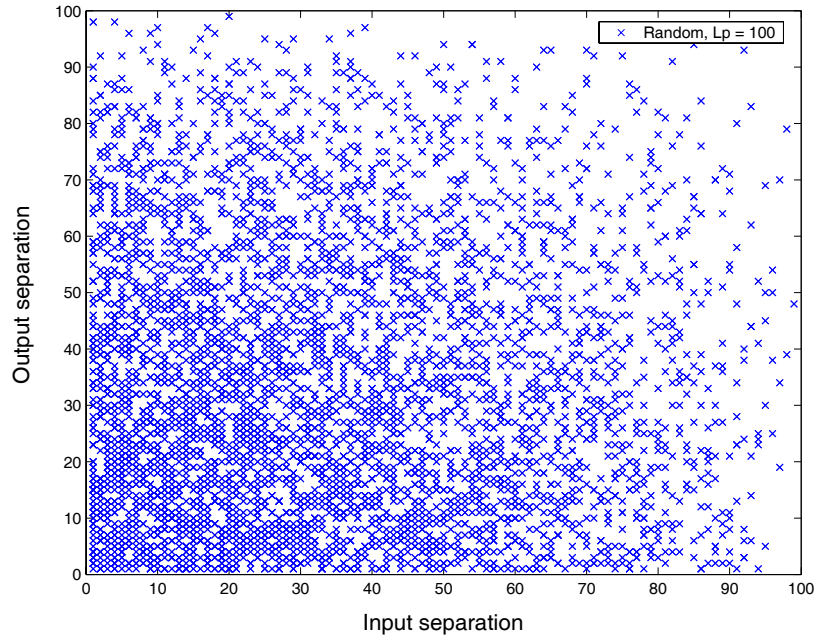


Figure 5.3. The input-output separation spectrum of a random interleaver with  $L_p = 100$ .

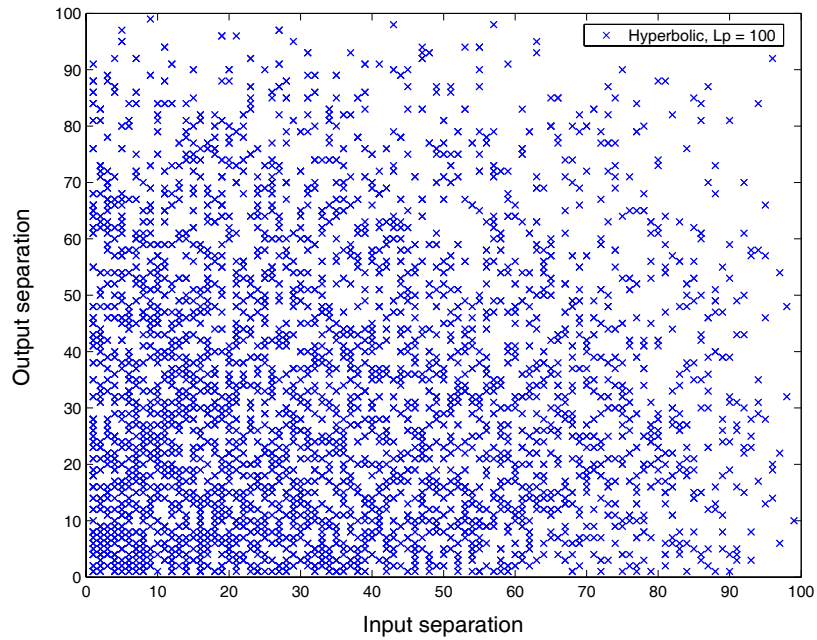


Figure 5.4. The input-output separation spectrum of a hyperbolic interleaver with  $p' = 101$ ,  $a = 1$ , and  $L_p = 100$ . A random circular shift is applied.

### 5.3 Bounds on the bit error probabilities

In this section, we derive a bound on the BER for scarcely populated multi-user UWB-IR systems when the effects of the AWGN are neglected ( $E_b/N_0$  tends to infinity) and the only source of errors are pulse collisions due to simultaneous transmission of signals corresponding to different users. In the following, we assume that the channel model is a binary symmetric channel (BSC) with the crossover probability  $p$  and that hard decision decoding is being performed at the receiver. We also assume that a pulse inter-arrival process is a Poisson process. Such an assumption allows us to relate the pulse collisions probability to the ALOHA collision probability, when the information unit is the pulse instead of the packet.

The probability that there are exactly  $\rho$  occurrences in a Poisson process is

$$P(X = \rho) = \frac{e^{-\lambda} \lambda^\rho}{\rho!}, \quad (5.19)$$

where  $\lambda$  is a positive real number equal to the expected number of occurrences that take place during a given interval. For the case of zero collisions,  $\rho = 0$ , one may write

$$P(X = 0) = e^{-\lambda}. \quad (5.20)$$

However, since a vulnerable interval equals to two time windows, which corresponds to the unslotted ALOHA case, the probability of a successful transmission is

$$P_1 = e^{-2\lambda}. \quad (5.21)$$

The pulse arrivals in a multi-user scenario are modeled by a Poisson process with the pulse arrival rate  $\lambda$  that equals to

$$\lambda = \lambda'(U - 1), \quad (5.22)$$

where  $\lambda'$  is the pulse arrival rate for a single-user UWB-IR system and  $\lambda' = T'_w/T_f$  with  $T'_w$  denoting the effective pulse duration in which the most pulse energy is concentrated and  $T_f = N_p T_w$  being the mean time between the pulses (frame time). We can write that

$$\lambda = \frac{T'_w}{T_f}(U - 1). \quad (5.23)$$

The resulting pulse collision probability can be expressed as

$$P_{col} = 1 - P_1 = 1 - e^{-2(U-1)\frac{T'_w}{T_f}}. \quad (5.24)$$

The crossover probability is

$$p = \frac{P_{col}}{2}, \quad (5.25)$$

where a division by two is performed to account for constructive effects of the pulse collisions.

### 5.3.1 Frame Repetition

In our UWB-IR system model an information bit / modulation symbol is represented by  $N_f$  frames each containing one pulse. Assuming that an information bit error occurs when more than or equal to  $N_f/2$  pulses are in error, the bit error probability is given by

$$P_b = \sum_{i=\lceil \frac{N_f}{2} \rceil}^{N_f} \binom{N_f}{i} p^i (1-p)^{N_f-i}, \quad (5.26)$$

where the  $\lceil x \rceil$  denotes the smallest integer not less than  $x$ .

Fig. 5.5 shows calculated upper bounds on the BER for different sets of UWB-IR system parameters, i.e.,  $N_f$  and  $N_p$  when frame repetition is applied. The data rates for the considered parameter settings are the same. We observe that for a two-user scenario, the best performance is achieved when a single information bit is represented by 8 pulses with 5-empty-chips-long separation ( $N_p = 6$ ), whereas for higher number of active users, i.e. when  $U > 3$ , lowering the number of pulses and at the same time increasing the number of empty chips yields better BER results. Explanation of this phenomenon lies in the fact that increasing the number of empty chips and thus time separation between the pulses lowers the pulse collision probability, since more pulses can be placed within the frame without causing any collisions. On the other hand, when  $U < 3$ , it is better to insure the correction capability introduced by a reasonable number of frames (here  $N_f = 8$ ), so that the possible errors caused by pulse collisions can be eliminated. Interestingly, the BER curves do not approach 1 nor 0.5 when  $U \rightarrow \infty$ , although the crossover probability  $p$  tends to 0.5 value. It is due to the fact that when  $p \rightarrow 0.5$  and is plugged into (5.26), then depending on  $N_f$ ,  $P_b \rightarrow 0.6875$ , 0.63672 or 0.59819, for  $N_f = 4, 8$ , and 16, respectively.

### 5.3.2 SOC Coding

The bit error rate performance may be bounded by the known union upper bound [80]. However, due to obtained large values of the crossover probability,  $p > 0.1$  for  $U > 1$ , this bound becomes unacceptably loose. A bit error rate analysis based on this bound might be appropriate when the data rate of the considered UWB-IR systems is much smaller or/and channel conditions are better (e.g. no multipath fading, ISI, nor IPI present) so that the crossover probability is much smaller than 0.1.

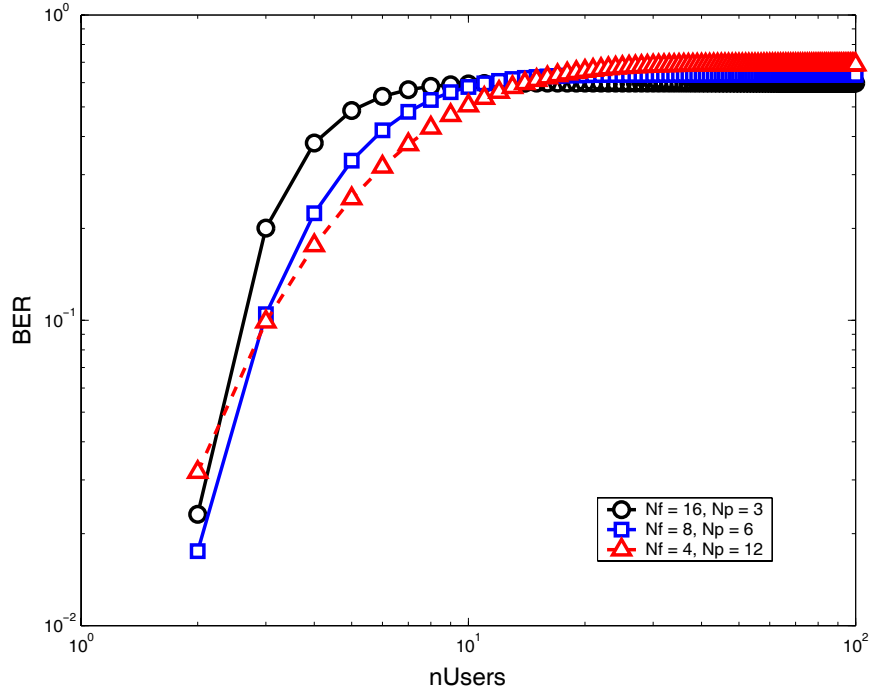


Figure 5.5. Bounds on the BER of UWB-IR systems with FR and without ICM for different system parameter settings  $N_f$  and  $N_p$ . We set  $T'_w = T_w = 0.167$  ns that allows to capture 100% of the pulse energy.

## 5.4 Simulation results - interleaving in scarcely populated UWB-IR systems

In this section, the BER performance of multi-user UWB-IR systems using SOC coding and FR is evaluated by using Monte Carlo simulations. The assumptions made during simulations are the same as listed in Section 4.2. Channel model scenario CM3 characterizing a NLOS transmission is considered.

The performance of scarcely populated high data rate (125Mbps) UWB-IR systems with hyperbolic congruence sequence based chip interleaving is evaluated through Monte Carlo simulations with 40 independent channel realizations and 2000 information bits in every packet. For every channel realization a unique sequence is assigned to the intended user in order to eliminate performance dependence on the selected sequences and average the results. For interferers, the value of  $a$  determining the sequence is pseudorandomly chosen from the set  $\{1, 2, \dots, U - 1\}$ . In order to model a situation that takes place often in practice that none of the users starts its transmission at the same time as the others, a random circular shift is added to the sequences. Perfect power control is assumed, i.e., powers of the signals corresponding to every active user are equal. The data rates of the considered synchronous

UWB-IR systems are identical and the bandwidth expansions introduced by SOC coding and FR are equal.

Fig. 5.6 and 5.7 show the BER performance of scarcely populated UWB-IR systems with and without the ICM technique when the total number of users  $U = 1, 2, 3$ , or  $4$ . As can be seen from both figures, the best BER performance is achieved when there is only one active user in the system. Increasing the number of active users worsens the BER. For  $U > 1$ , when  $E_b/N_0$  values are high, Fig. 5.6 and 5.7 reveal an error floor indicating that the performance is determined by the MUI, ISI, and IPI types of interference rather than the noise. The only exception is an  $U = 2$  multi-user UWB-IR system with ICM and SOC coding applied, for which, for the BER range as in the figures, we do not observe the error floor. For the parameter setting as in our system model, i.e., the number of chips per frame,  $N_p = 6$ , the length of the SOC code,  $n = 8$ , and the number of frames per symbol,  $N_f = 8$ , the maximal number of users is 6. However, when considering target BER values lower than  $10^{-2}$ , we notice that the maximal number of users served by the UWB-IR system with the ICM technique and SOC coding or FR applied is 3 or 2, respectively. This observation may suggest that for multi-user scenarios with high data rate transmissions ( $>100\text{Mbps}$ ) over multipath fading channels, channel codes much stronger than SOC are required, especially for UWB-IR systems based on a single delay branch differential autocorrelation receiver. As illustrated in both figures, for a single-user scenario, the coding gain introduced by the ICM technique is about 1 dB at the  $10^{-4}$  BER level. When  $U > 1$ , we observe larger coding gain, however, at the higher BER values. The time-filtering operation performed at the receiver introduces a significant improvement in the BER performance that may be visible when comparing Fig. 5.6 and 5.7 with Fig. 4.5. For both methods of protection against errors, i.e., SOC coding and FR, hyperbolic and random chip interleaving yield similar BER performance. This phenomenon has its roots in similar values of interleaver parameters. Moreover, for both interleaver types, the most important parameter, i.e., spread equals  $S = 1$ . It is imperative to point out here that interleavers based on hyperbolic congruence sequences do not have major drawbacks of random interleavers, i.e., lack of compact representation that could lead to simple implementation and lack of adequate analysis. Fig. 5.8 presents a comparison of the derived bound on the BER and actual BER performance obtained from simulations for the case of no ICM technique applied. When the number of active users  $U = 2$ , the bound provides a good approximation of the BER. However, for  $U = 3$  and high values of the BER, the bound becomes loose, which can be noticed as an offset that is due to the inaccuracy of the modeling of MUI by the Poisson process.

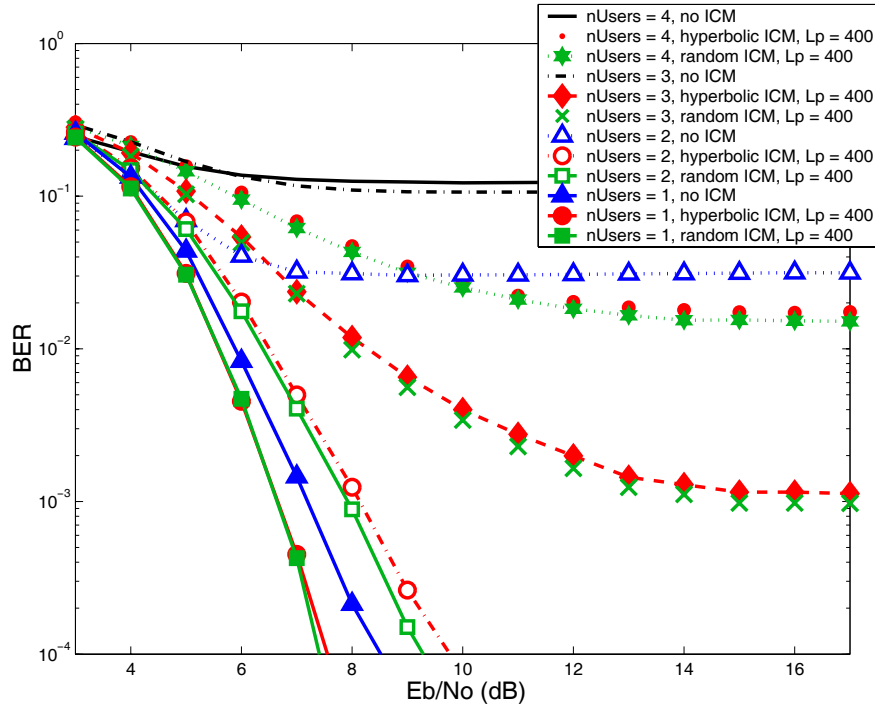


Figure 5.6. The bit error rate of UWB-IR systems with SOC coding and with or without ICM. Two types of length  $L_p = 400$  sequences considered, namely hyperbolic and random.

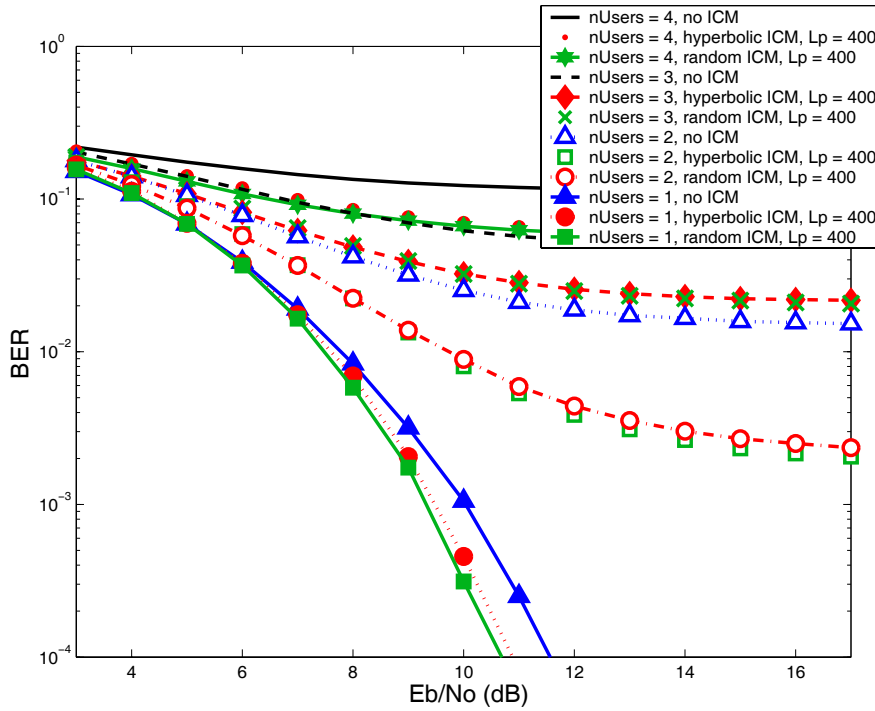


Figure 5.7. The bit error rate of UWB-IR systems with FR and with or without ICM. Two types of length  $L_p = 400$  sequences considered, namely hyperbolic and random.

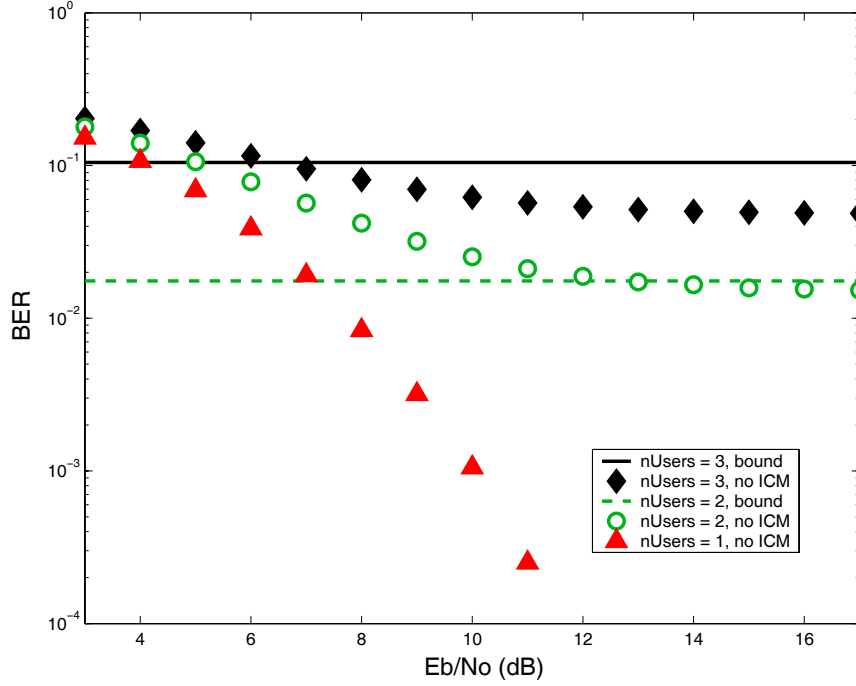


Figure 5.8. The bit error rate of UWB-IR systems with FR and without ICM - bounds and simulation results.

## 5.5 Summary

In this chapter, a multi-user UWB-IR system model architecture is presented. A particular focus has been given to the design of a chip interleaver applied in scarcely populated UWB-IR systems that has good correlation and randomness properties and a defined architecture.

Our contribution includes the design of the chip interleaver based on time-hopping hyperbolic congruence sequences and its main parameters determination. Comparing to the random interleavers, the proposed deterministic chip interleavers yielding similar BER performance, have the advantage of simpler implementation.

Moreover, in this chapter, the bit error rate performance of scarcely populated UWB-IR systems operating the IEEE 802.15.3a multipath fading has been characterized. Our results indicate that the application of the ICM technique based on the proposed chip interleaver improves the BER performance and comparing to random interleavers studied in Chapter 4, has the advantage of simpler implementation. The presented Poisson-based theoretical analysis may be helpful in a rough approximation of the BER performance of UWB-IR systems operating on correlated channels (when no chip interleaving is applied). For such cases, the Poisson assumption exemplifies the worst case scenario.



# Chapter 6

## UWB-IR based Body Area Networks

In this chapter, a concept of application of the UWB-IR technology in the realization of a body area network (BAN) is presented. The effects of the UWB propagation channel around the body are taken into account. The bit error rate performance is evaluated by means of Monte Carlo simulations.

This chapter is organized as follows. In Section 6.1, an introduction to the concept of body area networks is presented. Main features, topologies, and applications of BANs are discussed. Moreover, typical network topologies for the BANs are briefly mentioned. The introduction ends with the list of technical challenges that are related to the development of BANs. Sections 6.2.1 and 6.2.2 deal with the system model and channel model for a BAN, respectively. In Section 6.3, the results of Monte Carlo simulations for BAN based on the UWB-IR technology are provided. Section 6.4 summarizes this chapter.

### 6.1 Introduction

Healthcare will be facing major challenges in the near future due to population aging and rapid increase of care costs worldwide. Since the beginning of recorded human history young children have outnumbered elderly people. Very soon this will change. For the first time in history people age 65 and over will outnumber children under age 5. This trend is emerging around the globe.

According to U.S. Census Bureau projections, a substantial increase in the number of elderly people in the U.S. will occur during the 2010 to 2030 period. "The older population in 2030 is projected to be twice as large as in 2000, growing from 35 million to 72 million and representing nearly 20 percent of the total U.S. population at the latter date" [44]. Europe has the highest proportion of people older than 65 which in 2007 was around 14 % of the

total population compared with 11% for North America and only 6% for Asia. It is expected that Europe will have the fastest rate of ageing over the next 50 years. It is projected that the share of elderly people in the total population in Europe will double by 2050 [65].

According to the projections in [64], by 2020 25% of the EU's population will be over 65. It is expected that spending on pensions, health and long-term care will increase by 4-8% of GDP in coming decades, with total expenditures tripling by 2050. However, older Europeans are also important consumers with a combined wealth of over 3000 billion Euro. ICT will increasingly allow elderly people to stay active and productive for longer; to continue to engage in society with more accessible online services; and to enjoy a healthier and better quality life for longer. The majority of elderly people do not enjoy the benefits of the digital age yet - low cost communications and online services that could support some of their real needs - since only 10% use the Internet. Severe vision, hearing or dexterity problems, frustrate many elderly people's efforts (21% of the over 50s) to engage in the information society.

Considering the above, it is understandable why improvements in the quality of the patient's care have recently received a lot of attention. Information and communications technologies may be instrumental in improving the patients' care and the their quality of life by means of monitoring of the vital signs at the hospital and at home. Recent advances in the area of miniaturization of the wireless sensors and Micro-Electro-Mechanical Systems (MEMS) have laid a foundation for the development of ubiquitous and pervasive human wellbeing monitoring. Connectivity among the sensors placed on or in the human body can be achieved through the body area network. Such sensors may provide information on human vital signs including temperature, blood pressure, and oxygen levels just to mention a few.

Driven by the strong demands from the medical societies and ICT industries and to harmonize activities related to the development of BANs technologies, the IEEE has set up in December 2007 the 802.15.6 standardization committee. Its main objective is to define new physical and media access control layers for wireless BANs.

### 6.1.1 Definitions

A body area network refers to the network connecting devices on or around a human body. The connected devices may include miniature life sign sensors able to collect vital information with regard to the blood pressure, glucose rate, temperature, electroencephalogram (EEG), electrocardiogram (ECG), etc. Each sensor may have its own power supply consisting of a battery or energy scavenging device. Sensors may communicate with a central node worn on the body which also acts as a gateway to the outside world. A BAN differs from the personal area network (PAN) in the operational range. A PAN is typically referred to as a network covering distances up to 10 m, whereas a BAN has much smaller operation range that is limited to the close vicinity of the human body. A BAN can consist of a number of sensors

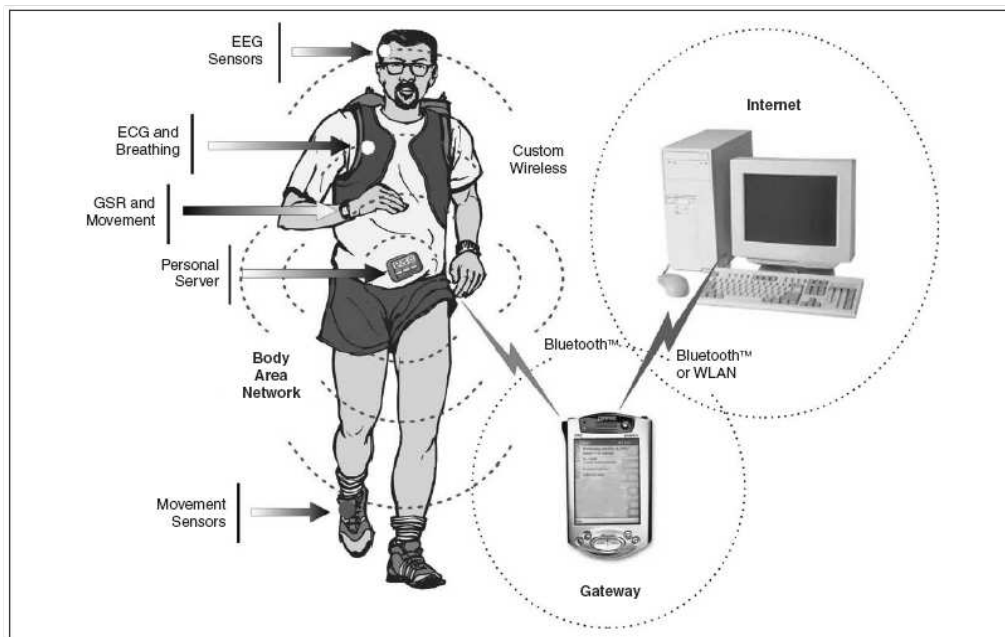


Figure 6.1. A body area network of intelligent sensors in the telemedical environment.

that may operate not only around but also inside the human body. The former type refers to the wearable BANs that are considered for both medical and non-medical applications, and the latter refers to the implant BANs that are mainly considered for medical and healthcare applications.

A vision of a body area network in the telemedical environment is shown in Fig. 6.1 [51].

### 6.1.2 Main features

Typical features of the BAN network include low transmission power, low overall power consumption, miniaturized design, and relatively low data rate over a short ( $< 2\text{m}$  distance). In order to preserve the battery power, the radio part of a BAN network may work in a burst mode with a minimal duty cycle that results in a burst data rate of up to several Mbps yet with the average data rate being several orders of magnitude lower. A distinctive feature of a BAN is also the possibility to use a human body as a propagation medium. Considering the above features, the ultra-wideband technology is a serious candidate for the physical layer of a BAN.

### 6.1.3 Applications

There is a wide range of potential applications of BANs including medical healthcare services, assistance to people with disabilities, and body interaction and entertainment [53]. A typical healthcare application scenario is patient's monitoring. To this group of applications fall monitoring of patients with chronic diseases, e.g. high blood pressure (hypertension), abnormalities of heart rhythm (arrhythmias) and diabetes. The BAN technology would allow continuous monitoring of patient's vital signs through ECG, blood pressure, and glucose level sensors that may be implanted in or attached to the human body. The potential benefits lay in the early diagnosis of the patient's at risk, prevention of the associated mortality, and reduction of the workload of nurses and thus increased efficiency of patient's management in the hospital [53]. Moreover, systems based on BANs that have the potential to detect abnormal events such as falls, losses of consciousness or unexpected behaviors that may lead to the health problems of the elderly people have been the main subject of research in the EU Confidence program. Thanks to the very fine spatial resolution (of the order of cm), the ultra-wideband technology can be a serious candidate for the underlying technology for such systems.

Another potential usage scenarios related to the healthcare include aging people support and care, home patients monitoring, and physical rehabilitation assistance. These scenarios are of high importance considering the increase in the average life expectancy and number of the elderly persons in the developed countries. The concept of ubiquitous and pervasive human wellbeing monitoring regarding the physical, physiological, and biochemical parameters has recently received a lot of attention both from academia and industry. Such monitoring giving the feedback to the caregivers, family members should be, however, unobtrusive to the elderly patients.

The last category of applications include entertainment equipment such as, video game controllers, and audio and video streaming devices and wireless phones.

### 6.1.4 Topologies

A network topology determines the arrangement of different devices on the network and the way of communication between them. Each topology has its advantages and disadvantages with regard to the capacity, latency, robustness, and complexity of routing. The selection of the topology is done based on the application the network is envisaged to work for. The most known network topologies include point-to-point, star, mesh, star-mesh hybrid, and cluster tree. The point-to-point topology is based on direct communication between only two nodes. In a star topology, all nodes (slaves) are connected to the central node that is also known as the master node. In a BAN, a sports watch can act as a central node, whereas slaves can be GPS units, heart rate, and temperature sensors. A star topology is simple and imposes low power requirements on the slave nodes. It has low reliability (single point

of failure), poor scalability and limited spacial coverage. On the contrary, a mesh topology ensures large spacial coverage, is fault tolerant, and scalable. In a mesh network, every node can talk with the other as long as it is within its communications range. This type of networks are also known as multi-hop networks. In reality, however, practical networks rarely require nodes to communicate with every neighbor. Moreover, mesh networks introduce high latency. The complexity of routing and the requirement that all the nodes must have the same functionality may become an issue. A star-mesh hybrid topology combines the simplicity of a star topology and flexibility of the mesh topology. In star-mesh hybrid networks, there is a possibility to connect one or more star networks to the mesh network. In this way, the topology allows for large spacial coverage and highly reliable communication. The power consumption can be balanced among the master nodes and slave nodes. Disadvantages include high latency, low capacity when the number of hops is high, and high complexity if all the nodes can act as masters. The cluster tree topology is a special type of a mesh topology. In a cluster tree topology, there is always a single path between two nodes. The first node starting the network is a so-called root of the tree. Another nodes can join the network as "children" of the root node. All the nodes are aware of their "parent" and "children" nodes. Complexity of routing, in this highly hierarchical topology, is reduced. Large spatial area coverage is possible with low power consumption of the nodes far away from the root node. Disadvantages include high latency and the requirement that all the nodes must have the same basic functionality, i.e. routing. An overview of network topologies is shown in Fig. 6.2.

Considering the limitations of the battery consumption complexity of routing, for the Body Area Network application, the highest potential, mainly due to the simplicity and imposed low power requirements on the slave nodes, have the star, star-mesh, and cluster tree topologies.

### 6.1.5 Technological challenges

There are several technological challenges related to the development of BANs. The biggest challenge is extreme miniaturization of the modules and its effect on the functionality of the components. This requires use of naked chips, flexible substrates, and application of very small batteries. The integration of the all components should be done in a biocompatible package that does not pose any danger to the human skin [38]. An option in providing the energy can be the mechanical or thermal energy scavenging technique. The size of antenna may be an issue limiting the overall form factor of the module. A proper selection of location of the sensors on the human body and their attachment is of high importance since the possible movements of loosely attached sensors may create spurious oscillations resulting in false readings [52].

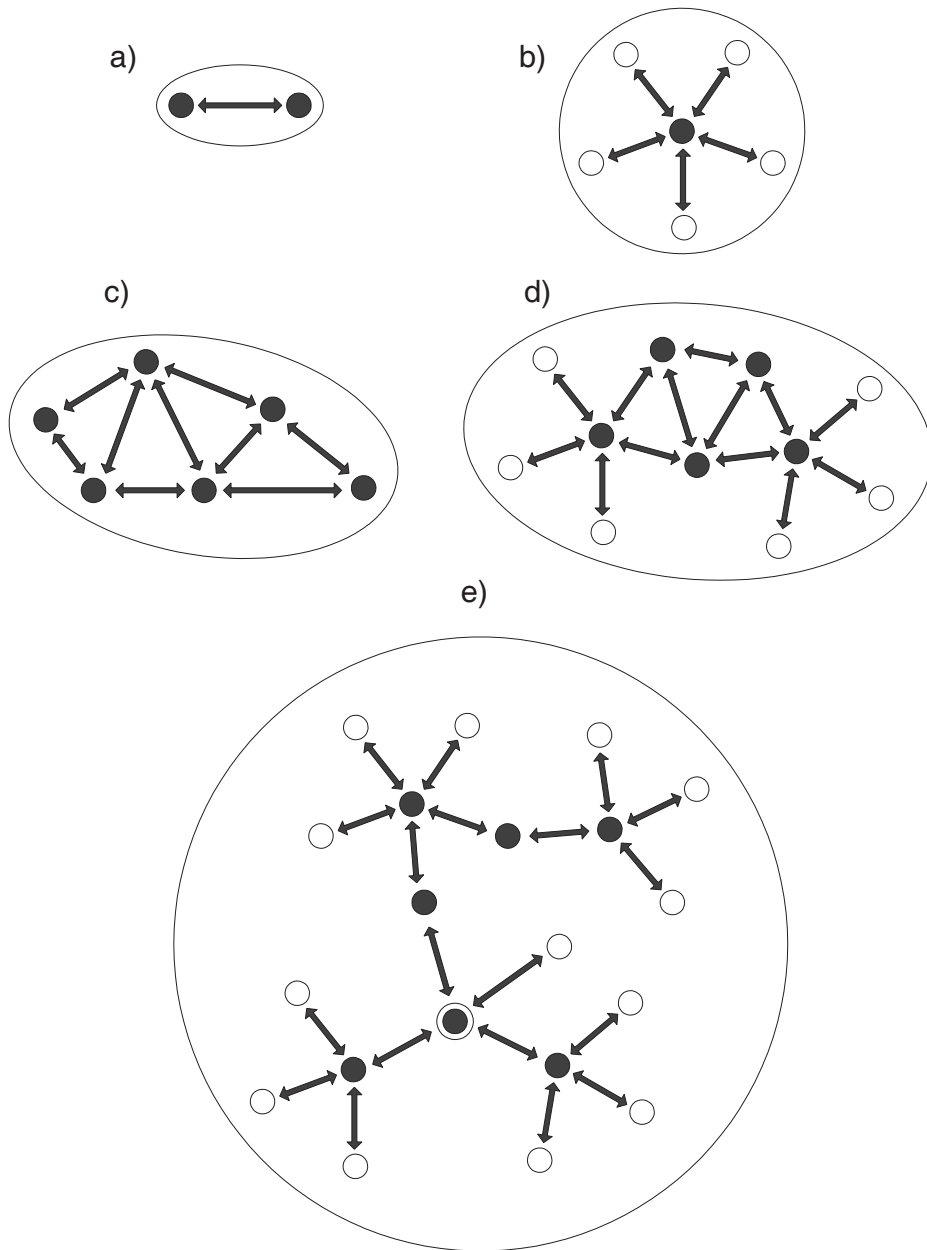


Figure 6.2. Common network topologies: a) point-to-point network, b) star network, c) mesh network, d) star-mesh hybrid network, e) cluster tree network.

### 6.1.6 Social issues

Social issues of BAN systems on the other hand are related to the security and legal issues. Since personal health related data is transmitted from sensors to the central node, an sufficient level of encryption should be present in order to protect BAN user's privacy. Legal issues encompass regulations restricting the access to the patient-identifiable information [52].

## 6.2 System model

The system model considered here is the same as described in Chapter 2 with the exception that the antenna effects, unlike previously considered separately, are now incorporated in the channel model. Moreover, the data rate of the UWB-IR system is lower and equals to 31.25 or 15.625 Mbps. This corresponds well to the BAN scenarios, where the data rates in the burst mode are typically of the order of several Mbps.

### 6.2.1 UWB-IR transmitter and receiver

Here, for the SOC scheme, we keep the constraint length of the SOC code constant,  $K = 5$ , and for the frame repetition case, the number of frames per symbol  $N_f = 8$ . To account for low data rate, comparing to the system model described in Chapter 2, we increase the number of chips per frame, so that it equals to  $N_p = 24$  or 48, for the data rate of 31.25 and 15.625 Mbps, respectively. The receiver architecture is based on the differential autocorrelation principle as explained in Chapter 2.

### 6.2.2 Body area radio propagation channel model

The channel model proposed for the IEEE 802.15.6 standard for Body Area Networks is here considered [108]. This model describes the medium for medical and non-medical devices that could be placed inside or on the surface of the human body. In majority it is based on the measurement campaign presented in [4].

There are three types of nodes defined:

- Implant node: a node that is placed inside the human body
- Body surface node: a node that is placed on the surface of the human skin or at most two centimeters away
- External node: a node that is not in contact with the human skin (between a few centimeters and up to 6 meters away from the body)

For every channel model scenario, there are number of frequency bands considered. In this chapter, we focus on channel model scenario CM3 which describes the channel for body surface - to body surface communication in the frequency band 3.1 - 10.6 GHz. This scenario refers to the IEEE 802.15.6 channel model and not to the IEEE 802.15.3a channel model discussed in Chapter 2.

The channel impulse response is given by [108]

Table 6.1. IEEE BAN UWB Channel Model Parameters.

Model Parameter	Value	Unit
$\gamma_0$	-4.60	dB
$\Gamma$	59.7	n/a
$\sigma_S$	5.02	dB
$1/\lambda$	1.85	ns
$\bar{M}$	38.1	n/a

Table 6.2. IEEE UWB BAN Channel Model Statistics.

Channel Metric	CM3	Unit
Est. mean $\bar{\tau}$	27.2	ns
Est. mean $\tau_{rms}$	19.0	ns
Est. mean $NP_{10dB}$	13.4	n/a
Est. mean $NP_{15dB}$	27.0	n/a
Est. mean $NP_{85\%}$	21.0	n/a
Est. mean $NP_{90\%}$	27.4	n/a
Est. mean IAT	3.02	ns

$$h(t) = \sum_{m=1}^M \alpha_m \exp(j\phi_m) \delta(t - t_m), \quad (6.1)$$

where  $\delta$  is a Dirac function and  $\alpha_m$  and  $t_m$  are the amplitude and arrival time of the  $m$ -th path, accordingly. The phase of the  $m$ -th path,  $\phi_m$  is modeled as a uniform distribution over  $[0, 2\pi)$ . The total number of paths is denoted by  $M$ . The path amplitudes satisfy

$$10 \log(|\alpha_m|^2) = \begin{cases} 0, & \text{if } m = 1 \\ \gamma_0 + 10 \log(\exp(-\frac{t_m}{\Gamma})) + S, & \text{if } m \neq 1. \end{cases} \quad (6.2)$$

where  $\Gamma$  is the exponential decay with a Ricean factor  $\gamma_0$  and  $S$  is a Normal distribution with zero mean and standard deviation  $\sigma_s$  to account for shadowing effects. The inter-arrival times of multipath components follow the Poisson distribution

$$p(t_m|t_{m-1}) = \lambda \exp[-\lambda(t_m - t_{m-1})], \quad (6.3)$$

$$p(M) = \frac{\bar{M}^M \exp(-\bar{M})}{M!}, \quad (6.4)$$

where  $\lambda$  is the path arrival rate and  $\bar{M}$  is the average number of paths.



Table 6.1 presents values of the BAN channel model parameters considered in this chapter [108]. The values of the main channel statistics averaged over an ensemble of 500 channel realizations are given in Table 6.2. Definitions of these statistics can be found in Chapter 4.

As can be observed from Table 6.2, the estimated mean values of delays, i.e., mean excess delay and RMS delay spread are quite high and equal 27.2 ns and 19.0 ns, respectively. The estimated mean number of paths that are 15 dB from the peak multipath arrival is 27.0 and the number of paths required to capture 90 % of the energy is 27.4. The estimated value of the interarrival time is equal to 3.02 ns. This means that multipath components are separated in time, which is also visible in Fig. 6.3. Unlike for the previous channel model considered in Chapter 4, the channel model describing the propagation effects around the human body indicates presence of only several multipath components of very high amplitude. Moreover, decaying of the amplitude of the subsequent multipath components shown in Fig. 6.4 is not that strong as for the previous channel model presented in Chapter 2 and studied in Chapter 4. Fig. 6.5 shows the received energy as a function of the number of multipath components. It can be observed, that first paths contain considerable amount of energy, around 10 % which is typical for the line-of-sight scenario. Fig. 6.6 shows the mean number of significant multipath components required to capture a given amount of energy when the multipath components are sorted out in the ascending order of their energy. From this figure we may see that min. 10 paths are required to capture 60 % of the energy. This is significantly lower than for the case of the IEEE 802.15.3a channel model, which means that theoretically it could be possible to build a feasible RAKE receiver for the low-data-rate UWB-IR BANs, given the knowledge of the channel, i.e., the paths' amplitudes and arrival times, as some of them may have higher amplitudes and arrive later than the first ones. Fig. 6.7 and 6.8 show the cumulative distribution functions (CDFs) of the RMS delay spread and the number of significant paths,  $NP_{10dB}$ , respectively. The results are also fitted with a Gaussian distribution.

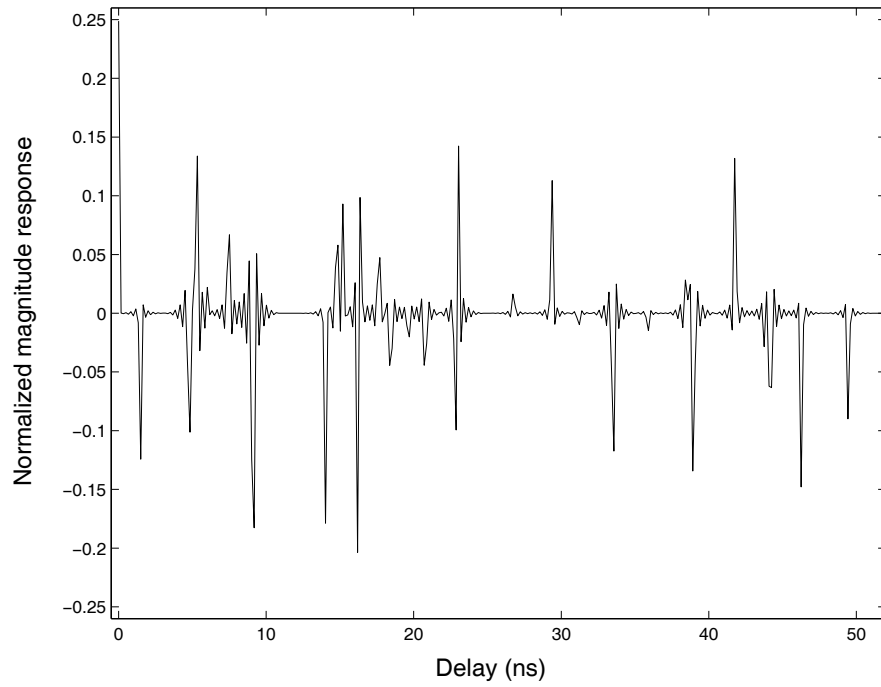


Figure 6.3. Snapshot of the channel impulse response for the CM3 of the BAN channel model.

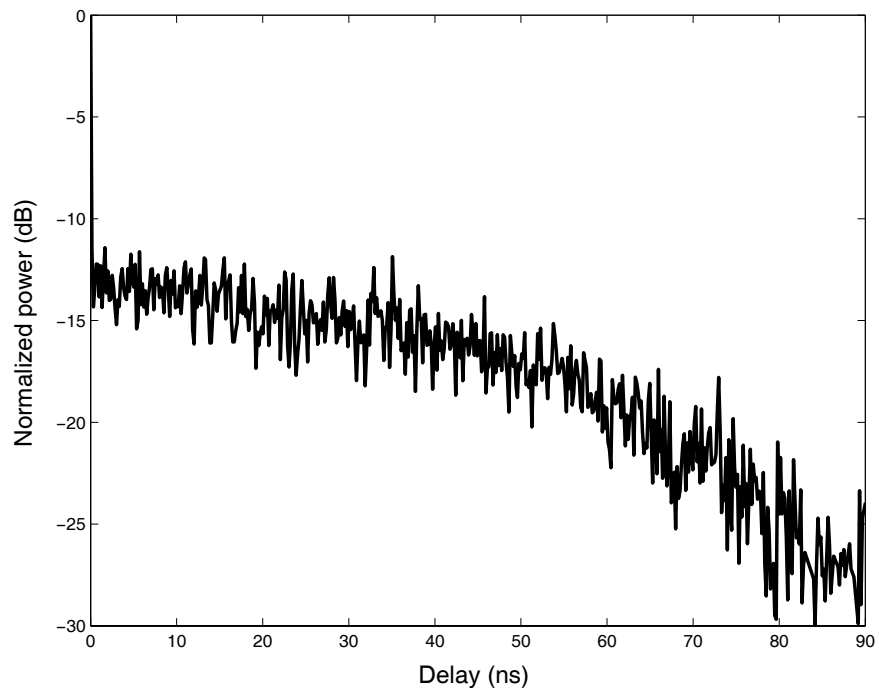


Figure 6.4. The average power decay profile for the CM3 of the BAN channel model.

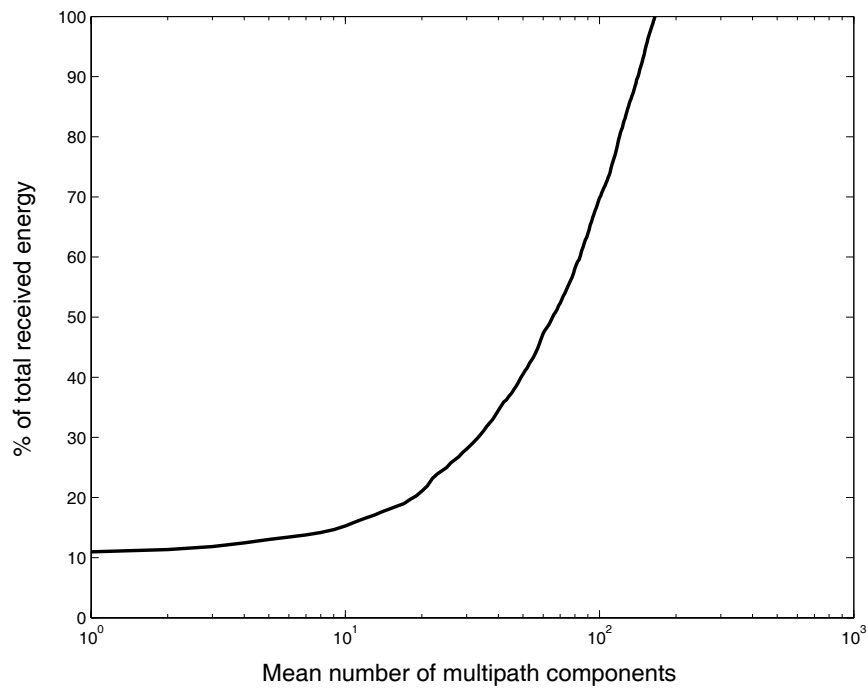


Figure 6.5. The received energy as a function of the number of multipath components for the CM3 of the BAN channel model.

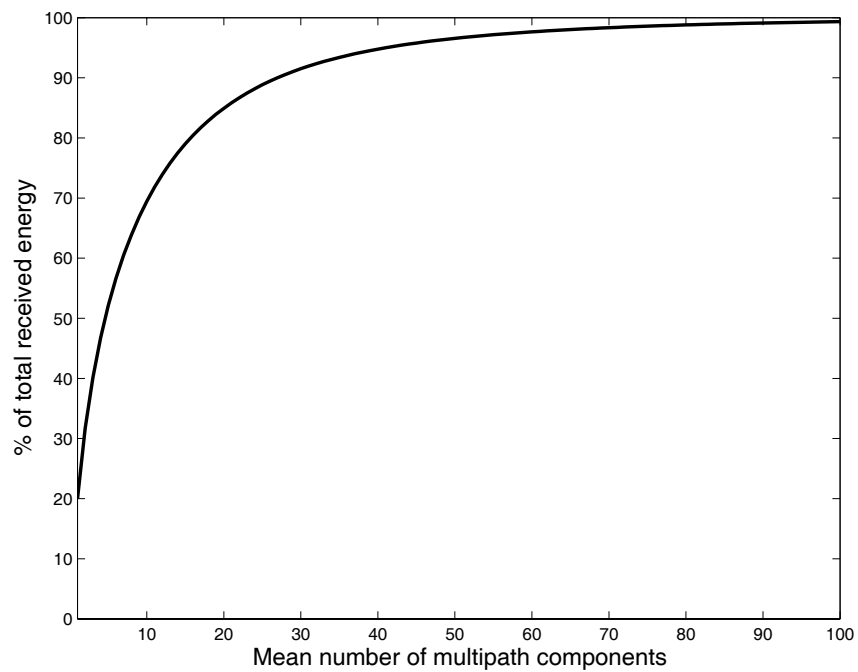


Figure 6.6. Mean number of significant multipath components required to capture a given amount of energy for the CM3 of the BAN channel model. The multipath components are sorted out in ascending order of their energy.

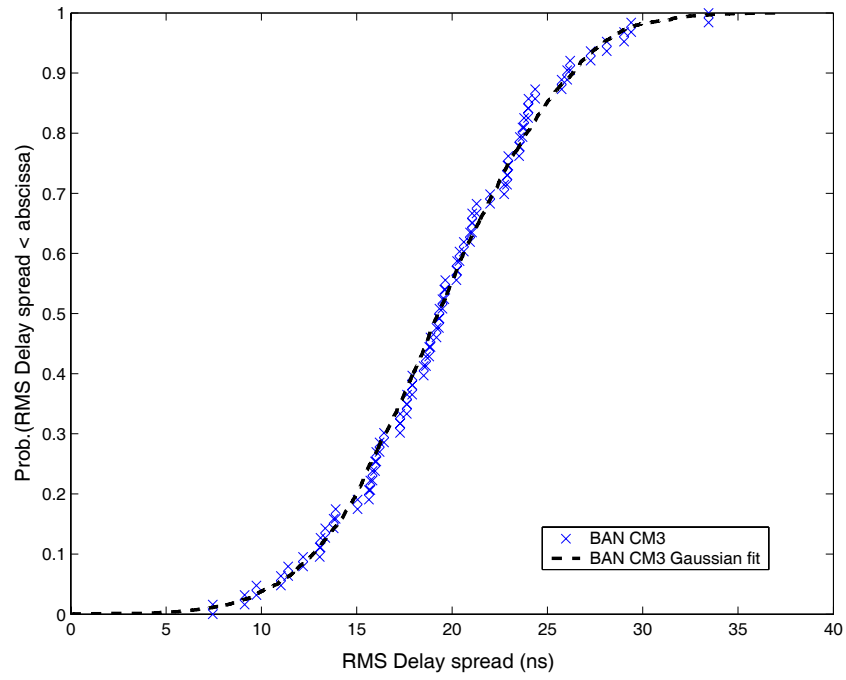


Figure 6.7. CDF of the RMS delay spread for CM3 of the BAN channel model.

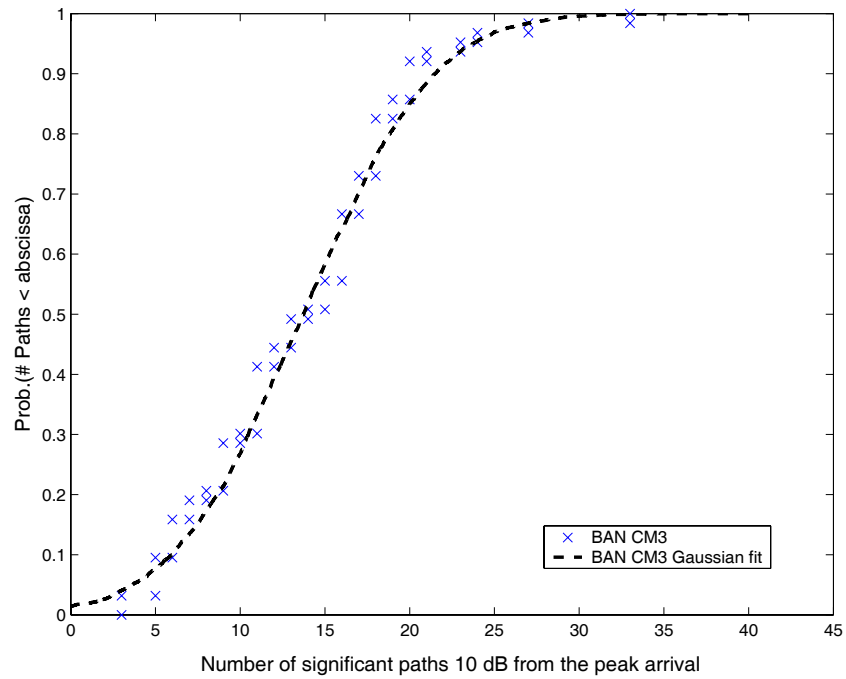


Figure 6.8. CDF of the number of significant paths (10 dB from the peak arrival) for CM3 of the BAN channel model.

## 6.3 Performance evaluation

The bit error rate performance of UWB-IR BANs has been evaluated by means of Monte Carlo simulations. Two data rates have been considered, namely 31.25 Mbps and 15.625 Mbps. The channel model describing multipath propagation of the electromagnetic wave around the human body and presented in the previous section has been used. It is assumed that the channel is constant during the duration of a packet consisting of 2000 bits. Moreover, every channel realization is independent. Perfect synchronization is assumed. For the ICM+PR technique, a random chip interleaver with  $L_p = 400$  chips is used, which corresponds to a time period  $\tau_L = 66.8$  ns. Considering that the maximum value of the estimated mean excess delay of the channel is  $\bar{\tau} = 27.2$  ns, such a length of interleaver ensures sufficient interleaving.

Similarly to performance analyzes presented in the previous chapters, two channel coding schemes are considered, i.e., SOC and FR. Furthermore, for every scheme, two cases are examined, i.e., with or without the proposed ICM+PR technique.

Fig. 6.9 shows the BER performance of a UWB-IR BAN with a data rate of 31.25 Mbps with and without the ICM+PR for SOC coding for which  $K = 5$ ,  $n = 8$ ,  $N_f = 1$ ,  $N_p = 24$  and FR for which  $N_f = 8$ ,  $n = 1$ ,  $N_p = 24$ . It can be observed that the BER performance of a UWB-IR BAN with SOC coding is better than that with the FR, and the difference in BER at the  $10^{-4}$  level equals ca. 5 dB. Application of the ICM+PR technique introduces coding gain, which is evident for the FR scheme and at the BER =  $10^{-4}$  level equals ca. 3 dB. For the SOC scheme, the introduced coding gain at the same BER level, equals only about 0.25 dB. It has been observed, that for the FR scheme and values of  $E_b/N_0 < 6.5$  dB, the BER performance with ICM+PR technique is slightly worse than that of no ICM+PR case. This phenomenon, also visible in Fig. 6.10, seems to be generally true for LOS scenarios irrespective of the data rate (also for high-data-rate UWB-IR systems) and was explained in Chapter 4, Section 4.2.4.

Fig. 6.10 shows the BER performance of a UWB-IR BAN with a data rate of 15.625 Mbps for SOC coding and FR and with and without the ICM+PR techniques. Similarly to Fig. 6.9, SOC coding offers better BER performance than FR scheme. However, for the lower data rate system, the introduced coding gain is smaller and on the BER =  $10^{-4}$  level equals ca. 2.5 dB. As observed, for UWB-IR BANs with the data rate of 15.625 Mbps and FR scheme, only for values of  $E_b/N_0 > 8$  dB it is beneficial to apply the ICM+PR technique. It can be predicted that the lower the data rate of the system with FR scheme is, the higher the  $E_b/N_0$  value required for beneficial application of the ICM+PR is. This can be explained in the fact that lowering the data rate means increasing separation in time between the consecutive pulses and as a consequence diminishing the negative impact of the ISI, IFI, and IPI effects. The ICM+PR technique exploits the temporal diversity brought by the UWB channel through multipaths. However, when the pulse separation is

large comparing to the channel excess delay, the benefit of using the ICM+PR becomes less evident and more dependent on the noise level.

Performance of the RAKE receivers in the BANs with BPSK signaling has been studied in [32]. A pulse duration of 0.5 ns has been assumed. The analysis was based on outage probability calculations. It has been concluded that in an indoor environment, many RAKE fingers are required to achieve optimal performance. Moreover, the number of RAKE fingers required to approach the optimal performance increases with distance, as the energy of paths traveling close to human torso is rapidly attenuated. For LOS scenarios, no influence of ground reflection has been noticed, as they have generally low energy compared to the first multipath arrival. However, in NLOS scenarios, ground reflections contribute to the better performance. In [32] it has been suggested to consider transmitted-reference scheme or multi-hop network around the body to combat the path loss near the body.

A comparison of linear and nonlinear UWB multi-user detector (MUD) based receivers with the RAKE receiver is presented in [84]. The number of users is varied from 2 to 5. It is shown that the presented scheme outperforms the RAKE receiver in the presence of multi-user interference.

A study of symbol-wise maximum likelihood detectors for pulse amplitude modulation and transmit-reference pulse amplitude modulation with partial information about the channel for Body Area Networks is presented in [110]. It is shown that the knowledge of the average power delay profile at the receiver improves performance substantially.

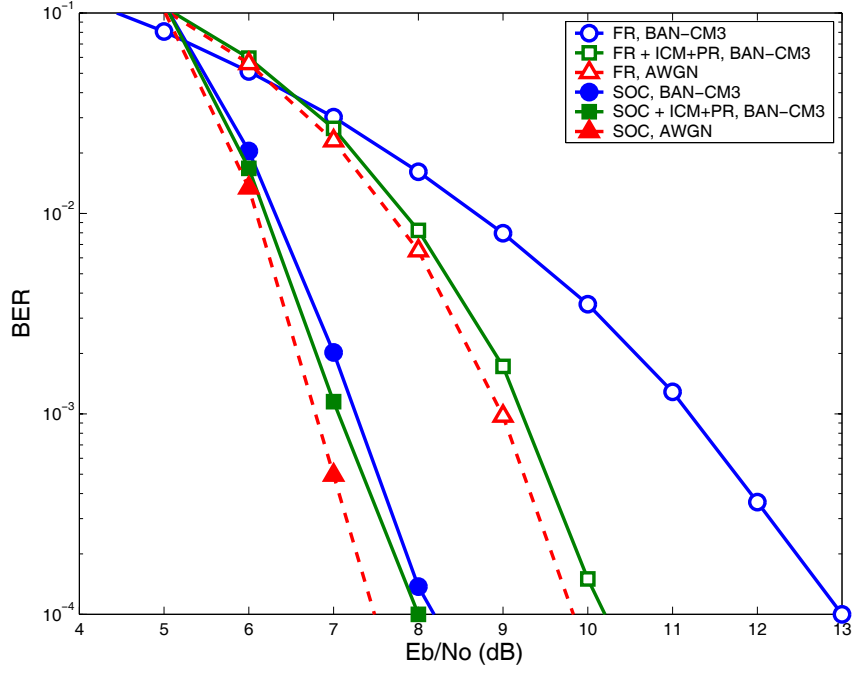


Figure 6.9. The effect of PR and ICM on the BER of UWB-IR BAN with SOC coding,  $K = 5$ ,  $n = 8$ ,  $N_f = 1$ ,  $N_p = 24$  and FR,  $N_f = 8$ ,  $n = 1$ ,  $N_p = 24$  in the BAN-CM3 scenario.

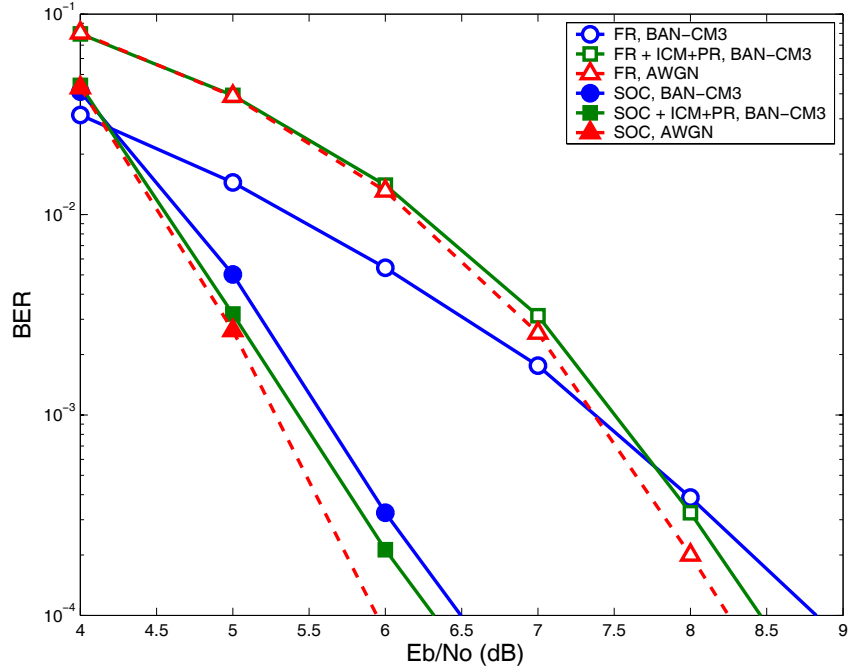


Figure 6.10. The effect of PR and ICM on the BER of UWB-IR BAN with SOC coding,  $K = 5$ ,  $n = 8$ ,  $N_f = 1$ ,  $N_p = 48$  and FR,  $N_f = 8$ ,  $n = 1$ ,  $N_p = 48$  in the BAN-CM3 scenario.

## 6.4 Summary

In this chapter, the bit error rate performance of UWB-IR body area networks has been analyzed. The channel describing the propagation effects around the human body is the one accepted in the IEEE 802.15.6 standard.

The obtained results indicate that SOC coding offers superior performance to FR scheme. The ICM + PR method offers BER performance improvements which are significant for FR scheme with the data rate of 31.25 Mbps. For the case of a lower data rate, and in particular for 15.625 Mbps, the ICM + PR technique also introduces performance improvements but only for values of  $E_b/N_0 > 8$  dB. However, receivers normally operate at such values of  $E_b/N_0$ , and the presented methods may also find application in feasible low-data-rate UWB-IR BANs.



# Chapter 7

## Conclusions

The main subject of this thesis is the design and performance evaluation of novel error control techniques particularly suitable for feasible UWB-IR systems operating in harsh radio channel environments. The performance is evaluated with respect to the bit error rate and signal-to-noise ratio. The considered non-coherent receiver architecture is based on the differential autocorrelation principle. The following three main system cases have been considered:

- single-user high-data-rate UWB-IR systems
- multi-user high-data-rate UWB-IR systems
- single-user low-data-rate UWB-IR systems for BAN applications.

The next section provides the main contributions that are the results of the research described in this thesis. Moreover, directions for future research related to the topics presented in the thesis and worth further investigation are indicated and discussed.

### 7.1 Contributions of this thesis

#### 7.1.1 Single-user high-data-rate UWB-IR systems

Single-user high-data-rate UWB-IR systems are considered in Chapter 2 and 4. Information on channel coding schemes that are used in single- and multi-user systems is provided in Chapter 3.

The main contributions include performance evaluation of UWB-IR systems with differential autocorrelation receiver for different sets of system parameters and different methods of protection against errors (superorthogonal convolutional coding, frame repetition, and bit repetition) on a realistic channel model and considering the inter-pulse-, inter-frame- and inter-symbol- interference. Another contribution is a design of the interleaved coding-modulation scheme which alleviates the problem of ISI, IFI, and IPI present in high data rate UWB-IR systems. The performance of the above mentioned scheme was evaluated on the chip and frame level. Additionally, studies on pulse based polarity randomization (PR) have been performed. To better understand the nature of the BER performance improvement introduced by the ICM+PR method, a statistical analysis of the multipath fading channel statistics considering four scenarios has been carried out. The main conclusions are as follows:

1. The proposed ICM + PR technique allows for alleviation of the impairments on the receiver caused by ISI, IFI, and IPI that are due to the multipath fading.
2. It has been shown that rearranging the order of chips (in case of chip-level ICM) or frames (in case of frame-level ICM), in a one-to-one random manner, results in the BER performance improvement. This improvement is particularly apparent in case of UWB-IR with FR.
3. It has been shown that pulse-based PR may constitute a sort of alternative to the chip-level ICM (without application of PR) since it yields a comparable BER performance without introducing any delay.
4. Our simulation results indicate that altering the system parameters settings (within the considered values) and maintaining the data rate does not affect the BER performance of UWB-IR systems with FR. However, visible influence favoring low code-rate codes takes place for the case of UWB-IR systems with SOC coding.
5. The obtained results for every channel scenario demonstrate robustness of the ICM+PR method against multipath fading, yielding comparable BER performance. On the contrary, the channel statistics have considerable influence on the BER performance of coded UWB-IR systems without ICM + PR.
6. The presented simulation results are in good agreement with the derived lower and upper bounds on the BER.

### 7.1.2 Multi-user high-data rate UWB-IR systems

Multi-user high-data-rate UWB-IR systems are studied in Chapter 5. Our focus is narrowed to scarcely populated systems, for which most of the analyzes done so far and based on

a Gaussian approximation to model the interference stemming from the concurrent transmitters, are inaccurate. The presented performance assessment of scarcely populated UWB-IR systems with the proposed interleaved coding-modulation scheme is done by means of a Poisson based analysis and Monte Carlo simulations.

The main contributions include a design of a deterministic chip interleaver based on time-hopping hyperbolic congruence sequences for the ICM method. This interleaver comparing to random interleavers, has the advantage of simpler implementation. The performance of UWB-IR systems based on the ICM method with both types of interleavers has been mutually compared. In order to understand the factors that stand behind comparable BER performance, an analysis of correlation properties and randomness characteristics of the both types of interleaver sequences has been made. Moreover, improvements in the architecture of the differential autocorrelation receiver have been proposed. The main conclusions are as follows:

1. The proposed ICM method introduces performance improvements also for scarcely populated multi-user scenarios.
2. Application of time-hopping hyperbolic congruence sequences to construct a chip interleaver for the ICM method yields BER performance improvement that is comparable to random interleavers. However, hyperbolic congruence sequences may be favored due to their simple implementation in a real communication system.
3. The presented Poisson-based analysis may be helpful in a rough approximation of the BER performance of UWB-IR systems without chip interleaving (without the ICM method).

### 7.1.3 Single-user low-data rate UWB-IR systems for BAN applications

Performance of UWB-IR based body area networks is investigated in Chapter 6. The system model used is the same as presented in Chapter 2, with the exception of lower data rates and different channel model that describes the propagation medium around the human body. The main contributions include the performance evaluation of UWB-IR BANs with and without the ICM + PR method for SOC coding or FR scheme by means of Monte Carlo simulations. The considered data rates of the BANs are 31.25 and 15.625 Mbps. The channel model used in our simulations is the one which is proposed for the IEEE 802.15.6 standard for Body Area Networks.

The main conclusions are as follows:

1. For low-data-rate UWB-IR systems, frame repetition and SOC coding enable better BER performance than that for the case of high-data-rate systems.
2. The ICM + PR technique may introduce performance improvements which are significant for the case of FR.
3. FR with the ICM + PR technique offers the BER performance that is for the data rate of 31.25 Mbps and at the BER=  $10^{-4}$  level 2 dB away from the performance of SOC coding.

## 7.2 Future research directions

The assumptions made and the results presented in this thesis open up a wide range of future topics. The common assumption in this thesis was that the synchronization between the transmitter and receiver is perfect. It would be interesting to analyze the effects of the clock misalignments on the BER performance of the differential receiver itself and also the presented ICM + PR method.

The sources of interference considered in this thesis are the ones that stem from the multipath fading effects and multi-user pulse overlap. However, there are other sources of interference present in the UWB frequency band that may influence the performance, including narrowband and wideband interference, e.g., WLANs based on the IEEE 802.11a standard that operate in the 5.15 -5.35 MHz frequency range. Also, the effects of interference stemming from the microwave ovens so popular nowadays at homes may constitute an interesting future topic.

In this thesis, superorthogonal convolutional coding, frame and bit repetition are considered as methods of protection against errors. An extension of the work presented here to turbo codes or regular LDPC codes, could be an interesting future topic. In this context, the performance of low complexity suboptimal iterative decoding algorithms could be analyzed.

Although differential autocorrelation receiver operating on symbols yields the best performance, such a receiver could also operate on frames resulting in a frame differential scheme [74]. Its performance would be worse but implementation simpler due to the relaxed requirement on the length of the delay lines used. A performance analysis of such a receiver in combination with the proposed ICM method could constitute an interesting extension of the work presented in this thesis.

Recently, application of the UWB-IR technology for high accuracy ranging has received lots of attention. A study on feasible architectures allowing for combination of ranging and communication may be an interesting topic.

# Bibliography

- [1] *Proc. IEEE of the International Symposium on Turbo Codes and Related Topics*, Brest, France, Sept. 1997.
- [2] *Proc. IEEE of the International Symposium on Turbo Codes and Related Topics*, Brest, France, Sept. 2000.
- [3] R. Aiello and A. Batra, *Ultra-wideband Systems Technologies and Applications*. Oxford, UK: Elsevier, 2006.
- [4] T. Aoyagi, “Channel model for WBANs - NICT,” *Tech. Rep. P802.15-08-0416-04-0006, IEEE P802.15 Working Group for Wireless Personal Area Networks (WPANs)*, Nov. 2008.
- [5] P. Azmi, M. Nasiri-Kenari, and J. Salehi, “Low-rate super-orthogonal channel coding for fiber-optic CDMA communication systems,” *IEEE Trans. Commun.*, vol. 19, no. 6, pp. 847–855, June 2001.
- [6] S. Bagga, “A delay filter for and IR-UWB front-end,” in *Proc. IEEE Int. Conference on Ultra-Wideband (ICUWB’2005)*, Switzerland, Sept. 2005.
- [7] A. Batra, J. Balakrishnan, and A. Dabak, “Physical layer submission to 802.15 task group 3a: multi-band orthogonal frequency division multiplexing,” *IEEE P802.15 Working Group for Wireless Personal Area Networks (WPANs)*, Sept. 2004.
- [8] A. Batra, S. Lingam, and J. Balakrishnan, “Multi-band OFDM: a cognitive radio for UWB,” in *Proc. IEEE Int. Symp. on Circ. and Syst., (ISCAS’06)*, May 2006, p. 4097.
- [9] E. Berlekamp, *Algebraic Coding Theory*. Aegean Park Press, 1984.
- [10] C. Berrou, A. Glavieux, and P. Thitimajshima, “Near Shannon Limit error-correcting coding and decoding: turbo-codes,” in *Proc. IEEE Int. Comm. Conference (ICC’03)*, Geneve, Switzerland, May 2003, pp. 1064–1070.
- [11] C. Bi, J. Y. Hui, L. Bodenheimer, and H. Spielberg, “Embedded turbo coding in pattern position modulation for ultra-wideband radio systems,” in *Proc. IEEE Int. Symp. on Inform. Theory*, vol. 5, Chicago, USA, June 2004, p. 512.

- [12] R. Bose and D. Ray-Chaudhuri, "On a class of error-correcting binary codes," *Information and Control Journal*, vol. 3, pp. 68–79, 1960.
- [13] Y. Chao and R. Scholtz, "Novel UWB transmitted reference schemes," in *Proc. IEEE Int. Conf. on Signals, Systems and Computers (Asilomar'04)*, Nov. 2004, pp. 652–656.
- [14] X. Chen and S. Kiaei, "Monocycle shapes for ultra wideband system," in *Proc. IEEE Int. Symp. on Circuits and Systems (ISCAS'02)*, vol. 1, May 2002, pp. 597–600.
- [15] J. Choi, "Random sign repetition time-hopping UWB with multiuser detection," *Eurasip Journal on Wireless Communications and Networking*, vol. 5, no. 4, pp. 590–598, Sept. 2005.
- [16] J. Choi and W. Stark, "Performance of ultra-wideband communications with suboptimal receivers in multipath channels," *IEEE J. Sel. Areas. Commun.*, vol. 20, no. 9, pp. 1754–1766, Dec. 2002.
- [17] —, "Performance of autocorrelation receivers for ultra-wideband communications with PPM in multipath channels," in *Proc. IEEE Int. Conf. on Ultra Wideband Systems and Technologies (UWBST'02)*, May 2002, pp. 213–217.
- [18] S.-W. Choi and S.-S. Choi, "200 Mbps Viterbi decoder for UWB," in *Proc. IEEE Int. Conf. on Advanced Comm. Techn. ICACT'05*, vol. 2, Feb. 2005, pp. 904–907.
- [19] J. Conroy, J. LoCicero, and D. Ucci, "Communication techniques using monopulse waveforms," in *Proc. IEEE Int. Military Communications Conf. (MILCOM'99)*, vol. 2, Oct. 1999, pp. 1181–1185.
- [20] S. N. Crozier, "New high-spread high-distance interleavers for turbo codes," in *Proc. Biennial Symp. Commun.*, May 2000, pp. 3–7.
- [21] L. Dinioi and S. Benedetto, "Variable-size interleaver design for parallel turbo decoder architectures," *IEEE Trans. Commun.*, vol. 53, no. 11, pp. 1833–1840, Nov. 2005.
- [22] P. Elias, "Error-free coding," *Institute of Radio Eng. Trans.*, vol. PGIT-4, pp. 29–37, 1954.
- [23] —, "Coding for noisy channels," *Institute of Radio Eng. Nat. Convention Record*, vol. 3, no. 1, pp. 37–46, 1955.
- [24] R. Fano, "A heuristic discussion on probabilistic decoding," *Institute of Radio Eng., Transactions on Information Theory*, vol. IT-9, no. 2, pp. 67–74, 1963.
- [25] FCC, "Revision of part 15 of the commission's rules regarding ultra-wideband transmission systems," *First Report and Order, ET Docket, FCC 02-8*, pp. 98–153, Feb./Apr. 2002.

- [26] J. Foerster, "The performance of a direct-sequence spread ultrawideband system in the presence of multipath, narrowband interference, and multiuser interference," in *Proc. IEEE Int. Conf. on Ultra Wideband Systems and Technologies (UWBST'02)*, May 2002, pp. 87–91.
- [27] R. J. Foerster, "Channel modeling sub-committee report (final)," *Tech. Rep. P802.15-02/490r1-SG3a, IEEE P802.15 Working Group for Wireless Personal Area Networks (WPANs)*, Feb. 2003.
- [28] G. Forney, "Codes on graphs: normal realizations," *IEEE Trans. Info. Theory*, vol. 47, no. 2, pp. 520–548, Feb. 2001.
- [29] A. R. Forouzan, M. Nasiri-Kenari, and J. A. Salehi, "Performance analysis of ultra-wideband time-hopping spread-spectrum multiple-access systems: uncoded and coded schemes," *IEEE Trans. Wireless. Commun.*, vol. 1, no. 4, pp. 671–681, Oct. 2002.
- [30] A. Forouzan, M. Nasiri-Kenari, and J. Salehi, "Low-rate convolutionally encoded time-hopping spread spectrum multiple access systems," in *Proc. IEEE PIMRC'00*, vol. 2, Sept. 2000, pp. 1555–1558.
- [31] —, "Performance analysis of ultra-wideband time-hopping code division multiple access systems: uncoded and coded schemes," in *Proc. IEEE ICC'01*, vol. 10, June 2001, pp. 3017–3032.
- [32] A. Fort, C. Desset, and L. Biesen, "Body area UWB RAKE receiver communication," in *Proc. IEEE Int. Conf. on Commun (ICC'06)*, June 2006, pp. 4682–4687.
- [33] P. Frenger, P. Orten, and T. Ottosson, "Convolutional codes with optimum distance spectrum," *IEEE Commun. Lett.*, vol. 3, no. 11, pp. 317–319, Nov. 1999.
- [34] R. Gallager, "Low-density parity-check codes," *IRE Trans. Info. Theory*, vol. 8, no. 1, pp. 21–28, Jan. 1962.
- [35] S. Gezici and H. Poor, "Optimal and suboptimal linear receivers for Impulse Radio UWB systems," in *Proc. IEEE Int. Conf. on Ultra Wideband (ICUWB'06)*, Massachusetts, USA, Sept. 2006, pp. 161–166.
- [36] B. Ginsburg and A. P. Chandrakasan, "Dual time-interleaved successive approximation register ADCs for an ultra-wideband receiver," *IEEE Journal of Solid-State Circuits*, vol. 42, pp. 247–257, Feb. 2007.
- [37] N. Guo, B. Sadler, and R. Qiu, "Reduced-complexity UWB time-reversal technique and experimental results," *IEEE Trans. Wireless. Commun.*, vol. 6, no. 12, pp. 4221–4226, Dec. 2007.
- [38] B. Gyselinckx, "Human++: autonomous wireless sensors for body area networks," in *Proc. IEEE Custom Integrated Circ. Conf.*, 2005, pp. 12–19.

- [39] S. Haddad, *Ultra low-power biomedical signal processing: an analog wavelet filter approach for pacemakers*. Ph.D. dissertation, Delft University of Technology, 2006.
- [40] J. Hagenauer and P. Hoeher, "A Viterbi algorithm with soft-decision outputs and its applications," in *Proc. IEEE Global Telecommunications Conference (Globecom'89)*, Dallas, Texas, Nov. 1989, pp. 1680–1686.
- [41] M. Hamalainen, V. Hovinen, R. Tesi, J. Iinatti, and M. Latva-aho, "On the UWB system coexistence with GSM900, UMTS/WCDMA, and GPS," *IEEE Trans. Commun.*, vol. 20, no. 9, pp. 1712–1721, Dec. 2002.
- [42] R. Hamming, "Error detecting and error correcting codes," *Bell System Technical Journal*, vol. 29, pp. 147–160, Apr. 1950.
- [43] H. Harmuth, *Transmission of Information by Orthogonal Functions*. New York: Springer, 1969.
- [44] W. He, *65+ in the United States 2005*, Available at <http://www.census.gov/prod/2006pubs/p23-209.pdf>, last accessed November 2009.
- [45] G. Hingorani and J. Hancock, "A transmitted-reference system for communication in random or unknown channels," *IEEE Trans. Commun. Techn.*, vol. 13, no. 3, pp. 293–301, Sept. 1965.
- [46] R. Hoor and H. Tomlinson, "Delay-hopped transmitted-reference communications," in *Proc. IEEE Conf. on Ultra Wideband Systems and Technologies (UWBST'02)*, May 2002, pp. 265–270.
- [47] Z. Irahhaute, A. Yarovoy, H. Nikookar, G. J. M. Janssen, and L. P. Ligthart, "The effect of antenna and pulse waveform on ultra-wideband link budget with impulse radio transmission," in *Proc. Europ. Microwave Week Conf.*, Amsterdam, The Netherlands, Oct. 2004, pp. 261–264.
- [48] K. Ishibashi, H. Ochiai, and R. Kohno, "On the performance of bit-interleaved coded DAPSK over Rayleigh fading channels," in *Proc. IEEE Int. Conf. on Commun (ICC'03)*, June 2004, pp. 732–736.
- [49] F. Jelinek, "Fast sequential decoding algorithm using a stack," *IBM Journal of Research and Development*, 1969.
- [50] A. V. Jovancevic and E. L. Titlebaum, "New coding schemes for increased number of users or messages in frequency-hopped multilevel FSK," in *Proc. IEEE VTC'96*, vol. 3, Apr. 1996, pp. 1732–1735.
- [51] E. Jovanov, "Stress monitoring using a distributed wireless intelligent sensor system," *Proc. IEEE Engineering in Medicine and Biology Magazine.*, vol. 22, no. 3, pp. 49–55, May 2003.



- [52] —, “A wireless body area network of intelligent motion sensors for computer assisted physical rehabilitation,” in *Proc. Journal of NeuroEng. and Rehab.*, Mar. 2005, pp. 1–10.
- [53] R. Kohno, K. Hamaguchi, H.-B. Li, and K. Takizawa, “R&D and standardization of body area network (BAN) for medical healthcare,” in *Proc. IEEE Int. Conf. on Ultra-wideband, ICUWB’08*, vol. 3, Hannover, Germany, Sept. 2008, pp. 5–8.
- [54] P. Komulainen and K. Pehkonen, “Performance evaluation of superorthogonal codes in AWGN and flat Rayleigh fading channels,” *IEEE J. Select. Areas Commun.*, vol. 16, no. 2, pp. 196–205, Feb. 1998.
- [55] C. Krall, C. Vogel, and K. Witrisal, “Time-interleaved digital-to-analog converters for UWB signal generation,” in *Proc. IEEE Int. Conference on Ultra-Wideband (ICUWB’2007)*, Singapore, Sept. 2007, pp. 366–371.
- [56] R. Kschischang, B. Frey, and H. Loeliger, “Factor graphs and the sum-product algorithm,” *IEEE Trans. Info. Theory*, vol. 47, no. 2, pp. 498–519, Feb. 2001.
- [57] J. Kunish and J. Pamp, “Measurement results and modelling aspects for the UWB radio channel,” in *Proc. IEEE Conf. on Ultra Wideband Systems and Technologies*, Baltimore, USA, May 2002, pp. 19–24.
- [58] D. MacKay, “Good-error correcting codes based on very sparse matrices,” *IEEE Trans. Info. Theory*, vol. 45, no. 2, pp. 399–432, Mar. 1999.
- [59] D. Mandelbaum, “Decoding beyond the designed distance of certain algebraic codes,” *IEEE Global Telecomm. Conf.*, pp. 772–776, 2000.
- [60] S. V. Maric and E. L. Titlebaum, “A class of frequency hop codes with nearly ideal characteristics for use in multiple-access spread-spectrum communications and radar and sonar systems,” *IEEE Trans. Commun.*, vol. 40, no. 9, pp. 1442–1447, Sept. 1992.
- [61] J. Massey, *Threshold Decoding*. MIT Press, 1963.
- [62] —, “Shift register synthesis and BCH decoding,” *IEEE Trans. Info. Theory*, vol. IT-15, pp. 122–127, Jan. 1969.
- [63] T. Matsumoto, H. Ochiai, and R. Kohno, “Super-orthogonal convolutional coding with orthogonal pulse waveform for ultra wideband communications,” in *Proc. IEEE Conf. on Ultrawideband Systems and Techn. (UWBST’04) and Int. Workshop on UltraWideband Systems (IWUWBS’04)*, May 2004, pp. 202–206.
- [64] Ageing well in the information society. Available at [http://ec.europa.eu/information\\_society/activities/einclusion/policy/ageing/launch/](http://ec.europa.eu/information_society/activities/einclusion/policy/ageing/launch/), last accessed March 2009: Initiative of the European Commission, June 2005.

- [65] EU25 population aged 65 and over expected to double between 1995 and 2050. Available at <http://ec.europa.eu/eurostat>, last accessed April 2009: Eurostat Press Office, September 2006.
- [66] European Commission decision on allowing the use of the radio spectrum for equipment using ultra-wideband technology in a harmonised manner in the Community. Available at [http://ec.europa.eu/information\\_society/policy/radio\\_spectrum/docs/ref\\_docs/.../uwb\\_04\\_orig\\_web.pdf](http://ec.europa.eu/information_society/policy/radio_spectrum/docs/ref_docs/.../uwb_04_orig_web.pdf), last accessed June 2007: Commission of the European Communities.
- [67] Revision of Part 15 of the Commission's Rules Regarding Ultra-Wideband Transmission Systems. Available at [http://www.fcc.gov/Bureaus/Engineering\\_Technology/Orders/2002/fcc02048.pdf](http://www.fcc.gov/Bureaus/Engineering_Technology/Orders/2002/fcc02048.pdf), last accessed June 2007: First Note and Order, Federal Communications Commission, ET-Docket 98-153, Adopted February 14, 2002, released April 22, 2002.
- [68] C. Meng-Hsuan and R. Scholtz, "Receiver improvement for ultra-wideband transmitted-reference systems," in *Proc. IEEE Wireless Communications and Networking Conference (WCNC'05)*, Mar. 2005, pp. 746–751.
- [69] L. Michael, M. Ghavami, and R. Kohno, "Multiple pulse generator for ultra-wideband communication using Hermite polynomial based orthogonal pulses," in *Proc. IEEE Int. Conf. on Ultra Wideband Systems and Technologies (UWBST'02)*, May 2002, pp. 47–51.
- [70] O. Moreno and S. V. Maric, "A new family of frequency-hop codes," *IEEE Trans. Commun.*, vol. 48, no. 8, pp. 1241–1244, Aug. 2000.
- [71] S. Morosi and T. Bianchi, "On the comparison between pulse repetition and cyclic prefix communication techniques in impulse radio UWB systems," in *Proc. IEEE Int. Symp. on Personal, Indoor and Mobile Commun. (PIMRC'06)*, June 2006.
- [72] H. Nguyen, I. Kocacs, and P. Eggers, "A time reversal transmission approach for multiuser UWB communications," *IEEE Trans. Antennas and Propagation*, vol. 54, no. 11, pp. 3216–3224, Nov. 2006.
- [73] I. Oppermann and B. S. Vucetic, "Complex spreading sequences with a wide range of correlation properties," *IEEE Trans. Commun.*, vol. 45, no. 3, pp. 365–375, Mar. 1997.
- [74] M. Pausini, *Autocorrelation receivers for ultra wideband wireless communications*. Ph.D. dissertation, Delft Univ. of Techn., 2007.
- [75] M. Pausini and G. J. M. Janssen, "Analysis and comparison of autocorrelation receivers for IR-UWB signals based on differential detection," in *Proc. IEEE Int. Conf. on Acoustics, Speech, and Signal Processing ICASSP'04*, vol. 4, Quebec, Canada, May 2004, pp. 513–516.

- [76] J. Pearl, *Probabilistic Reasoning in Intelligent Systems: Networks of Plausible Inference*. Morgan Kaufmann, 1988.
- [77] W. Peterson, "Encoding and error-correction procedures for the Bode-Chaudhuri Codes," *Institute of Radio Eng., Transactions on Information Theory*, vol. IT-6, pp. 459–470, 1960.
- [78] D. Porcino and W. Hirt, "Ultra-wideband radio technology: potential and challenges ahead," *IEEE Comm. Magazine*, pp. 66–74, July 2003.
- [79] R. Price and P. Green, "A communication technique for multipath channels," *Proceedings of the IEEE*, vol. 46, pp. 555–570, Mar. 1958.
- [80] J. G. Proakis, *Digital Communications*. Singapore: McGraw-Hill Companies Inc., 2001.
- [81] R. Qiu, H. Liu, and X. Shen, "Ultra-wideband for multiple access communications," *Proc. IEEE Communications Magazine*, vol. 43, no. 2, pp. 80–87, Feb. 2005.
- [82] F. Ramirez-Mireles, "On the performance of ultra-wide-band signals in Gaussian noise and dense multipath," *IEEE J. Trans. Vehic. Techn.*, vol. 50, no. 1, pp. 244–249, Jan. 2001.
- [83] —, "Performance of ultra-wideband SSMA using time-hopping and M-ary PPM," *IEEE J. Select. Areas Commun.*, vol. 19, no. 6, pp. 1186–1196, June 2001.
- [84] P. Reddy and V. Ganapathy, "Performance of multi user detector based receivers for UWB body area networks," in *Proc. IEEE Int. Conf. on e-Health Networking (HealthCom'08)*, July 2008, pp. 227–231.
- [85] I. Reed and G. Solomon, "Polynomial codes over certain finite fields," *SIAM J. Appl. Math.*, vol. 8, pp. 300–304, 1960.
- [86] M. Rice and E. Perrits, "A simple figure of merit for evaluation interleaver depth for the land-mobile satellite channel," *IEEE Trans. Commun.*, vol. 49, no. 8, pp. 1343–1353, Aug. 2001.
- [87] T. Richardson and R. Urbanke, "The capacity of Low-Density Parity Check Codes under Message-Passing Decoding," *IEEE Trans. Info. Theory*, vol. 47, no. 2, pp. 599–618, Feb. 2001.
- [88] J. Romme and K. Witrisal, "Oversampled weighted autocorrelation receivers for transmitted-reference UWB systems," in *Proc. Vehic. Techn. Conf. (VTC'05)*, May 2005, pp. 1375–1380.

- [89] G. Ross, *The transient analysis of multiple beam feed networks for array systems*. Brooklyn, NY, USA: Ph.D. dissertation, Dept. Elec. Eng., Polytech. Inst. Brooklyn, 1963.
- [90] C. Rushforth, "Transmitted-reference techniques for random or unknown channels," *IEEE Trans. Info. Theory*, vol. 10, pp. 39–42, Jan. 1964.
- [91] M. Sablatash, "Adaptive and cognitive UWB radio and a vision for flexible future spectrum management," in *Proc. Canadian Workshop on Inform. Theory, (CWIT'07)*, June 2007, pp. 41–44.
- [92] R. Scholtz, "Multiple access with time-hopping impulse modulation," in *Proc. IEEE Military Communications Conf. (Milcom'93)*, Oct. 1993, pp. 447–450.
- [93] P. Shaft, "Low-rate convolutional code applications in spread-spectrum communications," *IEEE Trans. Commun.*, vol. 25, no. 8, pp. 815–821, Aug. 1977.
- [94] X. Shen, M. Guizani, R. Qiu, and T. Le-Ngoc, *Ultra-wideband Wireless Communications and Networks*. West Sussex, England: John Wiley and Sons, Ltd, 2006.
- [95] T. Strohmer, M. Emami, and J. Hansen, "Application of time-reversal with MMSE equalizer to UWB communications," in *Proc. IEEE Global Telecommunications Conference (Globecom'04)*, vol. 5, Texas, USA, Nov. 2004, pp. 3123–3127.
- [96] Y. Sugiyama, "A method for solving key equation for Goppa codes," *Information and Control*, vol. 27, pp. 87–99, 1975.
- [97] O. Y. Takeshita and D. J. Costello, "New deterministic interleaver designs for turbo codes," *IEEE Trans. Inf. Theory*, vol. 46, no. 6, pp. 1988–2006, Sept. 2000.
- [98] J. Tang and K. Parhi, "Viterbi decoder for high-speed ultra-wideband communication systems," in *Proc. IEEE Int. Conf. on Acoustics, Speech, and Signal Processing ICASSP'05*, vol. 5, Mar. 2005, pp. 37–40.
- [99] K. Usuda, H. Zhang, and M. Nakagawa, "Pre-RAKE performance for pulse based UWB system in a standarized UWB short range channel," in *Proc. IEEE Wireless Communications and Networking Conference (WCNC'04)*, Atlanta, USA, Mar. 2004, pp. 920–925.
- [100] A. J. Viterbi, *Principles of Spread Spectrum Communications*. Massachusetts, USA: Addison-Wesley Publishing Company, 1995.
- [101] E. Viterbi, "Error bounds for convolutional codes and an asymptotically optimum decoding algorithm," *IEEE Trans. Info. Theory*, vol. IT-13, pp. 260–269, Apr. 1967.
- [102] B. Vucetic and J. Yuan, *Turbo Codes: Principles and Applications*. Kluwer Academic, 2000.

- [103] M.-O. Wessman, A. Swensson, and E. Agrell, "Frequency diversity performance of coded multiband OFDM systems on IEEE UWB channels," in *Proc. IEEE VTC'04*, vol. 2, Los Angeles, USA, Sept. 2004, pp. 1197–1201.
- [104] N. Wiberg, *Codes and decoding on general graphs*. Ph.D. dissertation, Dept. Elect. Eng. Linköping Univ., 1996.
- [105] M. Win and R. Scholtz, "Ultra-wide bandwidth time-hopping spread-spectrum impulse radio for wireless multiple-access communications," *IEEE J. Select. Areas Commun.*, vol. 48, no. 4, pp. 679–689, Apr. 2000.
- [106] J. Wozencraft and B. Reiffen, *Sequential Decoding*. Cambridge, Massachusetts, USA: The MIT Press, 1961.
- [107] N. Yamamoto and T. Ohtsuki, "Adaptive internally turbo-coded ultra-wideband impulse radio," in *Proc. IEEE Int. Comm. Conf.*, vol. 5, May 2003, pp. 3535–3539.
- [108] K. Y. Yazdandoost, "Channel model for body area network (BAN)," *Tech. Rep. P802.15-08-0780-06-0006, IEEE P802.15 Working Group for Wireless Personal Area Networks (WPANs)*, Mar. 2009.
- [109] S. Yoshida and T. Ohtsuki, "Performance evaluation of adaptive internally turbo-coded ultra wideband-impulse radio (AITC-UWB-IR) in multipath channels," in *Proc. IEEE Veh. Techn. Conf.*, vol. 2, Sept. 2004, pp. 1179–1183.
- [110] T. Zasowski and A. Wittneben, "Performance of UWB receivers with partial CSI using a simple body area network channel model," *IEEE J. Sel. Areas. Commun.*, vol. 27, no. 1, pp. 17–26, Jan. 2009.
- [111] J. Zhang, R. Kennedy, and T. Abhayapala, "New results on the capacity of M-ary PPM ultra-wideband systems," in *Proc. IEEE Int. Conf. on Commun (ICC'03)*, May 2003, pp. 2867–2871.
- [112] D. Zhao and W. A. Serdijn, "A time-interleaved sampling delay circuit for IR UWB receivers," in *Proc. IEEE Int. Symp. on Circuits and Systems*, Taiwan, May 2009.
- [113] S. Zhao and H. Liu, "Transmitter-side multipath preprocessing for pulsed UWB systems considering pulse overlapping and narrowband interference," *IEEE Trans. Vehicular Techn.*, vol. 56, no. 6, pp. 3502–3510, Nov. 2007.
- [114] J. Zheng and C. Xiao, "Improved models for the generation of multiple uncorrelated Rayleigh fading waveforms," *IEEE Comm. Lett.*, vol. 6, no. 6, pp. 256–258, June 2002.
- [115] J. Zhou and R. Qiu, "Spatial focusing of time-reversed UWB electromagnetic waves in a hallway environment," in *Proc. IEEE Symposium of the System Theory Tennessee Technological University*, Tennessee, USA, Mar. 2006, pp. 318–322.

- [116] K. Zigangirov, "Some sequential decoding procedures," *Problemy Peredachi Informatsii*, vol. 2, pp. 13–25, 1966.

# List of Abbreviations

ACS	Add Compare Select
ASIC	Application Specific Integrated Circuits
AWGN	Additive White Gaussian Noise
BAN	Body Area Network
BER	Bit Error Rate
BPAM	Binary Pulse Amplitude Modulation
BPPM	Binary Pulse Position Modulation
BPSK	Binary Phase Shift Keying
BR	Bit Repetition
CM	Channel Model Scenario
DAM	Differential Autocorrelation Modulation
DVB	Digital Video Broadcasting
EIRP	Equivalent Isotropic Radiated Power
FCC	Federal Communications Commission
FFT	Fast Fourier Transform
FPGA	Field Programmable Gate Array
FR	Frame Repetition
GA	Gaussian Approximation
HDTV	High Definition Television
IAT	Inter-Arrival Time
ICM+PR	Interleaved Coding-Modulation and Polarity Randomization
ICT	Information and Communication Technology
IEEE	Institute of Electrical and Electronics Engineers
IFI	Inter-Frame Interference
IFFT	Inverse Fourier Transform
IPI	Inter-Pulse Interference
ISI	Inter-Symbol Interference
ISM	Industrial Scientific and Medical
LOS	Line-Of-Sight
LDPC	Low Density Parity Check
LPI/D	Low Probability of Interception/Detection

NLNA	Non-linear low noise amplifier
NLOS	Non-Line-Of-Sight
MB-OFDM	Multiband OFDM
MEMS	Micro-Electro-Mechanical Systems
MRC	Maximal Ratio Combining
OFDM	Orthogonal Frequency Division Multiplexing
PAN	Personal Area Network
PCB	Printed Circuit Board
PDGR	Pulse De-Grouping
PDR	Polarity De-Randomizer
PPM	Pulse Position Modulation
PSD	Power Spectral Density
PSM	Pulse Shape Modulation
QoS	Quality-of-Service
QPSK	Quadrature Phase Shift Keying
RF	Radio Frequency
RMS	Root Mean Square
SNR	Signal-to-Noise Ratio
SOC	Superorthogonal Convolutional
TF	Time Filtering
TH	Time Hopping
TR	Transmitted Reference
UWB	Ultra-Wideband
UWB-IR	Ultra-Wideband Impulse Radio
WES	Weight Enumerating Sequence
WiFi	Wireless Fidelity
WiMAX	Worldwide Interoperability for Microwave Access
WLAN	Wireless Local Area Network
WPAN	Wireless Personal Area Network



# List of Symbols

$\alpha_{m,l}$	multipath gain coefficient of the $m$ -th path corresponding to the $l$ -th cluster
$A_\kappa$	signal amplitude of the user $\kappa$
$\beta$	information error weight
$B$	bandwidth
$\mathbf{b}$	modulated symbols sequence
$d_f$	free distance of code
$\mathbf{d}$	code bit sequence
$\Delta(i)$	delay function of an interleaver
$E$	energy per component of the code (per dimension)
$E_b$	energy per information bit
$\mathbf{f}$	frame sequence
$\mathcal{F}(\cdot)$	Fourier transform operator
$G(f)$	transfer function of the receiver front-end including antenna
$G_p$	processing gain
$h(t)$	channel impulse response
$H(s)$	transfer function of a filter
$\gamma$	dispersion of an interleaver
$\gamma_{out}$	output signal-to-noise ratio of the differential autocorrelation receiver
$I(t)$	multi-user interference term
$K$	constraint length of a code
$L_u$	size of information bit interleaver
$L_d$	size of code bit interleaver
$L_f$	size of frame interleaver
$L_p$	size of chip interleaver
$\lambda_{\tilde{a},\tilde{b}}(\tau)$	Hamming cross-correlation between sequences $\tilde{a}$ and $\tilde{b}$ for relative time delay $\tau$
$\bar{\lambda}$	normalized Hamming cross-correlation
$n(t)$	zero mean additive white Gaussian noise

$N$	total number of chips in a packet
$N_u$	number of information bits in a packet
$N_d$	number of code bits in a packet
$N_f$	number of frames per code bit
$N_p$	number of chips per frame
$N_0$	noise spectral density
$p$	crossover probability
$\mathbf{p}$	polarity randomization sequence
$P_b$	bit error probability
$P_{col}$	pulse collision probability
$\Pi_u$	interleaving operation on information bits
$\Pi_d$	interleaving operation on code bits
$\Pi_f$	interleaving operation on frames
$\Pi_p$	interleaving operation on chips
$\mathbf{r}''$	received sequence for one packet
$r''(t)$	received signal waveform after passing through an antenna and amplifier
$R$	code rate
$R_b$	bit rate
$\mathbf{s}$	sequence of chips
$s_i^{(\kappa)}(t)$	transmitted signal waveform for one packet from user $\kappa$
$S$	spread of an interleaver
$T(W, \beta)$	transfer function of a code
$T_w$	duration of the transmitted pulse
$\mathbf{u}$	sequence of information bits
$\mathbf{u}'$	sequence of interleaved information bits
$\hat{\mathbf{u}}$	sequence of deinterleaved decoded bits
$U$	number of users
$\varphi$	encoding function
$\{(\varsigma_d, d)\}$	distance spectrum of a code
$\Upsilon(i)$	placement operator for a hyperbolic congruence sequence
$\hat{y}_i$	output of the correlator for the $i$ -th symbol
$w(t)$	transmitted pulse
$X$	shadowing term
$\Omega_1(f)$	Fourier transform of the Gaussian monocycle

# Appendix A

## Publications by the Author

In the following, the publications by the author related to the thesis are listed in reverse chronological order.

### Journals

1. M.M. Pietrzyk, J.H. Weber, "On the Performance of UWB-IR with Interleaved Coding-Modulation and Polarity Randomization on AWGN and Multipath Fading Channels," IEEE Transactions on Vehicular Technology, vol. 57, no. 6, pp. 3578-3588, November 2008.

### Conferences

2. M.M. Pietrzyk, T. v.d. Gruen, "Ultra-wideband Technology-based Ranging Platform with Real-time Signal Processing," IEEE/ION Position, Location and Navigation Symposium, PLANS 2010, accepted for publication, California, USA, May 2010.
3. M.M. Pietrzyk, R. Retkowski, H. Fruehauf, T. v.d. Gruen, "Ultra-wideband Technology-Based Localization – Theoretical Boundaries and Implementation Aspects," Positioning and Navigation Symposium, POSNAV 2009, Dresden, Germany, October 2009.
4. C. Quemada, I. Val, M.M. Pietrzyk, T. v.d. Gruen, N. Gonzalez, I. Velez, "A Smart Care System for Elderly People to Support Independent Living: CONFIDENCE," Proceedings European Conference on Smart Systems Integration 2009, Brussels, Belgium, March 2009.
5. M.M. Pietrzyk, K. Popovski, T.A. Wysocki, B.J. Wysocki, and J.H. Weber, "Multi-User UWB-IR Systems with Interleaved Coding-Modulation on Multipath Fading Channels," Proceedings IET Forum on Waveform Diversity and Design in Communications, Radar and Sonar, Savoy Place, London, UK, ISBN 0-86341 -721-3, pp. 93-98, November 2006.

6. M.M. Pietrzyk, K. Popovski, T.A. Wysocki, B.J. Wysocki, and J.H. Weber, "Scarcely Populated UWB-IR Systems with Interleaved Coding-Modulation on Multipath Fading Channels," Proceedings the IEEE International Conference on Ultra-Wideband (ICUWB'2006), Waltham, Massachusetts, USA, ISBN 1-4244-0102-X, pp. 55-60, September 24-27, 2006.
7. M.M. Pietrzyk, K. Popovski, T.A. Wysocki, B.J. Wysocki, and J.H. Weber, "On the Performance of Scarcely Populated Coded UWB-IR Systems on Multipath Fading Channels," Proceedings 27th Symposium on Information Theory in the Benelux, Noordwijk, The Netherlands, ISBN-10: 90-71048-22-5, ISBN-13 (from January 2007): 978-90-71048-22-7, pp. 235-242, June 8-9, 2006.
8. M.M. Pietrzyk, J.H. Weber, "On the Influence of Channel Statistics on the Performance of Coded UWB-IR Systems," Proceedings 8th International Symposium on DSP and Communication Systems (DSPCS'2005) & 4th Workshop on the Internet, Telecommunications and Signal Processing (WITSP'2005), Noosa Heads, Sunshine Coast, Australia, ISBN: 09756934-1-7, 6 pgs., December, 2005.
9. M.M. Pietrzyk, J.H. Weber, "Impact of Channel Statistics on the Performance of Coded UWB-IR Systems," Proceedings 12th IEEE Symposium on Communications and Vehicular Technology in the Benelux (SCVT 2005), Enschede, The Netherlands, ISBN 90-365-2264-1, 8 pgs., November, 2005 - The Best Paper Award.
10. M.M. Pietrzyk, J.H. Weber, "Performance of UWB-IR with Polarity Randomization and Interleaved Coding-Modulation on Multipath Fading Channels," Proceedings 61st IEEE Vehicular Technology Conference (VTC 2005 Spring), Stockholm, Sweden, ISBN 0-7803-8887-9/05, 5 pgs., May 2005.
11. M.M. Pietrzyk, J.H. Weber, "Performance Evaluation of Coded UWB-IR on Multipath Fading Channels," Proceedings 7th International Symposium on Advanced Radio Technologies (ISART 2005), Boulder, Colorado, USA, pp. 145-149, March 2005.
12. M.M. Pietrzyk, J.H. Weber, "On the Performance of Interleaved Coding-Modulation in UWB-IR Systems on Multipath Fading Channels," Proceedings International Scientific Conference for Students and Young Scientists 'Telecommunication in XXI Century' (MKNSIMPN 2004), Kielce, Poland, 5 pgs., November 2004.
13. M.M. Pietrzyk, J.H. Weber, "Application of Error Correction Coding in Ultra-wideband Impulse Radio (UWB-IR) on a Multipath Fading Channel," Proceedings 11th IEEE Symposium on Communications and Vehicular Technology in the Benelux (SCVT 2004), Gent, Belgium, 5 pgs., November 2004.
14. M.M. Pietrzyk, "Ultra-wideband Radio - an Introduction to the Breakthrough Wireless Technology," Proceedings National Conference on Radio Communication, Radio and Television (KKRRiT 2003), Wroclaw, Poland, 4 pgs., June 2003.

15. M.M. Pietrzyk, S. Pietrzyk, W. Dziech, "Multiple Access and Collision Based Sub-carrier Allocation for OFDM Based Communication Systems," Proceedings National Conference on Radio Communication, Radio and Television (KKRRiT 2002), Gdansk, Poland, June 2002.
16. M.M. Pietrzyk, "The Future Generations of Mobile Communications based on Broad-band Access Technologies," Proceedings International Scientific Conference for Students and Young Scientists 'Telecommunication in XXI Century' (MKNSIMPN 2001), Kielce, Poland, 2001.

Relation of the listed publications and the chapters of the thesis is given in Table A.1.

Table A.1. Relationships between the publications and the chapters of this thesis, where  $\blacklozenge$  and  $\lozenge$  denote major and minor relationship, respectively.

Publication	Ch.1	Ch.2	Ch.3	Ch.4	Ch.5	Ch.6
1		$\blacklozenge$	$\blacklozenge$	$\blacklozenge$		
2	$\lozenge$	$\lozenge$				
3	$\lozenge$					
4	$\blacklozenge$					$\lozenge$
5		$\lozenge$	$\blacklozenge$		$\blacklozenge$	
6		$\lozenge$	$\blacklozenge$		$\blacklozenge$	
7		$\lozenge$	$\blacklozenge$		$\blacklozenge$	
8		$\blacklozenge$	$\blacklozenge$	$\blacklozenge$		
9		$\blacklozenge$	$\blacklozenge$	$\blacklozenge$		
10		$\blacklozenge$	$\blacklozenge$	$\blacklozenge$		
11		$\blacklozenge$	$\blacklozenge$	$\blacklozenge$		
12		$\blacklozenge$	$\blacklozenge$	$\blacklozenge$		
13		$\blacklozenge$	$\blacklozenge$	$\blacklozenge$		
14	$\blacklozenge$					
15						
16						

# Samenvatting (Summary in Dutch)

Er wordt voorzien dat draadloze systemen na de derde generatie (3G) connectiviteit voor alles en iedereen, waar en wanneer dan ook, mogelijk zullen maken. Deze zeer veelomvattende vorm van toekomstige communicatie zal een integratie van bestaande en toekomstige draadloze standaarden eisen, uiteenlopend van metropolitan area networks (MANs), wireless local area networks (WLANs), wireless personal area networks (WPANs) tot wireless body area networks (WBANs). Hedendaagse WLAN en WPAN technologieën kunnen niet voorzien in de behoeften van de connectiviteit van morgen, welke een hoge datasnelheid vereist, in staat is de omgeving gewaar te worden en gebaseerd is op omringende intelligentie en vergaande rekenparadigma's.

Ultra-wideband (UWB) is een veelbelovende technologie die een mogelijk oplossing biedt voor de eisen van de volgende generatie draadloze toestellen m.b.t. datasnelheid, kosten, vermogensverbruik en fysieke afmetingen. UWB kan misschien ook een belangrijke rol spelen in de realisatie van toekomstige heterogene netwerken. Deze technologie heeft recentelijk veel interesse gewekt in zowel de academische als de industriële wereld, resulterend in de specificatie van de IEEE 802.15.3 en IEEE 802.15.4 standaarden. De kracht van UWB ligt in de zeer grote instantane bandbreedte die wordt gebruikt en de mogelijkheid voor eenvoudige zender/ontvanger-architecturen.

Dit proefschrift behandelt verscheidene belangrijke aspecten van de UWB-technologie, inclusief het modeleren van realiseerbare ultra-wideband impulse radio (UWB-IR) systemen, de typering van hun prestaties, en geschikte methoden voor bescherming tegen fouten. Het belangrijkste doel van dit proefschrift is nieuwe technieken voor foutenbeheersing voor te stellen en te evalueren, in het bijzonder voor UWB-IR systemen welke opereren in omgevingen die onderhevig zijn aan ernstige multipath interferentie. De voorgestelde methoden buiten de temporele diversiteit uit welke meegebracht wordt door UWB-kanalen d.m.v. multipaths en aldus de verlichting mogelijk maakt van destructieve effecten van inter-symbol (ISI) en inter-pulse (IPI) interferentie. We ontdekten dat herordening van de volgorde van UWB chips of UWB frames tot een verbetering van de bit error rate (BER) leidt. Deze verbetering is in het bijzonder duidelijk voor UWB-IR systemen met frame repetition (FR) als methode voor bescherming tegen fouten. Voor UWB-IR systemen met superorthogonal convolutional (SOC) codering is de gintroduceerde winst kleiner.

Dit proefschrift start met de introductie van UWB-technologie en een literatuuroverzicht

m.b.t. de relevante onderwerpen. Vervolgens wordt het UWB-IR systeemmodel zoals beschouwd in het proefschrift gepresenteerd. Het verschaft details over de voorgestelde technieken, het kanaalmodel, de pulsform, antennetyperingen en ontvangerarchitectuur. Bovendien worden uitdagingen m.b.t. de hardware-implementatie geadresseerd. De beschouwde kanaalcoderingsschema's welke geschikt zijn voor UWB systemen zijn frame herhaling, bit herhaling en SOC codering. We presenteren de criteria voor hun selectie. Bovendien worden selecte aspecten van de hardware-implementatie van een decodeeralgoritme zoals beschikbaar in de literatuur besproken. De prestatie van UWB-IR systemen wordt getypeerd d.m.v. theoretische en op Monte-Carlo-simulatie gebaseerde analyses. De BER prestatie van eenpersoons UWB-IR systemen opererend op additive white Gaussian noise (AWGN) and multipath fading kanalen wordt in detail bestudeerd. De nieuwigheid van de gepresenteerde analyse is dat deze ISI en IPI effecten, RF front-end zaken en rele antennetyperingen beschouwt welke vaak door onderzoekers veronachtzaamd worden. Bovendien worden deze gepresenteerd, voor de eerste keer, voor het gegeven type eenvoudige incoherente ontvangerarchitectuur (differential autocorrelation receiver), kanaalcoderingsschema (SOC codering), en kanaalmodel (IEEE 802.15.3a multipath fading kanaal).

Onze resultaten geven aan dat voor UWB-IR systemen met SOC codering, en met gegeven systeemparameters zoals in detail behandeld in Hoofdstuk 4, het mogelijk is BER waarden in de orde van  $10^{-4}$  te behalen voor  $E_b/N_0$  (verhouding van de energie per bit tot de ruisdichtheid) waarden kleiner dan 12.5 dB. UWB-IR systemen met frame herhaling presteren veel slechter: voor hetzelfde BER niveau is de vereiste  $E_b/N_0$  meer dan 16 dB. Onze bevindingen laten ook zien dat het herschikken van de chip-volgorde in een willekeurige een-op-een manier een grotere prestatieverbetering geeft dan het herschikken van frames of bits. Bovendien heeft verandering van systeemparameters (binnen de beschouwde waarden) met handhaving van de datasnelheid geen effect op de BER prestatie van UWB-IR systemen met FR. Dit is niet het geval voor UWB-IR systemen met SOC codering, waarvoor een voorkeur voor lage code-rates zichtbaar is. De verkregen simulatieresultaten zijn in goede overeenstemming met de afgeleide onder- en bovengrenzen voor de BER.

Een nieuw ontwerp van een deterministische chip interleaver gebaseerd op time-hopping hyperbolische congruentiereeksen wordt eveneens voorgesteld. Dit schema, samen met SOC codering of frame herhaling, vormt een effectieve beschermingsmethode tegen fouten in dunbevolkte UWB-IR systemen welke opereren in omgevingen die onderhevig zijn aan ernstige multipath interferentie. De BER prestatie van UWB-IR systemen voor multipath fading kanalen met en zonder het voorgestelde schema wordt gevalueerd m.b.v. grenzen gebaseerd op de Poisson verdeling en intensieve Monte Carlo simulaties. Onze bijdrage bevat het ontwerp van de chip interleaver gebaseerd op time-hopping hyperbolische congruentiereeksen en het bepalen van de belangrijkste parameters ervan.

Onze bevindingen geven aan dat de Interleaved Coding-Modulation (ICM) methode ook voor scenario's met weinige gebruikers prestatieverbeteringen introduceert. De voorgestelde deterministische chip interleaver kan de voorkeur krijgen boven een random interleaver van-



wege de eenvoudigere implementatie. Onze resultaten laten zien dat de gepresenteerde Poisson-gebaseerde analyse behulpzaam kan zijn in een ruwe benadering van de BER prestatie van UWB-IR systemen zonder de ICM methode.

Het laatste deel van het proefschrift presenteert een studie naar de toepassing van de UWB-IR technologie bij body area networks (BANs). Het begint met een inleiding in het BAN concept. Vervolgens wordt een beschrijving van verscheidene beschouwde scenario's, systeem- en kanaalmodellen gegeven. Prestaties van BANs gebaseerd op UWB-IR technologie worden gevalueerd m.b.v. Monte-Carlo simulaties.

Onze resultaten geven aan dat voor BANs met lage datasnelheid frame herhaling en SOC codering betere BER prestaties mogelijk maken dan voor het geval van systemen met hoge datasnelheid. Bovendien biedt de ICM methode BER prestatieverbeteringen welke significant zijn voor het FR schema met een datasnelheid van 31.25 Mbps. In het geval van lagere datasnelheden dan 31.25 Mbps introduceert deze methode slechts verbeteringen wanneer de  $E_b/N_0$  groter is dan een zekere waarde.



# Streszczenie

Przewiduje się, że systemy bezprzewodowe powyżej trzeciej generacji udostępnią łączność dla każdego w każdym miejscu i czasie. Systemy komunikacyjne przyszłości będą wymagać integracji obecnych oraz przyszłych standardów bezprzewodowych obejmując sieci miejskie (MAN), bezprzewodowe sieci dostępne (WLAN), sieci osobiste (WPAN) oraz sieci body area networks (WBAN). Jednakże obecne technologie na jakich bazują sieci WPAN i WBAN nie są w stanie sprostać wymaganiom przyszłości, które dotyczą szybkości transmisji, inteligencji oraz możliwości przetwarzania danych.

Jedną z najbardziej obiecujących technologii spełniających te wymagania jest UWB (Ultra-wideband). Technologia ta stała się ostatnio bardzo popularna dzięki zastosowaniu w standardach IEEE 802.15.3 oraz IEEE 802.15.4. Przewaga technologii UWB nad technologiami szeroko- i wąskopasmowymi ma swoje źródło w bardzo szerokim paśmie użytkowym oraz możliwości budowy urządzeń nadajnik-odbiornik o uproszczonej konstrukcji.

Niniejsza rozprawa porusza szereg ważnych zagadnień dotyczących technologii UWB takich jak modelowanie systemów UWB opartych na przesyłaniu impulsów (UWB-IR), ocena stopy błędów, a także metody korekcji błędów transmisji. Głównym celem niniejszej rozprawy jest zaproponowanie i analiza oryginalnych technik korekcji błędów dla systemów UWB-IR pracujących w środowiskach transmisji wielodrogowej. Zaproponowane metody wykorzystują różnorodność czasową (temporal diversity) mającą swoje źródło w wielodrogowości, i pozwalają na zniwelowanie negatywnych efektów interferencji międzysymbolowych oraz międzyramkowych.



## Acknowledgements

This thesis would not have been possible without the support of many people.

First, I would like to express my gratitude to my promoter Prof. Ignas Niemegeers for giving me the opportunity to pursue my Ph.D. studies. In particular, I am very grateful to my mentor Dr. Jos Weber for his professional guidance, numerous fruitful discussions, and constructive criticism. I sincerely thank him for his support and encouragement at every stage of my Ph.D. I have learned a lot and feel privileged to have worked under his guidance.

I would also like to thank all the members of my Ph.D. Committee for reading the manuscript and their valuable feedback.

I am grateful to Prof. Tad Wysocki for making it possible to do a research visit at the University of Wollongong in Australia and for all support I have received. I am thankful to Dr. Beata Wysocki for her valuable discussions and support that have continued many years after my return to the Netherlands. I would also like to thank Dr. Keni Popovski for joint collaboration that resulted in several papers written together.

During my Ph.D., I enjoyed a pleasant environment created by colleagues from the Wireless and Mobile Communications and Network Architectures and Services Groups. In particular, I would like to thank Dr. Anthony Lo, Dr. Martin Jacobsson and Dr. Bao Linh Dang for being true friends and helping me when it was really needed. I also wish to extend my thanks to the secretaries: Marjon Verkaik-Vonk, Wendy Murtinu-Van Schagen, and Laura Bauman for their help with administrative matters. My special thanks go to Laura Bruns and Laura Zondervan for supporting me during my first year in Delft. I am indebted to Dr. Homayoun Nikookar and Dr. Gerard Janssen for their insights and our discussions on a UWB channel and receiver.

I wish to thank Thomas von der Grün from the Fraunhofer Institute for Integrated Circuits for creating possibilities to finish this thesis.

Last but not least, I owe this thesis to Aneta and our daughter Klaudia for their love and patience and our parents for their moral support and encouragement.



# Curriculum Vitae

Michał M. Pietrzyk

## Profile

Michał Pietrzyk was born in Kielce, Poland, on March 28, 1977. From 1992 until 1997 he attended Technical Electronics College, in Kielce, Poland, specializing in General Electronics. In June 1997, he earned the technical degree and was ranked the 1st over nearly 200 graduates. From 1997 until 2002, he studied Electrical Engineering at the Kielce University of Technology in Poland. He was awarded the Master of Science degree (with the highest honors) in Electrical Engineering with specialization in Telecommunications, in July 2002.

From July 2002 until Nov. 2002, he was with the Development Department of Radmor S.A., Gdynia, Poland, working as a Researcher and Software Engineer. He was involved in a military Software Radio Project. In Feb. 2003, he joined the Wireless and Mobile Communication Group, at the Delft University of Technology in the Netherlands as a Researcher and PhD Candidate specializing in design and performance evaluation of error control coding schemes particularly suitable for UWB systems. This work was performed within the confines of the AIRLINK Project under the Freeband Program. During his PhD studies, from Nov. 2005 to Feb. 2006, he was a Visiting Researcher at the University of Wollongong, NSW, Australia. Since Nov. 2007, he has been working as a Research Engineer and Project Manager at the Fraunhofer Institute in Germany. His research areas include wireless communications, UWB technology, localization techniques, error-control coding, and cognitive radios.

Mr. M. Pietrzyk has served as an invited reviewer for international journals including IEEE Transactions on Wireless Communications, IEEE Transactions on Communications, EURASIP Journals on Wireless Communications and Networking, Electronics and Telecommunications Research Institute (ETRI) journals, IEEE Communications Letters and conferences: IEEE Global Communications Conference (GLOBECOM'06), IEEE International Conference on Ultra-wideband (ICUWB'06), IEEE Wireless Communications and Networking Conference (WCNC'07), just to mention a few.

During his PhD studies, he mentored three M.Sc. and two Bachelor students in the area of channel coding for UWB communications. He is a member of the IEEE and IET.

## Awards

- The IEEE ICUWB 2006 conference paper ranked between top 10%-30% of papers and nominated for the Best Paper Award, Sept. 2006.

- The second prize in the Best Paper Contest for the paper "Impact of Channel Statistics on the Performance of Coded UWB-IR Systems" presented at the 12th IEEE Symposium on Communications and Vehicular Technology, Enschede, The Netherlands, 2005.
- The President's Award for the outstanding graduate student (top 5% among all the graduates from the Kielce University of Technology), Kielce, Poland, 2002.

### **Invited Presentations**

- M.M. Pietrzyk, "Error Control Techniques for UWB-IR Communications," École Polytechnique Fédérale de Lausanne, Lausanne, Switzerland, April 2007.
- M.M. Pietrzyk, "Error Correction Techniques for UWB-IR Systems," Communications Research Group, University of Oxford, UK, November 2006.
- M.M. Pietrzyk, "Channel Coding for UWB Technology and Recent Results on Application of Orthogonal Sequences in UWB-IR Systems with Interleaved Coding-Modulation and Polarity Randomization," National ICT Australia (NICTA), Canberra, Australia, January 2006.
- M.M. Pietrzyk, "On Channel Coding for UWB Communications," two presentations for the Wireless Research Group, University of Wollongong, Australia, November 2005.

### **Other international activities**

- Technical Program Committee (TPC) Member of the 3rd International Conference on Signal Processing and Communication Systems (ICSPCS'2009), Nebraska, USA, Sept. 2009.